

Adaptive Guidance and Control of Small Unmanned Aerial Vehicles

A thesis accepted by the Faculty of Aerospace Engineering and Geodesy of the
University of Stuttgart in partial fulfillment of the requirements for the degree of
Doctor of Engineering Sciences (Dr.-Ing.)

by

Toufik Souanef

born in Batna, Algeria

Committee chair: Prof. Dr.techn. Thomas Hobiger

Main Referee: Prof. Dr.-Ing. Walter Fichter

Co-Referee: Prof. Dr.-Ing. Florian Holzapfel

Date of defense: 6 September 2019

**Institute of Flight Mechanics and Control
University of Stuttgart
2019**

Preface

I would like to express my gratitude and appreciation to my advisor, Professor Walter Fichter, for his "adaptive guidance", patience and detailed advice through these years.

I would also like to express my appreciation to my committee member Professor Florian Holzapfel. Thanks for the valuable questions and comments, which helped me towards the improvement and completion of my thesis.

Many thanks to Doctor Werner Grimm for his support in reviewing my dissertation. My warmest appreciation to all my labmates. Thank you for your help and discussions.

Special thanks to my family for their love and support.

Contents

Preface	iii
Nomenclature	ix
Abstract	xi
Kurzfassung	xiii
1 Introduction	1
1.1 Motivation	1
1.2 Adaptive Control Techniques for UAV Applications	2
1.2.1 Path-Following of Small UAVs	3
1.2.2 Fault-Tolerant Control	3
1.3 Research Objective and \mathcal{L}_1 Adaptive Control	4
1.4 Thesis Contributions	6
2 \mathcal{L}_1 Adaptive Control of Systems with Disturbances of Unknown Bounds	9
2.1 \mathcal{L}_1 Adaptive Controller for SISO Systems	10
2.1.1 Controller Design	11
2.1.2 Controller Analysis	13
2.2 \mathcal{L}_1 Adaptive Controller for MIMO Systems	20
2.2.1 Controller Design	21
2.2.2 Controller Analysis	22
2.3 Summary	29

3	\mathcal{L}_1 Adaptive Guidance of Fixed-wing UAVs	31
3.1	The Path-Following Problem	32
3.2	\mathcal{L}_1 Adaptive Straight-Line Path-Following in the Horizontal Plane	33
3.2.1	Controller Design	33
3.2.2	Simulation Results	37
3.3	\mathcal{L}_1 Adaptive Circular Path-Following	43
3.3.1	Controller Design	44
3.3.2	Simulation Results	46
3.4	Flight Test Results	47
3.5	Summary	49
4	\mathcal{L}_1 Adaptive Guidance of Fixed-wing UAVs for 3D Curved Paths	51
4.1	Problem Formulation	52
4.2	\mathcal{L}_1 Adaptive Path-Following of Three Dimensional Curved Paths	57
4.3	Simulation Results	58
4.3.1	Simulation Results for a Dubins Path	59
4.3.2	Simulation Results for a Helix Path	64
4.4	Summary	65
5	Fault-Tolerant \mathcal{L}_1 Adaptive Control Based on Multiple Models	69
5.1	Multiple Model \mathcal{L}_1 Adaptive Control of SISO Systems	70
5.1.1	Controller Design	71
5.1.2	The Switching Logic	73
5.1.3	Controller Analysis	74
5.2	Control of a Small UAV in Case of Inversion of the Elevator Command	76
5.2.1	Controller Design	76
5.2.2	Simulation Results	77
5.3	Multiple Model \mathcal{L}_1 Adaptive Control of MIMO Systems	79
5.4	UAV Lateral-Directional Control in Case of Inversion of the Commands	82
5.4.1	Controller Design	82
5.4.2	Simulation Results	83
5.5	Summary	85

6	Output Feedback Fault-Tolerant \mathcal{L}_1 Adaptive Control	87
6.1	Observer-based \mathcal{L}_1 Adaptive Control	88
6.1.1	Controller Design	88
6.1.2	Controller analysis	90
6.1.3	Flight Test Results	94
6.2	Multiple Model Output Feedback \mathcal{L}_1 Adaptive Control	97
6.2.1	Controller Design	97
6.2.2	Controller analysis	99
6.2.3	Flight Test Results	101
6.3	Summary	103
7	Conclusions and Outlook	105
7.1	Conclusions	105
7.2	Outlook	106
A	Appendix	109
A.1	Comments on \mathcal{L}_1 Stability Condition	109
A.1.1	\mathcal{L}_1 Adaptive Stability Condition	109
A.1.2	Simulation Results	112
A.1.3	Conclusion	112
A.2	\mathcal{L}_1 -Spaces and \mathcal{L}_1 -Norms.	113
	Bibliography	115
	Resume	127

Nomenclature

Symbols frequently used within this thesis are listed below in alphabetical order. Not included are symbols appearing only once or which are assumed to be clear from the context.

Symbols

A	System matrix
A_m	Desired matrix
b	Input vector
B	Input matrix
c	Measurement vector
C	Measurement matrix
\mathbb{I}	Identity matrix
\mathbb{R}	Reals set
u	Control input
x	State vector
y	System output

Greek Symbols

α	Angle of attack
β	Sideslip angle
η	System disturbance
γ	Vertical orientation angle
Γ	Adaptation gain
ψ	Horizontal orientation angle
θ	Vector of constant unknown parameters

Nomenclature

Subscripts and Superscripts

c	Commanded
m	Matched
p	Path
u	Unmatched

Operators

$\dot{(\cdot)}$	Time derivative
$\hat{(\cdot)}$	Estimate
\in	Element of
\forall	For all

Acronyms

2D	Two-Dimensions
3D	Three-Dimensions
BIBS	Bounded Input Bounded State
FPGA	Field Programmable Gate Array
LQR	Linear Quadratic Regulator
MIMO	Multi-Input-Multi-Output
MRAC	Model Reference Adaptive Control
SISO	Single-Input-Single-Output
SBC	Single Board Computer
UAV	Unmanned Aerial Vehicle

Abstract

This dissertation focuses on adaptive guidance and control of small fixed-wing Unmanned Aerial Vehicles (UAVs). Small UAVs are very sensitive to wind. Furthermore, they are generally built with low-cost material which makes them prone to frequent faults and failures. On the other hand, limited avionic equipment reduce the possibility to elaborate and implement complicated guidance and control systems. All these reasons motivate the use of a control method that is robust to faults and disturbances and relatively simple for implementation, namely \mathcal{L}_1 adaptive control.

First, an approach for \mathcal{L}_1 adaptive control is presented based on an adaptation law that borrows insights from the sliding mode control to estimate the unknown bounds of disturbances.

Next, an approach of path-following for fixed-wing UAVs is developed considering the presence of wind disturbances. The key idea is to formulate the path-following of a fixed-wing UAV as a control problem in the presence of parametric uncertainties and external disturbances. As a consequence, the common assumption that wind speed is constant can be relaxed. This permits the formulation of clear statements for robustness and performance. The path-following controller was demonstrated in flight under wind speed up to 10 m/s , representing 50% of the normal airspeed of the UAV.

Another contribution of this dissertation is the development of a method for fault tolerant control. The design is based on an \mathcal{L}_1 adaptive controller with a nominal reference model and a set of degraded reference models. In a degraded model the criteria of performance are reduced. The controller was tested in a real flight, and it was shown that the multiple model \mathcal{L}_1 adaptive controller permits to maintain the UAV in flight, in the presence of failures, while the controller with one nominal model fails.

Towards real flight tests, an approach for output feedback \mathcal{L}_1 adaptive

Abstract

control was designed. The main motivation is that the measure of the full state is not available on small UAVs. The proposed method is based on a state observer instead of the state predictor characteristic of \mathcal{L}_1 adaptive control. The main advantage is that a full state measurement can be avoided, and the design and the implementation of the controller are simplified.

Kurzfassung

Die vorliegende Dissertation befasst sich mit der adaptiven Regelung von kleinen unbemannten Luftfahrzeugen (Unmanned Aerial Vehicles - UAVs). Kleine UAVs sind sehr empfindlich gegenüber Wind. Des Weiteren sind sie häufig preisgünstig hergestellt, darum sind sie anfällig für Fehler und Ausfälle. Auf der anderen Seite erlaubt die begrenzte Avionikausstattung keine Implementierung komplizierter Lenk- und Steuersysteme. All diese Gründe sprechen für die Nutzung von Regelungsansätzen, die robust gegenüber Fehlern und Störungen und relativ einfach in der Implementierung sind. Hier bietet sich die \mathcal{L}_1 adaptive Regelung an.

Zuerst wird eine methodische Erweiterung für die \mathcal{L}_1 adaptive Regelung präsentiert. Grundlage hierfür ist ein Ansatz aus der Sliding Mode Regelung, um unbekannte Grenzen und Störungen abschätzen zu können. Mit dieser speziellen Methode werden nun verschiedene, für UAVs relevante Szenarien behandelt, nämlich die Bahnregelung unter Windeinfluss, die Regelung bei sehr starken Unsicherheiten bis hin zu Vorzeichenfehlern, sowie die praktische Realisierung ohne vollständige Zustandsmessung.

Zunächst wird unter Berücksichtigung von Störungen durch Wind eine Methode für die Bahnregelung von Starrflügel UAVs entwickelt. Die Basis hierfür ist die Systemformulierung der Bahnregelung eines UAVs unter Einfluss von parametrischen Unsicherheiten und externen Störungen. Die Wegpunktfolge eines Starrflügler-UAV wird also als Kontrollproblem bei parametrischen Unsicherheiten und externen Störungen formuliert. Folglich kann auf die allgemeine Annahme verzichtet werden, dass die Windgeschwindigkeit konstant ist. Dies ermöglicht die Formulierung klarer Aussagen zur Robustheit und Leistungsfähigkeit. Der Wegfolgeregler wurde im Flug unter Windgeschwindigkeit bis zu 10 m/s , demonstriert, was 50% der normalen Geschwindigkeit des UAVs entspricht.

Kurzfassung

Ein weiterer Beitrag dieser Dissertation ist die Entwicklung einer fehler-toleranten Regelung. Der Entwurf basiert wiederum auf der \mathcal{L}_1 adaptiven Regelung, in diesem Fall mit einem nominalen und einer Reihe von de-gradierten Referenzmodellen. In den degradierten Referenzmodellen sind die Kriterien der Leistung reduziert.

Für reale Flugtests wurde ein Ansatz für die \mathcal{L}_1 adaptive Regelung mit Ausgangsrückführung entworfen. Bei kleinen UAVs ist eine Messung des gesamten Zustands üblicherweise nicht verfügbar. Das vorgeschlagene Modell basiert auf einem Zustandsbeobachter, anstatt eines Prädiktors, wie er üblicherweise in der \mathcal{L}_1 adaptiven Regelung verwendet wird. Damit wird eine vollständige Zustandsmessung vermieden und der Entwurf und die Implementierung des Reglers werden vereinfacht. Da eine Zustandsraumdarstellung beibehalten wird, kann die Systemdynamik, einschließlich der Unsicherheiten und Störungen mit physikalischem Vorwissen angegeben werden, was die praktische Anwendung vereinfacht.

Die Robustheit der \mathcal{L}_1 adaptiven Regelung gegenüber großen Unsicherheiten und Störungen bei der Flugregelung einer kleinen UAV wurde sowohl in Simulationen als auch in Flugtests demonstriert.

1

Chapter 1

Introduction

1.1	Motivation	1
1.2	Adaptive Control Techniques for UAV Applications	2
1.2.1	Path-Following of Small UAVs	3
1.2.2	Fault-Tolerant Control	3
1.3	Research Objective and \mathcal{L}_1 Adaptive Control	4
1.4	Thesis Contributions	6

1.1 Motivation

Unmanned Aerial Vehicles (UAVs), commonly known as drones and referred to as Remotely Piloted Aircrafts (RPA) by the International Civil Aviation Organization (ICAO), are aircrafts without a human pilot aboard [1]. According to the assigned missions or to their size, there are many different classes of UAVs [106].

This work focuses on small fixed-wing UAVs (that is, with wingspans less than 2 meters and payload smaller than 2 kg) [9]. Small UAVs are gaining growing interest because of their low cost, high maneuverability, and simple maintenance. They are used for a wide range of military and civilian tasks [6, 89].

Despite the advantages of small UAVs, their guidance and control is still a challenging problem because of their small size, light weight, relatively low speeds, reduced payload capacity, unknown dynamics, limited sensors suite



Figure 1.1: Twinstar II small fixed-wing UAV.

and insufficient onboard computing.

In this context, a major limitation of small UAVs is their extreme sensitivity to wind, because of their relatively low speeds. For such UAVs, wind speeds are commonly 20% to 60% of the desired airspeed [77]. If the path-following (guidance) system does not account for wind, the trajectory tracking ability of UAVs will be reduced. Therefore, there is a need to design path-following methods that are robust against wind disturbances.

Furthermore, the operation of UAVs, especially in urban environments, needs a high degree of safety and reliability. However, small UAVs are generally built with low-cost material, which increases the probability of occurrence of faults and failures. For that reason, the design of fault-tolerant control systems is required [12, 32, 82, 114]. Nevertheless, applying most of such advanced control techniques for small UAVs is difficult, because of their limited onboard computing resources.

A solution to these issues can be provided through the use of adaptive control [5, 52, 64, 74]. Adaptive control was introduced to meet the challenge of automatically adjusting the controller parameters in the presence of uncertain and time varying aircraft dynamics [44]. Extensive research in the field of adaptive control has enabled the design, analysis, and synthesis of robust and performant adaptive systems [33].

1.2 Adaptive Control Techniques for UAV Applications

Regarding guidance and control of small UAVs, adaptive control is a suitable method for the following reasons:

- It shows good robustness against disturbances, which makes it a natural candidate for path-following in windy conditions.
- Adaptive control does not need an accurate model of the UAV. Actually, obtaining precise models of UAVs is not simple. This is because wind tunnel tests are expensive and long [48], while identification methods, sensibly less expensive than wind tunnel tests are sensitive to payload changes, sensor measurements and accuracy, and they typically assume the availability of the full state vector measurement [30].
- The ability of adaptive control to automatically reconfigure its parameters without a fault detection scheme makes it easy for implementation. This leads to a relatively simple design and reduced computing effort [32, 34, 63], which makes it suitable for low-cost fault-tolerant flight control systems.

In the following, the previous researches on path-following in wind, and control in the presence of faults are presented and discussed.

1.2.1 Path-Following of Small UAVs

The objective of path-following is the design of a control law that generates commands to the attitude controller to follow a given reference trajectory. Path-following of fixed-wing UAVs is designed based on missile guidance [11] and control techniques, particularly nonlinear control [46, 93]. A recent survey of different path-following approaches for fixed-wing UAVs is given in [101]. It should be stressed that wind effect is not explicitly addressed by most researchers.

The previous approaches dealing with the problem of path-following of fixed-wing UAVs under wind are based on the modification of the planned path [24, 72, 80, 90] and control [8, 15, 69, 77, 88]. Their common issue is that they assume that wind speed is constant. In [115] an adaptive control design for UAV path-following with slowly time-varying wind is presented. All these assumptions are not realistic, because wind speed is not constant in practice, and it can change quickly.

1.2.2 Fault-Tolerant Control

Fault-tolerant control is defined as a control system that possess the ability to accommodate failures automatically [114]. Fault-tolerant control systems

1 Introduction

are classified as either passive or active. Passive fault-tolerant control is based on robust control [35, 110] while assuming the worst case conditions. As a consequence, the designed controllers turn to be conservative from performance viewpoint [55]. Active fault-tolerant controllers are composed of a fault detection scheme, and a supervision module. On the basis of the information of the former, the supervision module may decide how to reconfigure the controller [32, 34]. However, applying such advanced control systems for small UAVs is difficult, because of their limited computing resources.

A compromise between the two approaches is adaptive control, which is based on the reconfiguration of the controller parameters without involving a fault detection module. Adaptive fault-tolerant control is built on the design of a desired model of the plant [13, 104]. However, after the occurrence of a fault, it is not possible, in practice, to recover the nominal system performance, particularly for non-redundant systems such as small UAVs. Maintaining the optimal performance may lead to an overload of the actuators, and possibly to hard failures that may cause loss of integrity of the system.

A solution to this problem was presented in [56, 113] based on performance degradation of the nominal controller. The method considers the combination of the model following control with a fault detection scheme. The design is made under the assumption that the model of the plant has no uncertainties, which is not realistic, especially for post-fault systems. Furthermore, only actuator faults are addressed while structural faults are not considered.

1.3 Research Objective and \mathcal{L}_1 Adaptive Control

The objective of this thesis is to make a contribution to the adaptive guidance and control of small fixed-wing UAVs in the presence of faults and/or atmospheric disturbances.

The proposed approach is based on \mathcal{L}_1 adaptive control [49]. The benefit of \mathcal{L}_1 adaptive control is its capacity for fast and robust adaptation that leads to desired transient performance for both system signals, input and output. These characteristics make it suitable for systems with unknown dynamics and subject to possible faults and external disturbances, such as small UAVs.

\mathcal{L}_1 Adaptive Control

As shown in Fig. 1.2, the \mathcal{L}_1 adaptive controller consists of three components: the state predictor, the adaptive law with fast adaptation, and the control law with a low-pass filter. The state predictor is a designed dynamic system that contains a vector of adaptive parameters. The adaptive law is used to update adaptive parameters such that the error between the predicted state and the real state are small enough. The control law is designed to ensure that the output tracks any given references. Using this structure the \mathcal{L}_1 adaptive controller ensures robust tracking performance with fast adaptation.

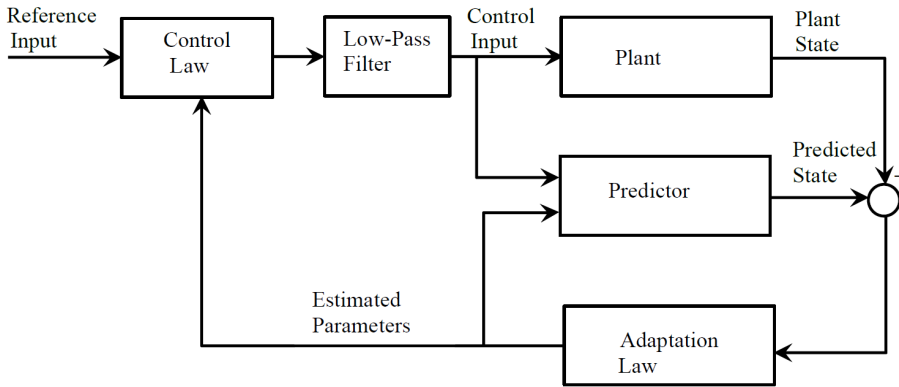


Figure 1.2: General architecture of \mathcal{L}_1 adaptive control.

\mathcal{L}_1 Adaptive Flight Control Applications

The development of \mathcal{L}_1 adaptive control was motivated by the need to certify adaptive flight critical systems with a more affordable validation and verification process [50]. The \mathcal{L}_1 adaptive control has been applied for various flight control systems including subscale model of transport aircraft [3, 28, 43, 41, 42, 47, 67, 102], fixed-wing UAVs [10, 21, 57, 59, 91, 75, 107], rotorcraft UAVs [23, 39, 45, 54, 57, 58, 78, 116], tailless unstable aircraft [81], variable-stability learjet [2], hypersonic glider [7, 25], missiles [19, 37, 68, 95], aerial refueling [108] and cooperative control of multiple UAVs [109]. Furthermore, \mathcal{L}_1 adaptive control was successfully tested in flight for the benchmark problems of the wing rock phenomenon [20, 22] and the Rohr's counter example [29].

1 Introduction

It should be noted that \mathcal{L}_1 adaptive control was not used previously for the design of the guidance system. In [101] it is stated that in [59, 60] \mathcal{L}_1 adaptive control is applied to the path-following of a fixed-wing UAV, while in fact, the \mathcal{L}_1 adaptive controller augments the low-level controller in the presence of uncertainties and external disturbances.

Limitations of \mathcal{L}_1 Adaptive Control

A limitation of \mathcal{L}_1 adaptive control is that it is formulated under the assumption that the bounds of external disturbances, such as wind, are known. However, these bounds are hard to quantify in practice. Therefore, if an external disturbance goes beyond its supposed bound this will result in poor performance of the controller. For this reason, applying \mathcal{L}_1 adaptive control to the path-following of small UAVs in wind requires to solve this issue.

Another problem is that despite good performances of \mathcal{L}_1 adaptive control, it is still true that when the uncertainties induced by disturbances, faults or failures are too large, they may make the system unstable. In fact, if the uncertainties caused by a fault become larger than the system design, the \mathcal{L}_1 norm stability condition [49] will not be satisfied. This motivates the development of a multiple model \mathcal{L}_1 adaptive control, in order to increase the robustness of the system in the presence of faults and/or large disturbances.

Furthermore, in practical applications, such as control of low-cost UAVs, the entire states of the plant are not accessible for measurement. This makes necessary the use of output feedback methods for \mathcal{L}_1 adaptive control. Relatively few approaches are described for output feedback \mathcal{L}_1 adaptive control [61]. The approach in [18] is limited to first order systems. In [19] an architecture based on a piecewise constant adaptation law is presented. Its main drawback is that the stability condition is not easy to verify [62]. This is why it is necessary to design output-feedback approaches that take into account this property of small fixed wing UAVs.

1.4 Thesis Contributions

The engineering contributions of this dissertation, in the field of flight control, are:

- **Developing and flight testing of an adaptive path-following controller that is robust against wind.** This approach relaxes what is commonly assumed that wind speed is constant. The controller

was demonstrated in flight under wind gusts, with speed up to 10 m/s , representing 50% of the desired airspeed of the UAV.

- **Designing and flight demonstration of an adaptive reconfigurable controller that considers explicitly the degradation of the UAV through severe faults.** The approach is based on a multiple model \mathcal{L}_1 adaptive control with a nominal model and a degraded model. The multiple model based controller was able to maintain the UAV in flight under hard failures, while the controller with one model has failed.

The following contributions to \mathcal{L}_1 adaptive control theory were completed in the context of the dissertation:

- **Developing an approach for \mathcal{L}_1 adaptive control that uses the sliding surface structure.** This method addresses the control of systems with disturbances of unknown bounds such as wind.
- **Conceiving a multiple model \mathcal{L}_1 adaptive controller.** It is shown that the system is stable and presents quantifiable performance bounds both for the system output and the control signal.
- **Designing and flight testing an approach for output feedback \mathcal{L}_1 adaptive control that maintains a flight mechanical formulation of the state space representation.** The controller was tested in a real flight, for the pitch rate control of a small fixed-wing UAV, and has proved its robustness against uncertainties and elevator loss of effectiveness.

Chapter 2

2 \mathcal{L}_1 Adaptive Control of Systems with Disturbances of Unknown Bounds

2.1	\mathcal{L}_1 Adaptive Controller for SISO Systems	10
2.1.1	Controller Design	11
2.1.2	Controller Analysis	13
2.2	\mathcal{L}_1 Adaptive Controller for MIMO Systems	20
2.2.1	Controller Design	21
2.2.2	Controller Analysis	22
2.3	Summary.	29

As is stated in the introduction, a drawback of \mathcal{L}_1 adaptive control is that it is formulated under the assumption that the bounds of external disturbances are known. However, this is not always the case in practice. Therefore, if an external disturbance goes beyond its supposed bound this will result in conservative performance of the control system. Resolving this issue requires a method for estimating the bounds of the perturbations.

In this chapter, based on [96], is presented an \mathcal{L}_1 adaptive control approach that borrows insights from the sliding mode control to design the adaptive laws. The main advantage is that the estimation of both the disturbances and their bounds is achieved by using a sliding surface. As a consequence, the performance and the robustness of the control system are improved without assuming prior information about external perturbations. In addition,

combining the state predictor and the low-pass filter of the input command contributes to eliminate the high frequency oscillations that cause chattering, and ensures continuity of the control signal.

Adaptive control has been used with sliding mode control to estimate the unknown upper bounds of disturbances and achieve global asymptotic stability [38, 51, 83, 87, 111]. The drawback of these approaches is that there is no systematic way to quantify the transient performance. Moreover, fast adaptation may lead to poor robustness characteristics [53]. An \mathcal{L}_1 adaptive controller with sliding mode based adaptive law was presented in [71]. This method was designed for a relatively restrictive class of systems, that is with matched disturbances and no uncertainties in the input gain.

The objectives of this chapter are the following:

- Improving the robustness of \mathcal{L}_1 adaptive control systems in the presence of matched and unmatched disturbances with unknown bounds by using the sliding surface structure from sliding mode control.
- Proving stability and achieving quantifiable performance bounds both for the system output and the control signal.
- Extending the obtained results for SISO systems to MIMO systems.

2.1 \mathcal{L}_1 Adaptive Controller for SISO Systems

Given a class of Single-Input Single-Output systems defined by

$$\begin{aligned} \dot{x}(t) &= A_m x(t) + b(\omega u(t) + \theta^\top x(t) + \eta_m(t)) + \eta_u(t, x), \\ y(t) &= c^\top x(t), \quad x(0) = x_0. \end{aligned} \tag{2.1}$$

where $A_m \in \mathbb{R}^{n \times n}$ is a known Hurwitz matrix that defines the desired dynamics of the system; $b, c \in \mathbb{R}^n$ are known constant vectors; $x(t) \in \mathbb{R}^n$ is the state vector which is assumed available through measurement; $u(t) \in \mathbb{R}$ is the control input; $y(t) \in \mathbb{R}$ is the system output; $\omega \in \mathbb{R}$ is an unknown constant with known sign representing the model input uncertainties; $\theta \in \mathbb{R}^n$ is a vector of constant unknown parameters representing model uncertainties; $\eta_m(t) \in \mathbb{R}$ is an unknown matched disturbance; and $\eta_u(t, x) \in \mathbb{R}^n$ is an unknown unmatched disturbance.

Assumption 2.1 The pair (A_m, b) is controllable.

Assumption 2.2 The non-linear functions $\eta_m(t)$ and $\eta_u(t, x)$ are uniformly bounded, i.e., there exist unknown real constants $L_m > 0$ and $L_u > 0$, such that for all $t \geq 0$ the following bounds hold:

$$|\eta_m(t)| \leq L_m \text{ and } \|\eta_u(t, x)\| \leq L_u.$$

Assumption 2.3 The unknown model parameters are bounded, i.e., $\theta \in \Theta$, where Θ is a known compact convex set and $0 < \omega_l \leq \omega \leq \omega_u$.

The objective is to design a state-feedback controller to ensure that the output of the system tracks a given piecewise continuous bounded reference signal $r(t)$.

2.1.1 Controller Design

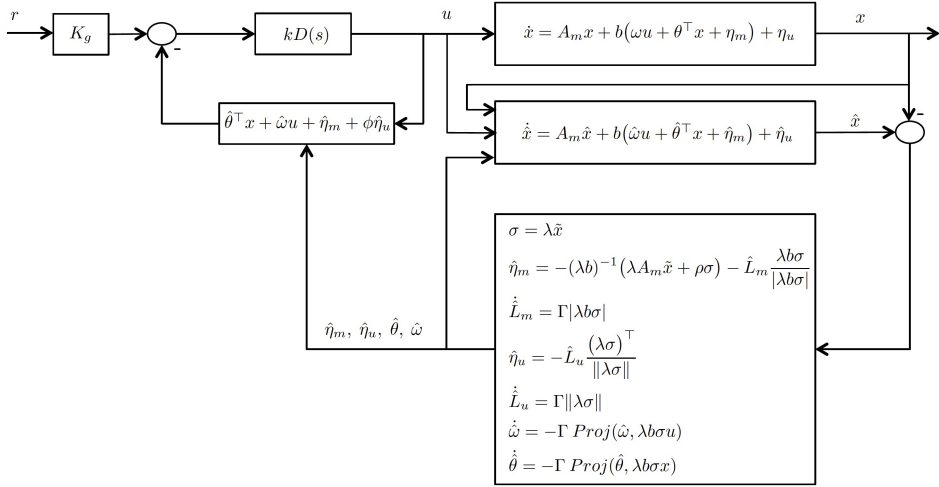


Figure 2.1: Block diagram of the \mathcal{L}_1 adaptive controller.

We consider the architecture of the \mathcal{L}_1 adaptive controller which is composed of the state predictor, the adaptation law and the control law.

The state predictor is defined as

$$\begin{aligned} \dot{\hat{x}}(t) &= A_m \hat{x}(t) + b(\hat{\omega}(t)u(t) + \hat{\theta}^\top(t)x(t) + \hat{\eta}_m(t)) + \hat{\eta}_u(t), \\ \hat{y}(t) &= c^\top \hat{x}(t), \quad \hat{x}(0) = x_0, \end{aligned} \quad (2.2)$$

where $\hat{x}(t)$ is the predicted state and, $\hat{\theta}(t)$, $\hat{\omega}(t)$, $\hat{\eta}_m(t)$, and $\hat{\eta}_u(t)$ are the estimates of the unknown system parameters and external disturbances.

2 \mathcal{L}_1 Adaptive Controller for Disturbances with Unknown Bounds

The sliding surface is defined as

$$\sigma(t) = \lambda \tilde{x}(t), \quad (2.3)$$

where $\tilde{x}(t) = \hat{x}(t) - x(t)$ is the state estimation error and $\lambda \in \mathbb{R}^{1 \times n}$ is a constant row vector, chosen such that $\lambda b \neq 0$ and the coefficients $\lambda_i : i = 1..n$ form a stable manifold.

The estimation of the matched disturbance $\eta_m(t)$ is defined by

$$\hat{\eta}_m(t) = -(\lambda b)^{-1}(\lambda A_m \tilde{x}(t) + \rho \sigma(t)) - \hat{L}_m(t) \frac{\lambda b \sigma(t)}{|\lambda b \sigma(t)|}, \quad (2.4)$$

where $\rho > 0$ is arbitrary, and the estimated bound $\hat{L}_m(t)$ is given by

$$\dot{\hat{L}}_m(t) = \Gamma |\lambda b \sigma(t)|, \quad L_{m0} = \hat{L}_m(0), \quad (2.5)$$

where $\Gamma \in \mathbb{R}^+$ is the adaptation rate.

The estimation of the unmatched disturbance $\eta_u(t, x)$ is defined by

$$\hat{\eta}_u(t) = -\hat{L}_u(t) \frac{(\lambda \sigma(t))^\top}{\|\lambda \sigma(t)\|}, \quad (2.6)$$

where the estimated bound $\hat{L}_u(t)$ is computed by

$$\dot{\hat{L}}_u(t) = \Gamma \|\lambda \sigma(t)\|, \quad L_{u0} = \hat{L}_u(0). \quad (2.7)$$

The unknown parameters ω and θ are estimated by

$$\begin{aligned} \dot{\hat{\omega}}(t) &= -\Gamma \text{Proj}(\hat{\omega}(t), \lambda b \sigma(t) u(t)), \\ \dot{\hat{\theta}}(t) &= -\Gamma \text{Proj}(\hat{\theta}(t), \lambda b \sigma(t) x(t)), \end{aligned} \quad (2.8)$$

where the projection-type adaptive law permits to maintain the unknown parameters within their predefined sets [86].

The control law is given by

$$u(s) = kD(s) \left(K_g r(s) - \hat{v}(s) - \phi(s) \hat{\eta}_u(s) \right), \quad (2.9)$$

where $k > 0$ is arbitrary, $D(s)$ is a transfer function that leads to a strictly proper stable filter $C(s) = \omega k D(s) / (1 + \omega k D(s))$ with $C(0) = 1$; the static gain is chosen as $K_g = -1 / (c^\top A_m^{-1} b)$; $\hat{v}(s)$ is the Laplace transformation of

$\hat{v}(t) = \hat{\theta}^\top(t)x(t) + \hat{\omega}(t)u(t) + \hat{\eta}_m(t)$; $\phi(s) = c^\top(sI - A_m)^{-1}H_m^{-1}(s)$; $H_m(s) = c^\top(s\mathbb{I} - A_m)^{-1}b$; and $\hat{\eta}_u(s)$ is the Laplace transformation of $\hat{\eta}_u(t)$.

Remark 2.1 It is straightforward to note that the adaptation laws of the external disturbances in equations (2.4) and (2.6) use the estimated bounds from equations (2.5) and (2.7). This relaxes the assumption that the bounds of the external disturbances are known, which is required in \mathcal{L}_1 adaptive control based on projection-type adaptive laws [17].

2.1.2 Controller Analysis

Let

$$L = \max_{\theta \in \Theta} \|\theta\|_1, \quad H(s) = (s\mathbb{I} - A_m)^{-1}b, \quad G(s) = H(s)(1 - C(s)). \quad (2.10)$$

The \mathcal{L}_1 adaptive controller defined via equations (2.2) to (2.9) is subject to the \mathcal{L}_1 norm condition:

$$\|G(s)\|_{\mathcal{L}_1} L < 1, \quad (2.11)$$

where $\|\cdot\|_{\mathcal{L}_1}$ denotes for the \mathcal{L}_1 norm (Appendix A2).

Moreover, the design of $C(s)$ needs to ensure that

$$G_u(s) = (s\mathbb{I} - A_m)^{-1} - C(s)H(s)\phi(s), \quad (2.12)$$

is proper and stable. Furthermore, since the transfer matrix $G_u(s)$ is proper and stable it has a \mathcal{L}_1 norm [49].

Closed-Loop Reference System

The reference system, i.e. the closed-loop system with nominal parameters, in this case is the same as in all \mathcal{L}_1 adaptive control architectures. It is defined by

$$\begin{aligned} \dot{x}_r(t) &= A_m x_r(t) + b(\omega u_r(t) + \theta^\top x_r(t) + \eta_m(t)) + \eta_u(t, x_r), \\ y_r(t) &= c^\top x_r(t), \quad x_r(0) = x_0. \end{aligned} \quad (2.13)$$

The reference control law is given by

$$u_r(s) = \frac{C(s)}{\omega} \left(K_g r(s) - \theta^\top x_r(s) - \eta_m(s) - \phi(s)\eta_u(s) \right). \quad (2.14)$$

Lemma 2.1 If the filter $C(s)$ is designed such that it verifies the \mathcal{L}_1 norm condition in (2.11) and the requirement in (2.12), then the closed-loop reference system in (2.13) and (2.14) is Bounded-Input Bounded-State (BIBS) stable with respect to the reference input and initial conditions.

Proof. The closed-loop reference system (2.13) and (2.14) can be written

$$\begin{aligned} x_r(s) = & H(s)C(s)K_g r(s) + G(s)\theta^\top x_r(s) \\ & + G(s)\eta_m(s) + G_u(s)\eta_u(s) + x_{in}(s), \end{aligned} \quad (2.15)$$

where $x_{in}(s) = (s\mathbb{I} - A_m)^{-1}x_0$.

Then, for all $t \in [0, \tau]$ we have

$$\begin{aligned} \|x_{r_\tau}\|_{\mathcal{L}_\infty} \leq & \|C(s)H(s)\|_{\mathcal{L}_1} K_g \|r_\tau\|_{\mathcal{L}_\infty} + \|G(s)\|_{\mathcal{L}_1} L \|x_{r_\tau}\|_{\mathcal{L}_\infty} \\ & + \|G(s)\|_{\mathcal{L}_1} \|\eta_{m_\tau}\|_{\mathcal{L}_\infty} + \|G_u(s)\|_{\mathcal{L}_1} \|\eta_{u_\tau}\|_{\mathcal{L}_\infty} + \|x_{in_\tau}\|_{\mathcal{L}_\infty}, \end{aligned} \quad (2.16)$$

where $\|\cdot\|_{\mathcal{L}_\infty}$ denotes for the \mathcal{L}_∞ norm and $\|(\cdot)_\tau\|_{\mathcal{L}_\infty}$ denotes for the truncated \mathcal{L}_∞ norm at the time instant τ (Appendix A2).

Substituting the upper bounds of η_m and η_u and solving for $\|x_{r_\tau}\|_{\mathcal{L}_\infty}$ in the equation above to obtain the following bound

$$\begin{aligned} \|x_{r_\tau}\|_{\mathcal{L}_\infty} \leq & \frac{\|C(s)H(s)\|_{\mathcal{L}_1} K_g \|r_\tau\|_{\mathcal{L}_\infty} + \|G(s)\|_{\mathcal{L}_1} L_m}{1 - \|G(s)\|_{\mathcal{L}_1} L} \\ & + \frac{\|G_u(s)\|_{\mathcal{L}_1} L_u + \|x_{in}\|_{\mathcal{L}_\infty}}{1 - \|G(s)\|_{\mathcal{L}_1} L}. \end{aligned} \quad (2.17)$$

If the \mathcal{L}_1 norm condition in (2.11) is verified then $\|x_{r_\tau}\|_{\mathcal{L}_\infty}$ is uniformly bounded for all $\tau > 0$, and the proof is complete. \square

Transient and Steady-State Performance

In the following, it is stated that the prediction error $\tilde{x}(t)$, and the estimation errors of the disturbances, their bounds and the unknown parameters are uniformly bounded.

Lemma 2.2 The following bound holds for the norm of the prediction error:

$$\|\tilde{x}\|_{\mathcal{L}_\infty} \leq \delta, \quad (2.18)$$

where $\delta > 0$ is arbitrary small.

Furthermore, if the closed-loop system is stable then the prediction error $\tilde{x}(t)$ converges to zero, i.e.,

$$\lim_{t \rightarrow \infty} \tilde{x}(t) = 0. \quad (2.19)$$

Proof. In this section, the dependence of the parameters on (t) is dropped unless it is not clear from the context.

From (2.1) and (2.2), the prediction error dynamics can be written

$$\dot{\tilde{x}} = A_m \tilde{x} + b(\tilde{\omega}u + \tilde{\theta}^\top x + \tilde{\eta}_m) + \tilde{\eta}_u, \quad (2.20)$$

where $\tilde{\theta} = \hat{\theta} - \theta$, $\tilde{\omega} = \hat{\omega} - \omega$, $\tilde{\eta}_m = \hat{\eta}_m - \eta_m$ and $\tilde{\eta}_u = \hat{\eta}_u - \eta_u$. We define also $\tilde{L}_m = \hat{L}_m - L_m$ and $\tilde{L}_u = \hat{L}_u - L_u$.

Consider the Lyapunov function candidate

$$V = \frac{1}{2}\sigma^2 + \frac{1}{2}\Gamma^{-1}(\tilde{\theta}^\top \tilde{\theta} + \tilde{\omega}^2 + \tilde{L}_m^2 + \tilde{L}_u^2). \quad (2.21)$$

Its derivative is given by

$$\dot{V} = \sigma \dot{\sigma} + \Gamma^{-1}(\tilde{\theta}^\top \dot{\tilde{\theta}} + \tilde{\omega} \dot{\tilde{\omega}} + \tilde{L}_m \dot{\tilde{L}}_m + \tilde{L}_u \dot{\tilde{L}}_u). \quad (2.22)$$

From (2.3) and (2.20) the derivative of the sliding surface can be written

$$\dot{\sigma} = \lambda A_m \tilde{x} + \lambda b(\tilde{\theta}^\top x + \tilde{\omega}u + \tilde{\eta}_m) + \lambda \tilde{\eta}_u. \quad (2.23)$$

Replacing in (2.22), it follows that

$$\begin{aligned} \dot{V} = & \sigma \left(\lambda A_m \tilde{x} + \lambda b(\tilde{\theta}^\top x + \tilde{\omega}u + (\hat{\eta}_m - \eta_m)) + \lambda(\hat{\eta}_u - \eta_u) \right) \\ & + \Gamma^{-1}(\tilde{\theta}^\top \dot{\tilde{\theta}} + \tilde{\omega} \dot{\tilde{\omega}} + \tilde{L}_m \dot{\tilde{L}}_m + \tilde{L}_u \dot{\tilde{L}}_u). \end{aligned} \quad (2.24)$$

Given $\hat{\eta}_m$ and $\hat{\eta}_u$ from (2.4) and (2.6); and $\hat{\theta}$ and $\hat{\omega}$ from (2.8), it can be written

$$\begin{aligned} \dot{V} = & -\rho\sigma^2 - \lambda b\sigma\eta_m - \lambda\sigma\eta_u \\ & - |\lambda b\sigma| \hat{L}_m - \|\lambda\sigma\| \hat{L}_u + \Gamma^{-1}(\tilde{L}_m \dot{\tilde{L}}_m + \tilde{L}_u \dot{\tilde{L}}_u). \end{aligned} \quad (2.25)$$

Hence, the following upper bound can be derived

$$\begin{aligned} \dot{V} \leq & -\rho\sigma^2 + |\lambda b\sigma| \|\eta_m\| + \|\lambda\sigma\| \|\eta_u\| \\ & - |\lambda b\sigma| \hat{L}_m - \|\lambda\sigma\| \hat{L}_u + \Gamma^{-1}(\tilde{L}_m \dot{\tilde{L}}_m + \tilde{L}_u \dot{\tilde{L}}_u). \end{aligned} \quad (2.26)$$

Using assumption 2.2, it can be written

$$\dot{V} \leq -\rho\sigma^2 - |\lambda b\sigma|\tilde{L}_m - \|\lambda\sigma\|\tilde{L}_u + \Gamma^{-1}(\tilde{L}_m\dot{\tilde{L}}_m + \tilde{L}_u\dot{\tilde{L}}_u). \quad (2.27)$$

Considering the adaptation laws from (2.5) and (2.7), it follows that

$$\dot{V}(t) \leq -\rho\sigma^2. \quad (2.28)$$

Therefore, the sliding surface σ , the estimation errors of the unknown parameters $\tilde{\theta}$ and $\tilde{\omega}$; and the disturbances bounds errors \tilde{L}_m and \tilde{L}_u are uniformly bounded. Consequently, the estimation errors of the external disturbances $\tilde{\eta}_m$ and $\tilde{\eta}_u$ are also uniformly bounded.

Given that on the sliding surface the trajectories are governed by $\sigma(\tilde{x}, t) = 0$, and since the coefficients of the sliding surface form a stable manifold and $\tilde{x}(0) = 0$, i.e., the system is initialized on the sliding surface, then there exists always an arbitrarily small real $\delta > 0$ verifying

$$\|\tilde{x}\|_{\mathcal{L}_\infty} \leq \delta. \quad (2.29)$$

This result comes from the fundamental propriety of sliding mode control, stipulating that if the system is on the sliding surface, it stays on the nearby sliding surface despite disturbances [105].

Moreover, from (2.28) it can be written

$$\int_0^t \sigma(t)^2 dt \leq \frac{1}{\rho} (V(0) - V(t)). \quad (2.30)$$

Since $V(0)$ is bounded and $V(t)$ is bounded and non-increasing, therefore

$$\lim_{t \rightarrow \infty} \int_0^t \sigma(t)^2 dt \quad (2.31)$$

is bounded.

If the closed-loop system is stable, i.e., $u(t)$ and $x(t)$ are bounded then $\dot{\sigma}(t)$ in equation (2.23) is bounded. By applying Barbal't's Lemma it follows that

$$\lim_{t \rightarrow \infty} \sigma^2(t) = 0 \text{ and } \lim_{t \rightarrow \infty} \sigma(t) = 0. \quad (2.32)$$

Consequently

$$\lim_{t \rightarrow \infty} \tilde{x}(t) = 0, \quad (2.33)$$

and the proof is complete. \square

Next, in the following theorem, the performance bounds of the \mathcal{L}_1 adaptive controller are shown.

Theorem 2.1 Given the system (2.1), the reference system (2.13), (2.14) and the \mathcal{L}_1 adaptive controller (2.2) to (2.9), we have

$$\|x_r - x\|_{\mathcal{L}_\infty} \leq \gamma_1, \quad (2.34)$$

$$\|u_r - u\|_{\mathcal{L}_\infty} \leq \gamma_2, \quad (2.35)$$

where

$$\gamma_1 = 2 \frac{\|G(s)\|_{\mathcal{L}_1}}{1 - \|G(s)\|_{\mathcal{L}_1} L} L_m + 2 \frac{\|G_u(s)\|_{\mathcal{L}_1}}{1 - \|G(s)\|_{\mathcal{L}_1} L} L_u + \frac{\|H(s)C(s)H_m^{-1}(s)c^\top\|_{\mathcal{L}_1} \delta}{1 - \|G(s)\|_{\mathcal{L}_1} L},$$

and

$$\gamma_2 = \left\| \frac{C(s)}{\omega} \right\|_{\mathcal{L}_1} (L\gamma_1 + 2(L_m + \|\phi(s)\|_{\mathcal{L}_1} L_u)) + \left\| \frac{C(s)}{\omega} H_m^{-1}(s)c^\top \right\|_{\mathcal{L}_1} \delta.$$

Proof. The control law in (2.9) can be written as

$$\begin{aligned} u(s) = & \frac{C(s)}{\omega} \left(K_g r(s) - \theta^\top x(s) - \eta_m(s) \right) \\ & - \frac{C(s)}{\omega} \left(\phi(s) (\eta_u(s) + \tilde{\eta}_u(s)) - \tilde{v}(s) \right), \end{aligned} \quad (2.36)$$

where $\tilde{v}(s)$ is the Laplace transformation of $\tilde{v}(t) = \tilde{\omega}u(t) + \tilde{\theta}^\top x(t) + \tilde{\eta}_m(t)$ and $\tilde{\eta}_u(s)$ is the Laplace transformation of $\tilde{\eta}_u(t)$.

Hence, the Laplace transformation of the closed loop system (2.1) and (2.36) can be written

$$\begin{aligned} x(s) = & H(s)C(s)K_g r(s) + G(s)\theta^\top x(s) + G(s)\eta_m(s) \\ & + G_u(s)\eta_u(s) - H(s)C(s)(\tilde{v}(s) + \phi(s)\tilde{\eta}_u(s)) + x_{in}(s). \end{aligned} \quad (2.37)$$

Taking the difference of (2.15) and (2.37) it follows that

$$\begin{aligned} x_r(s) - x(s) = & G(s)\theta^\top (x_r(s) - x(s)) \\ & - G(s)(\eta_m(s) - \eta_{mr}(s)) \\ & - G_u(s)(\eta_u(s) - \eta_{ur}(s)) \\ & + H(s)C(s)(\tilde{v}(s) + \phi(s)\tilde{\eta}_u(s)). \end{aligned} \quad (2.38)$$

2 \mathcal{L}_1 Adaptive Controller for Disturbances with Unknown Bounds

From (2.20) the Laplace transformation of the prediction error dynamics can be written

$$\tilde{x}(s) = H(s)\tilde{v}(s) + (sI - A_m)^{-1}\tilde{\eta}_u(s). \quad (2.39)$$

Multiplying both terms of (2.39) by $H_m^{-1}(s)c^\top$ one obtains

$$H_m^{-1}(s)c^\top \tilde{x}(s) = \tilde{v}(s) + \phi(s)\tilde{\eta}_u(s). \quad (2.40)$$

Substituting in (2.38) it follows that

$$\begin{aligned} x_r(s) - x(s) = & G(s)\theta^\top(x_r(s) - x(s)) - G(s)(\eta_m(s) - \eta_{mr}(s)) \\ & - G_u(s)(\eta_u(s) - \eta_{ur}(s)) + H(s)C(s)H_m^{-1}(s)c^\top \tilde{x}(s). \end{aligned} \quad (2.41)$$

Solving for $x_r(s) - x(s)$, the following bound holds for $t \in [0, \tau]$

$$\begin{aligned} \|(x_r - x)_\tau\|_{\mathcal{L}_\infty} \leq & \frac{\|G(s)\|_{\mathcal{L}_1}}{1 - \|G(s)\|_{\mathcal{L}_1}L} \|(\eta_{m\tau} - \eta_{mr})_\tau\|_{\mathcal{L}_\infty} \\ & + \frac{\|G_u(s)\|_{\mathcal{L}_1}}{1 - \|G(s)\|_{\mathcal{L}_1}L} \|(\eta_u - \eta_{ur})_\tau\|_{\mathcal{L}_\infty} \\ & + \frac{\|H(s)C(s)H_m^{-1}(s)c^\top\|_{\mathcal{L}_1}}{1 - \|G(s)\|_{\mathcal{L}_1}L} \|\tilde{x}_\tau\|_{\mathcal{L}_\infty}. \end{aligned} \quad (2.42)$$

Given the upper bound of $\tilde{x}(t)$ from Lemma 2.2, and the disturbance bounds from assumption 2.2, it follows that

$$\begin{aligned} \|(x_r - x)_\tau\|_{\mathcal{L}_\infty} \leq & 2 \frac{\|G(s)\|_{\mathcal{L}_1}}{1 - \|G(s)\|_{\mathcal{L}_1}L} L_m \\ & + 2 \frac{\|G_u(s)\|_{\mathcal{L}_1}}{1 - \|G(s)\|_{\mathcal{L}_1}L} L_u \\ & + \frac{\|H(s)C(s)H_m^{-1}(s)c^\top\|_{\mathcal{L}_1}}{1 - \|G(s)\|_{\mathcal{L}_1}L} \delta, \end{aligned} \quad (2.43)$$

which leads to the bound in (2.34).

To show the second bound in (2.35), by taking the difference of (2.14)

and (2.36), one can derive

$$\begin{aligned}
 u_r(s) - u(s) &= -\frac{C(s)}{\omega} \theta^\top \left((x_r(s) - x(s)) \right) \\
 &\quad + \frac{C(s)}{\omega} (\eta_m(s) - \eta_{mr}(s)) \\
 &\quad + \frac{C(s)}{\omega} \phi(s) (\eta_u(s) - \eta_{ur}(s)) \\
 &\quad + \frac{C(s)}{\omega} (\phi(s) \tilde{\eta}_u(s) + \tilde{v}(s)).
 \end{aligned} \tag{2.44}$$

Hence

$$\begin{aligned}
 u_r(s) - u(s) &= -\frac{C(s)}{\omega} \theta^\top \left((x_r(s) - x(s)) \right) \\
 &\quad + \frac{C(s)}{\omega} (\eta_m(s) - \eta_{mr}(s)) \\
 &\quad + \frac{C(s)}{\omega} \phi(s) (\eta_u(s) - \eta_{ur}(s)) \\
 &\quad + \frac{C(s)}{\omega} H_m^{-1}(s) c^\top \tilde{x}(s).
 \end{aligned} \tag{2.45}$$

Consequently, the following bound holds for $t \in [0, \tau]$

$$\begin{aligned}
 \|(u_r - u)_\tau\|_{\mathcal{L}_\infty} &\leq \left\| \frac{C(s)}{\omega} \right\|_{\mathcal{L}_1} L \|(x_r - x)_\tau\|_{\mathcal{L}_\infty} \\
 &\quad + 2 \left\| \frac{C(s)}{\omega} \right\|_{\mathcal{L}_1} (L_m + \|\phi(s)\|_{\mathcal{L}_1} L_u) \\
 &\quad + \left\| \frac{C(s)}{\omega} H_m^{-1}(s) c^\top \right\|_{\mathcal{L}_1} \|\tilde{x}_\tau\|_{\mathcal{L}_\infty},
 \end{aligned} \tag{2.46}$$

which holds uniformly for all $\tau \geq 0$, leading to the bound in (2.35). \square

Implementation Issues

In practical applications, the sliding surface $\sigma(t)$ does not go to zero due to sampled computation, noisy measurements or other uncertainties. This results in a persistent increase of the estimated bounds of (2.5) and (2.7), and may lead to bound over-estimation with negative effects [27, 85].

A solution to this problem is the dead-zone modification [84], which works by switching the estimator off when the absolute value of the sliding surface

gets below a certain threshold. Hence, equations (2.5) and (2.7) are modified to be:

$$\dot{\hat{L}}_m(t) = \begin{cases} \Gamma|\lambda b\sigma(t)| & \text{if } |\sigma(t)| > \epsilon_m, \\ 0 & \text{if not,} \end{cases} \quad (2.47)$$

and

$$\dot{\hat{L}}_m(t) = \begin{cases} \Gamma\|\lambda\sigma(t)\| & \text{if } |\sigma(t)| > \epsilon_u, \\ 0 & \text{if not} \end{cases} \quad (2.48)$$

where $\epsilon_m \in \mathbb{R}^+$ and $\epsilon_u \in \mathbb{R}^+$ are real constants.

In the following, the proposed approach is extended to the control of MIMO systems.

2.2 \mathcal{L}_1 Adaptive Controller for MIMO Systems

Given a class of MIMO systems defined by

$$\begin{aligned} \dot{x}(t) &= A_m x(t) + B(\omega u(t) + \theta^\top x(t) + \eta_m(t)) + \eta_u(t, x), \\ y(t) &= Cx(t), \quad x(0) = x_0, \end{aligned} \quad (2.49)$$

where $A_m \in \mathbb{R}$ is a known Hurwitz matrix that defines the desired dynamics of the system; $B^{n \times m}$, $C \in \mathbb{R}^{m \times n}$ are known constant matrices; $x(t) \in \mathbb{R}^n$ is the state vector which is assumed available through measurement; $u(t) \in \mathbb{R}^m$ is the control input vector; $y(t) \in \mathbb{R}^m$ is the output vector; $\omega \in \mathbb{R}^{m \times m}$ is an unknown constant matrix; $\theta^\top \in \mathbb{R}^{m \times n}$ is a matrix of constant unknown parameters representing model uncertainties; $\eta_m(t) \in \mathbb{R}^m$ is an unknown matched disturbance; and $\eta_u(t, x) \in \mathbb{R}^n$ is an unknown unmatched disturbance.

Assumption 2.4 The non-linear functions $\eta_m(t)$ and $\eta_u(t, x)$ are uniformly bounded, i.e., there exist unknown real constants $L_m > 0$ and $L_u > 0$, such that for all $t \geq 0$ the following bounds hold:

$$\|\eta_m(t)\| \leq L_m \text{ and } \|\eta_u(t, x)\| \leq L_u.$$

Assumption 2.5 The unknown model parameters are bounded, i.e., $\theta \in \Theta$, where Θ is a known compact convex set. The system input gain matrix ω is assumed to be an unknown (non-singular) strictly row-diagonally dominant matrix with $\text{sgn}(\omega_{ii})$ known. Also, it is assumed that there exists a known compact convex set Ω such that $\omega \in \Omega \subset \mathbb{R}^{m \times m}$.

2.2.1 Controller Design

The state predictor is defined as

$$\begin{aligned}\dot{\hat{x}}(t) &= A_m \hat{x}(t) + B(\hat{\omega}(t)u(t) + \hat{\theta}^\top(t)x(t) + \hat{\eta}_m(t)) + \hat{\eta}_u(t), \\ \hat{y}(t) &= C\hat{x}(t), \quad \hat{x}(0) = x_0,\end{aligned}\tag{2.50}$$

where $\hat{x}(t)$ is the predicted state and $\hat{\theta}(t)$, $\hat{\omega}(t)$, $\hat{\eta}_m(t)$, and $\hat{\eta}_u(t)$ are the estimates of the unknown system parameters and disturbances.

The sliding surface is defined as

$$\sigma(t) = \lambda \tilde{x}(t),\tag{2.51}$$

where $\tilde{x}(t) = \hat{x}(t) - x(t)$ is the state estimation error and $\lambda \in \mathbb{R}^{m \times n}$ is a constant arbitrary matrix, chosen such that λB is non-singular and the coefficients $\lambda(i, j) : i = 1..n; j = 1..m$ form a stable hyperplane.

The estimation of the matched disturbance $\eta_m(t)$ is defined by

$$\hat{\eta}_m(t) = -(\lambda B)^{-1}(\lambda A_m \tilde{x}(t) + \rho \sigma(t)) - \hat{L}_m(t) \frac{B^\top \lambda^\top \sigma(t)}{\|B^\top \lambda^\top \sigma(t)\|},\tag{2.52}$$

where $\rho > 0$ is arbitrary and the estimated bound $\hat{L}_m(t)$ is given by

$$\dot{\hat{L}}_m(t) = \Gamma \|\sigma^\top(t) \lambda B\|, \quad L_{m0} = \hat{L}_m(0),\tag{2.53}$$

where $\Gamma \in \mathbb{R}^+$ is the adaptation rate.

The estimation of the unmatched disturbance $\eta_u(t, x)$ is defined by

$$\hat{\eta}_u(t) = -\hat{L}_u(t) \frac{\lambda^\top \sigma(t)}{\|\lambda^\top \sigma(t)\|},\tag{2.54}$$

where the estimated bound $\hat{L}_u(t)$ is computed by

$$\dot{\hat{L}}_u(t) = \Gamma \|\sigma^\top(t) \lambda\|, \quad L_{u0} = \hat{L}_u(0).\tag{2.55}$$

The input gain matrix ω and unknown parameters matrix θ are estimated by

$$\begin{aligned}\dot{\hat{\omega}}(t) &= -\Gamma \text{Proj}(\hat{\omega}(t), u(t) \sigma^\top(t) \lambda B)^\top, \\ \dot{\hat{\theta}}(t) &= -\Gamma \text{Proj}(\hat{\theta}(t), x(t) \sigma^\top(t) \lambda B).\end{aligned}\tag{2.56}$$

The control law is given by

$$u(s) = K D(s) \left(K_g r(s) - \hat{\nu}_1(s) - \hat{\nu}_2(s) \right), \quad (2.57)$$

where $D(s)$ is an $m \times m$ strictly proper transfer matrix; $K \in \mathbb{R}^{m \times m}$; $K_g = -(CA_m^{-1}B)^{-1}$ is the pre-filter of the MIMO control law; $\hat{\nu}_1(s)$ is the Laplace transformation of $\hat{\nu}_1(t) = \hat{\theta}^\top(t)x(t) + \hat{\omega}(t)u(t) + \hat{\eta}_m(t)$; $H_m(s) = C(s\mathbb{I} - A_m)^{-1}B$; $H_0(s) = C(s\mathbb{I} - A_m)^{-1}$; and $\hat{\nu}_2 = H_m^{-1}(s)H_0(s)\hat{\eta}_u(s)$.

The design of $D(s)$ and K should lead to a strictly proper and stable filter transfer matrix

$$C(s) = \omega K D(s) (\mathbb{I} + \omega K D(s))^{-1},$$

with DC gain $C(0) = \mathbb{I}$.

2.2.2 Controller Analysis

Let

$$L = \max_{\theta \in \Theta} \|\theta\|_1, \quad H(s) = (s\mathbb{I} - A_m)^{-1}B, \quad G(s) = H(s)(\mathbb{I} - C(s)). \quad (2.58)$$

The \mathcal{L}_1 adaptive controller defined via equations (2.50)-(2.57) is subject to the following \mathcal{L}_1 norm condition:

$$\|G(s)\|_{\mathcal{L}_1} L < 1. \quad (2.59)$$

Moreover, the design of $C(s)$ needs to ensure that the transfer matrix

$$G_u(s) = (s\mathbb{I} - A_m)^{-1} - H(s)C(s)H_m^{-1}(s)H_0(s), \quad (2.60)$$

is a proper and stable.

Closed-Loop Reference System

The reference system, i.e. the closed-loop system with nominal parameters, is defined by

$$\begin{aligned} \dot{x}_r(t) &= A_m x_r(t) + B(\omega u_r(t) + \theta^\top x_r(t) + \eta_m(t)) + \eta_u(t, x), \\ y_r(t) &= C x_r(t), \quad x_r(0) = x_0. \end{aligned} \quad (2.61)$$

2.2 \mathcal{L}_1 Adaptive Controller for MIMO Systems

The reference control law is given by

$$u_r(s) = \omega^{-1}C(s)\left(K_g r(s) - \nu_{1r}(s) - \nu_{2r}(s)\right), \quad (2.62)$$

where $\nu_{1r}(s)$ is the Laplace transformation of $\nu_{1r}(t) = \theta^\top x_r(t) + \eta_m(t)$ and $\nu_{2r} = H_m^{-1}(s)H_0(s)\eta_u(s)$.

Lemma 2.3 If the filter $C(s)$ is designed such that it verifies the \mathcal{L}_1 norm condition in equation (2.59) and the requirement in (2.60), then the closed-loop reference system in equations (2.61) and (2.62) is BIBS stable with respect to the reference input and initial conditions.

Proof. The closed-loop reference system (2.61) and (2.62) can be written

$$\begin{aligned} x_r(s) = & H(s)C(s)K_g r(s) + G(s)\theta^\top x_r(s) \\ & + G(s)\eta_m(s) + G_u(s)\eta_u(s) + x_{in}(s), \end{aligned} \quad (2.63)$$

where $x_{in}(s) = (s\mathbb{I} - A_m)^{-1}x_0$.

Then, for all $t \in [0, \tau]$ we have

$$\begin{aligned} \|x_{r\tau}\|_{\mathcal{L}_\infty} \leq & \|H(s)C(s)\|_{\mathcal{L}_1}K_g\|r_\tau\|_{\mathcal{L}_\infty} + \|G(s)\|_{\mathcal{L}_1}L\|x_{r\tau}\|_{\mathcal{L}_\infty} \\ & + \|G(s)\|_{\mathcal{L}_1}\|\eta_{m\tau}\|_{\mathcal{L}_\infty} + \|G_u(s)\|_{\mathcal{L}_1}\|\eta_{u\tau}\|_{\mathcal{L}_\infty} + \|x_{in\tau}\|_{\mathcal{L}_\infty} \end{aligned} \quad (2.64)$$

Substituting the upper bounds of η_m and η_u and solving for $\|x_{r\tau}\|_{\mathcal{L}_\infty}$ in the equation above to obtain the following bound

$$\begin{aligned} \|x_{r\tau}\|_{\mathcal{L}_\infty} \leq & \frac{\|H(s)C(s)\|_{\mathcal{L}_1}K_g\|r_\tau\|_{\mathcal{L}_\infty} + \|G(s)\|_{\mathcal{L}_1}Lm}{1 - \|G(s)\|_{\mathcal{L}_1}L} \\ & + \frac{\|G_u(s)\|_{\mathcal{L}_1}L_u + \|x_{in}\|_{\mathcal{L}_\infty}}{1 - \|G(s)\|_{\mathcal{L}_1}L}. \end{aligned} \quad (2.65)$$

If the \mathcal{L}_1 norm condition in (2.59) is verified then $\|x_{r\tau}\|_{\mathcal{L}_\infty}$ is uniformly bounded for all $\tau > 0$, and the proof is complete. \square

Transient and Steady-State Performance

In the following, it is stated that the prediction error $\tilde{x}(t)$, and the estimation errors of the disturbances, their bounds and the unknown parameters are uniformly bounded.

Lemma 2.4 The following bound holds for the norm of the prediction error

$$\|\tilde{x}\|_{\mathcal{L}_\infty} \leq \delta, \quad (2.66)$$

where $\delta > 0$ is arbitrary small.

Furthermore, if the closed-loop system is stable then the prediction error $\tilde{x}(t)$ converges to zero, i.e.,

$$\lim_{t \rightarrow \infty} \tilde{x}(t) = 0. \quad (2.67)$$

Proof. In this section, the dependence of the parameters on (t) is dropped unless it is not clear from the context.

From (2.49) and (2.50), the prediction error dynamics can be written

$$\dot{\tilde{x}} = A_m \tilde{x} + B(\tilde{\omega}u + \tilde{\theta}^\top x + \tilde{\eta}_m) + \tilde{\eta}_u. \quad (2.68)$$

Consider the Lyapunov function candidate

$$V = \frac{1}{2} \sigma^\top \sigma + \frac{1}{2} \Gamma^{-1} \left(\text{tr}(\tilde{\theta}^\top \tilde{\theta}) + \text{tr}(\tilde{\omega}^\top \tilde{\omega}) + \tilde{L}_m^2 + \tilde{L}_u^2 \right). \quad (2.69)$$

It's derivative is given by

$$\dot{V} = \sigma^\top \dot{\sigma} + \Gamma^{-1} \left(\text{tr}(\tilde{\theta}^\top \dot{\tilde{\theta}}) + \text{tr}(\tilde{\omega}^\top \dot{\tilde{\omega}}) + \tilde{L}_m \dot{\tilde{L}}_m + \tilde{L}_u \dot{\tilde{L}}_u \right). \quad (2.70)$$

From (2.51) and (2.68) the derivative of the sliding surface can be written

$$\dot{\sigma} = \lambda A_m \tilde{x} + \lambda B(\tilde{\theta}^\top x + \tilde{\omega}u + \tilde{\eta}_m) + \lambda \tilde{\eta}_u. \quad (2.71)$$

Replacing in (2.70), it follows that

$$\begin{aligned} \dot{V} = & \sigma^\top \left(\lambda A_m \tilde{x} + \lambda B(\tilde{\theta}^\top x + \tilde{\omega}u + (\hat{\eta}_m - \eta_m)) + \lambda(\hat{\eta}_u - \eta_u) \right) \\ & + \Gamma^{-1} \left(\text{tr}(\tilde{\theta}^\top \dot{\tilde{\theta}}) + \text{tr}(\tilde{\omega}^\top \dot{\tilde{\omega}}) + \tilde{L}_m \dot{\tilde{L}}_m + \tilde{L}_u \dot{\tilde{L}}_u \right). \end{aligned} \quad (2.72)$$

Given the fact that for any scalar s , $\text{tr}(s) = s$, hence

$$\begin{aligned} \dot{V} = & \sigma^\top \lambda A_m \tilde{x} + \text{tr}(\sigma^\top \lambda B \tilde{\theta}^\top x) + \text{tr}(\sigma^\top \lambda B \tilde{\omega}u) \\ & + \sigma^\top \lambda B(\hat{\eta}_m - \eta_m) + \sigma^\top \lambda(\hat{\eta}_u - \eta_u) \\ & + \Gamma^{-1} \left(\text{tr}(\tilde{\theta}^\top \dot{\tilde{\theta}}) + \text{tr}(\tilde{\omega}^\top \dot{\tilde{\omega}}) + \tilde{L}_m \dot{\tilde{L}}_m + \tilde{L}_u \dot{\tilde{L}}_u \right). \end{aligned} \quad (2.73)$$

Using the property $\text{tr}(M1 M2) = \text{tr}(M2 M1)$ for any matrices $M1, M2$, we obtain

$$\begin{aligned} \dot{V} = & \sigma^\top \lambda A_m \tilde{x} + \text{tr}(\tilde{\theta}^\top x \sigma^\top \lambda B) + \text{tr}(\tilde{\omega}u \sigma^\top \lambda B) \\ & + \sigma^\top \lambda B(\hat{\eta}_m - \eta_m) + \sigma^\top \lambda(\hat{\eta}_u - \eta_u) \\ & + \Gamma^{-1} \left(\text{tr}(\tilde{\theta}^\top \dot{\tilde{\theta}}) + \text{tr}(\tilde{\omega}^\top \dot{\tilde{\omega}}) + \tilde{L}_m \dot{\tilde{L}}_m + \tilde{L}_u \dot{\tilde{L}}_u \right). \end{aligned} \quad (2.74)$$

2.2 \mathcal{L}_1 Adaptive Controller for MIMO Systems

Given $\hat{\eta}_m$ and $\hat{\eta}_u$ from (2.52) and (2.54) and the adaptation law (2.56) it can be written

$$\begin{aligned} \dot{V} = & -\rho\sigma^\top\sigma - \sigma^\top\lambda B\eta_m - \sigma^\top\lambda\eta_u \\ & - \|\sigma^\top\lambda B\|\hat{L}_m - \|\sigma^\top\lambda\|\hat{L}_u + \Gamma^{-1}(\tilde{L}_m\dot{\hat{L}}_m + \tilde{L}_u\dot{\hat{L}}_u). \end{aligned} \quad (2.75)$$

Hence, the following upper bound can be derived

$$\begin{aligned} \dot{V} \leq & -\rho\|\sigma\|^2 + \|\sigma^\top\lambda B\|\|\eta_m\| + \|\sigma^\top\lambda\|\|\eta_u\| \\ & - \|\sigma^\top\lambda B\|\hat{L}_m - \|\sigma^\top\lambda\|\hat{L}_u + \Gamma^{-1}(\tilde{L}_m\dot{\hat{L}}_m + \tilde{L}_u\dot{\hat{L}}_u). \end{aligned} \quad (2.76)$$

Using assumption 2.4, it follows that

$$\dot{V} \leq -\rho\|\sigma\|^2 - \|(\lambda B)^\top\sigma\|\tilde{L}_m - \|\lambda^\top\sigma\|\tilde{L}_u + \Gamma^{-1}(\tilde{L}_m\dot{\hat{L}}_m + \tilde{L}_u\dot{\hat{L}}_u). \quad (2.77)$$

Considering the adaptation laws from (2.53) and (2.55), it follows that

$$\dot{V} \leq -\rho\|\sigma\|^2. \quad (2.78)$$

Therefore, the sliding surface σ , the estimation errors of the unknown parameters $\tilde{\theta}$ and $\tilde{\omega}$; and the disturbances bounds errors \tilde{L}_m and \tilde{L}_u are uniformly bounded. Consequently, the estimation errors of the external disturbances $\tilde{\eta}_m$ and $\tilde{\eta}_u$ are also uniformly bounded.

Similarly to the proof of Lemma 2.2, since the coefficients of the sliding surface form a stable hyperplane and $\tilde{x}(0) = 0$, i.e., the system is initialized on the sliding surface, and given that on the sliding surface the trajectories are governed by $\sigma(\tilde{x}, t) = 0$, there always exists an arbitrarily small real $\delta > 0$ verifying

$$\|\tilde{x}\|_{\mathcal{L}_\infty} \leq \delta. \quad (2.79)$$

This result comes from the fundamental propriety of sliding mode control, stipulating that if the system is on the sliding surface, it stays on the nearby sliding surface despite disturbances [105].

Moreover, from (2.78) it can be written

$$\int_0^t \|\sigma(t)\|^2 dt \leq \frac{1}{\rho} (V(0) - V(t)). \quad (2.80)$$

Since $V(0)$ is bounded and $V(t)$ is bounded and non-increasing, therefore

$$\lim_{t \rightarrow \infty} \int_0^t \sigma(t)^2 dt \quad (2.81)$$

is bounded.

If the closed-loop system is stable, i.e., $u(t)$ and $x(t)$ are bounded then $\dot{\sigma}(t)$ in equation (2.71) is bounded. By applying Barbal't's Lemma it follows that

$$\lim_{t \rightarrow \infty} \|\sigma(t)\|^2 = 0 \text{ and } \lim_{t \rightarrow \infty} \|\sigma(t)\| = 0. \quad (2.82)$$

Consequently

$$\lim_{t \rightarrow \infty} \tilde{x}(t) = 0, \quad (2.83)$$

and the proof is complete. \square

Next, in the following theorem the performance bounds of the \mathcal{L}_1 adaptive controller are shown.

Theorem 2.2 Given the system (2.49), the reference system (2.61) and (2.62) and the \mathcal{L}_1 adaptive controller (2.50) to (2.57), we have

$$\|x_r - x\|_{\mathcal{L}_\infty} \leq \gamma_1, \quad (2.84)$$

$$\|u_r - u\|_{\mathcal{L}_\infty} \leq \gamma_2, \quad (2.85)$$

where

$$\gamma_1 = 2 \frac{\|G(s)\|_{\mathcal{L}_1}}{1 - \|G(s)\|_{\mathcal{L}_1} L} L_m + 2 \frac{\|G_u(s)\|_{\mathcal{L}_1}}{1 - \|G(s)\|_{\mathcal{L}_1} L} L_u + \frac{\|H(s)C(s)H_m^{-1}(s)C\|_{\mathcal{L}_1} \delta}{1 - \|G(s)\|_{\mathcal{L}_1} L},$$

and

$$\gamma_2 = \|\omega^{-1}C(s)\|_{\mathcal{L}_1} \left(L\gamma_1 + 2(L_m + \|H_m^{-1}(s)H_0(s)\|_{\mathcal{L}_1} L_u) + C(s)H_m^{-1}(s)\delta \right).$$

Proof. The control law in (2.57) can be written as

$$\begin{aligned} u(s) = & K D(s) \left(K_g r(s) - \omega u(s) - \theta^\top x(s) - \eta_m(s) \right) \\ & - K D(s) \left(H_m^{-1}(s) H_0(s) (\eta_u(s) + \tilde{\eta}_u(s)) - \tilde{v}(s) \right), \end{aligned} \quad (2.86)$$

2.2 \mathcal{L}_1 Adaptive Controller for MIMO Systems

where $\tilde{v}(s)$ is the Laplace transformation of $\tilde{v}(t) = \tilde{\omega}u(t) + \tilde{\theta}x(t) + \tilde{\eta}_m(t)$ and $\tilde{\eta}_u(s)$ is the Laplace transformation $\tilde{\eta}_u(t)$.

Consequently

$$u(s) = K D(s) \left(\mathbb{I} + \omega K D(s) \right)^{-1} \left(K_g r(s) - \theta^\top x(s) - \eta_m(s) \right) - K D(s) \left(\mathbb{I} + \omega K D(s) \right)^{-1} \left(H_m^{-1}(s) H_0(s) (\eta_u(s) + \tilde{\eta}_u(s)) - \tilde{v}(s) \right),$$

which leads to

$$u(s) = \omega^{-1} C(s) \left(K_g r(s) - \theta^\top x(s) - \eta_m(s) \right) - \omega^{-1} C(s) \left(H_m^{-1}(s) H_0(s) (\eta_u(s) + \tilde{\eta}_u(s)) - \tilde{v}(s) \right). \quad (2.87)$$

Hence, the Laplace transformation of the closed loop system (2.49) and (2.87) can be written

$$x(s) = H(s) C(s) K_g r(s) + G(s) \theta^\top x(s) + G(s) \eta_m(s) + G_u(s) \eta_u(s) - H(s) C(s) (\tilde{v}(s) + H_m^{-1}(s) H_0(s) \tilde{\eta}_u(s)) + x_{in}(s). \quad (2.88)$$

Taking the difference of (2.63) and (2.88) it follows that

$$x_r(s) - x(s) = G(s) \theta^\top (x_r(s) - x(s)) + G(s) (\eta_m(s) - \eta_{mr}(s)) + G_u(s) (\eta_u(s) - \eta_{ur}(s)) + H(s) C(s) (\tilde{v}(s) + H_m^{-1}(s) H_0(s) \tilde{\eta}_u(s)). \quad (2.89)$$

From (2.68) the Laplace transformation of the prediction error dynamics can be written

$$\tilde{x}(s) = H(s) \tilde{v}(s) + (s\mathbb{I} - A_m)^{-1} \tilde{\eta}_u(s). \quad (2.90)$$

Multiplying both terms of (2.90) by $H_m^{-1}(s)C$ one obtains

$$H_m^{-1}(s) C \tilde{x}(s) = \tilde{v}(s) + H_m^{-1}(s) H_0(s) \tilde{\eta}_u(s). \quad (2.91)$$

Substituting in (2.89) it follows that

$$x_r(s) - x(s) = G(s) \theta^\top (x_r(s) - x(s)) + G(s) (\eta_m(s) - \eta_{mr}(s)) + G_u(s) (\eta_u(s) - \eta_{ur}(s)) + H(s) C(s) H_m^{-1}(s) C \tilde{x}(s). \quad (2.92)$$

Solving for $x_r(s) - x(s)$, the following bound holds for $t \in [0, \tau]$

$$\begin{aligned} \|(x_r - x)_\tau\|_{\mathcal{L}_\infty} &\leq \frac{\|G(s)\|_{\mathcal{L}_1}}{1 - \|G(s)\|_{\mathcal{L}_1} L} \|(\eta_{m\tau} - \eta_{mr})_\tau\|_{\mathcal{L}_\infty} \\ &\quad + \frac{\|G_u(s)\|_{\mathcal{L}_1}}{1 - \|G(s)\|_{\mathcal{L}_1} L} \|(\eta_u - \eta_{ur})_\tau\|_{\mathcal{L}_\infty} \\ &\quad + \frac{\|H(s)C(s)H_m^{-1}(s)C\|_{\mathcal{L}_1}}{1 - \|G(s)\|_{\mathcal{L}_1} L} \|\tilde{x}_\tau\|_{\mathcal{L}_\infty}. \end{aligned} \quad (2.93)$$

Given the upper bound of $\tilde{x}(t)$ from Lemma 2.4, and the disturbance bounds from assumption 2.4, it follows that

$$\begin{aligned} \|(x_r - x)_\tau\|_{\mathcal{L}_\infty} &\leq 2 \frac{\|G(s)\|_{\mathcal{L}_1}}{1 - \|G(s)\|_{\mathcal{L}_1} L} L_m \\ &\quad + 2 \frac{\|G_u(s)\|_{\mathcal{L}_1}}{1 - \|G(s)\|_{\mathcal{L}_1} L} L_u \\ &\quad + \frac{\|H(s)C(s)H_m^{-1}(s)C\|_{\mathcal{L}_1}}{1 - \|G(s)\|_{\mathcal{L}_1} L} \delta, \end{aligned} \quad (2.94)$$

which leads to the bound in (2.84).

To show the second bound in (2.85), by taking the difference of (2.62) and (2.87), one can derive

$$\begin{aligned} u_r(s) - u(s) &= -\omega^{-1}C(s)\theta^\top \left((x_r(s) - x(s)) \right) \\ &\quad - \omega^{-1}C(s)(\eta_m(s) - \eta_{mr}(s)) \\ &\quad - \omega^{-1}C(s)H_m^{-1}(s)H_0(s)(\eta_u(s) - \eta_{ur}(s)) \\ &\quad + \omega^{-1}C(s)(H_m^{-1}(s)H_0(s)\tilde{\eta}_u(s) + \tilde{v}(s)). \end{aligned} \quad (2.95)$$

Hence

$$\begin{aligned} u_r(s) - u(s) &= -\omega^{-1}C(s)\theta^\top \left((x_r(s) - x(s)) \right) \\ &\quad - \omega^{-1}C(s)(\eta_m(s) - \eta_{mr}(s)) \\ &\quad - \omega^{-1}C(s)H_m^{-1}(s)H_0(s)(\eta_u(s) - \eta_{ur}(s)) \\ &\quad + \omega^{-1}C(s)H_m^{-1}(s)C(s)\tilde{x}(s), \end{aligned} \quad (2.96)$$

and (2.95) can be upper bounded as

$$\begin{aligned} \|(u_r - u)_\tau\|_{\mathcal{L}_\infty} &\leq \|\omega^{-1}C(s)\|_{\mathcal{L}_1} L \|(x_r - x)_\tau\|_{\mathcal{L}_\infty} \\ &\quad + 2\|\omega^{-1}C(s)\|_{\mathcal{L}_1} (L_m + \|H_m^{-1}(s)H_0(s)\|_{\mathcal{L}_1} L_u) \\ &\quad + \|\omega^{-1}C(s)\|_{\mathcal{L}_1} \|C(s)H_m^{-1}(s)C(s)\|_{\mathcal{L}_1} \|\tilde{x}_\tau\|_{\mathcal{L}_\infty}, \end{aligned} \quad (2.97)$$

which holds uniformly for all $\tau \geq 0$, leading to the bound in (2.85). \square

2.3 Summary

An \mathcal{L}_1 adaptive controller for both SISO and MIMO systems with matched and unmatched disturbances of unknown bounds was presented in this chapter. The adaptation laws, based on a sliding surface, permit to estimate the bounds of the perturbations. By doing so, the conservative assumption on prior information on upper bounds of external disturbances is relaxed. The proposed scheme guaranteed a fast transient response with bounded tracking performance. In the following, the design will be applied to the guidance and control of a small UAV in the presence of wind disturbances and/or faults or failures.

3

Chapter 3

\mathcal{L}_1 Adaptive Guidance of Fixed-wing UAVs

3.1	The Path-Following Problem	32
3.2	\mathcal{L}_1 Adaptive Straight-Line Path-Following in the Horizontal Plane	33
	3.2.1 Controller Design	33
	3.2.2 Simulation Results	37
3.3	\mathcal{L}_1 Adaptive Circular Path-Following	43
	3.3.1 Controller Design	44
	3.3.2 Simulation Results	46
3.4	Flight Test Results	47
3.5	Summary	49

Many applications of small UAVs require the system to autonomously follow a predefined path at a prescribed height. The most commonly used paths are straight lines and circular orbits. A requirement for a path-following design is that they must be accurate and robust to wind disturbances [101].

The aim of this chapter is to discuss the development of an adaptive guidance (path-following) approach, for a fixed-wing UAV, which explicitly considers that wind speed is time-varying.

The main idea, in this chapter, was to formulate the path-following of a fixed-wing UAV as a control design for systems in the presence of parametric uncertainties and external disturbances. Assuming that there is no prior information on wind, the proposed solution is based on the \mathcal{L}_1 adaptive

controller for disturbances of unknown bounds presented in the previous chapter.

The objectives of this chapter are:

- Formulating the path-following problem as a control design in the presence of unknown uncertainties and external disturbances.
- Developing an \mathcal{L}_1 adaptive straight-line path-following controller.
- Extending the approach to circular path-following.
- Demonstrating the performance of the proposed design in simulations as well as in real flight experiments.

3.1 The Path-Following Problem

The kinematic model of a fixed-wing UAV in the inertial frame is given from [9] as follows

$$\begin{aligned}\dot{p}_n &= V_a \cos(\psi) \cos(\gamma_a) + W_n, \\ \dot{p}_e &= V_a \sin(\psi) \cos(\gamma_a) + W_e, \\ \dot{p}_d &= -V_a \sin(\gamma_a) + W_d,\end{aligned}\tag{3.1}$$

where p_n , p_e , p_d are respectively the North, East and down (negative of the altitude) positions, V_a is the airspeed, ψ is the heading angle relative to the north, γ_a is the air referenced flight path angle, and W_n , W_e , and W_d are wind speeds in the inertial frame.

This model is derived under the assumption that the UAV is in steady level flight. In this case, the airspeed V_a is aligned with the x -direction of the body frame, which means that the sideslip angle β is zero.

Assuming a coordinated turn, i.e., the ailerons are used to change the UAV heading, the rate of variation of the heading angle is given by

$$\dot{\psi} = \frac{g}{V_a} \tan(\phi).\tag{3.2}$$

The objective is to compute the desired rolling angle ϕ_c and flight-path angle γ_c that maintain the UAV on the desired path, despite the presence of wind.

3.2 \mathcal{L}_1 Adaptive Straight-Line Path-Following in the Horizontal Plane

Assumption 3.1 In practice, the two most commonly used paths for UAVs are straight-lines and circular paths [101]. Both types of paths are usually defined on the horizontal plane, with constant altitude and speed.

Assumption 3.2 The dynamics of the pitch and roll are much faster than the dynamics of the altitude and the yaw motion.

Assumption 3.3 There is no available information on the wind, neither its velocity nor its direction.

Remark 3.1 In this chapter the time dependence of the variables is dropped unless if it is not clear from the context.

3.2 \mathcal{L}_1 Adaptive Straight-Line Path-Following in the Horizontal Plane

3.2.1 Controller Design

Using assumption 3.4, the horizontal kinematics of a fixed-wing UAV can be expressed by

$$\begin{aligned}\dot{p}_n &= V_a \cos(\psi) + W_n, \\ \dot{p}_e &= V_a \sin(\psi) + W_e, \\ \dot{\psi} &= \frac{g}{V_a} \tan(\phi).\end{aligned}\tag{3.3}$$

The desired path is defined by the straight-line from the precedent waypoint $P_k(p_{nk}, p_{ek})$ to the destination waypoint $P_{k+1}(p_{nk+1}, p_{ek+1})$, where (p_{nk}, p_{ek}) and (p_{nk+1}, p_{ek+1}) are respectively the horizontal coordinates of the waypoints P_k and P_{k+1} in the inertial frame, as shown in Fig. 3.1.

The cross-track error d is the shortest distance from the position of the UAV to the reference path, given by

$$d = -(p_n - p_{nk}) \sin(\psi_p) + (p_e - p_{ek}) \cos(\psi_p),\tag{3.4}$$

where ψ_p is the orientation of the path relative to the North direction defined by

$$\psi_p = \text{atan2}(p_{ek+1} - p_{ek}, p_{nk+1} - p_{nk}),\tag{3.5}$$

where the function atan2 returns an angle between $[0, 2\pi]$.

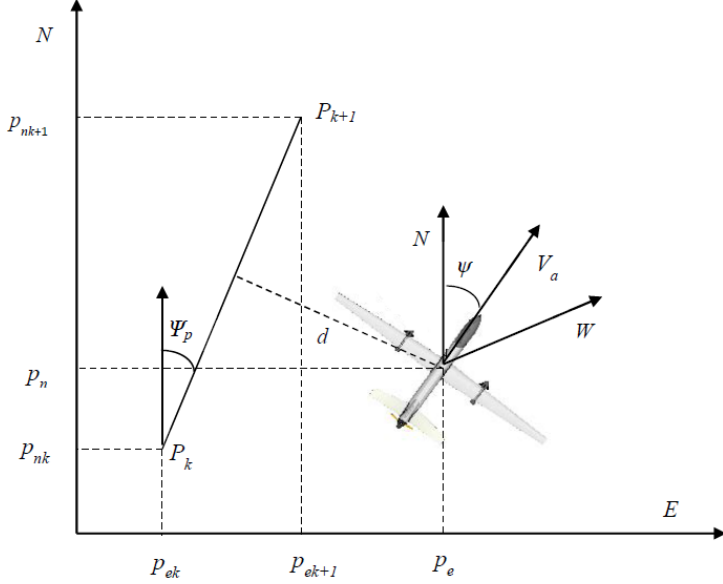


Figure 3.1: Path-following in the horizontal plane.

By differentiating (3.4) with respect to time and using (3.3) and (3.2), it follows that

$$\begin{aligned} \dot{d} &= -V_a \sin(\psi_e) + W_e \sin(\psi_p) - W_n \cos(\psi_p), \\ \dot{\psi}_e &= -\frac{g}{V_a} \tan(\phi_c), \end{aligned} \quad (3.6)$$

where $\psi_e = \psi_p - \psi$ is the orientation of the UAV relative to the desired path.

Remark 3.2 The use of the notations ϕ_c is justified by the fact that, in practice, this angle is the reference input of the low-level controller.

Letting $x = [d, \psi_e]^\top$ be the state vector and $u = \phi_c$ be the control input, the system is transformed to the following nonlinear state-space model

$$\dot{x} = f(x, u) + \zeta, \quad (3.7)$$

where

$$f(x, u) = \begin{bmatrix} -V_a \sin(x_2) \\ -\frac{g}{V_a} \tan(u) \end{bmatrix} \quad \text{and} \quad \zeta(t) = \begin{bmatrix} W_e \sin(\psi_p) - W_n \cos(\psi_p) \\ 0 \end{bmatrix}.$$

The regulated output y is the cross-track error d , i.e., the output vector is

$$c = [1 \ 0]^\top.$$

3.2 \mathcal{L}_1 Adaptive Straight-Line Path-Following in the Horizontal Plane

The objective is to design the control law $u(t)$ that stabilizes the system and consequently steers the UAV to the reference path. The proposed solution is based on the \mathcal{L}_1 adaptive controller. To this end, the linearized model is first derived.

Actually, a common procedure in adaptive control design is to linearize the nonlinear model at a given equilibrium or operating point, to design a linear controller based on the linearized system model, and to augment the linear controller with the adaptive controller. This allows for better robustness of the system [66].

For the equilibrium point $x_{eq} = [d_{eq} \ 0]^\top$, $u_{eq} = 0$ and $\zeta_{eq} = 0$, where d_{eq} is arbitrary, the linearized state space model of (3.7) is given by

$$\dot{\bar{x}} = A_p \bar{x} + b_p \bar{u}, \quad (3.8)$$

where

$$A_p = \begin{bmatrix} 0 & -V_a \\ 0 & 0 \end{bmatrix}, \quad b_p = \begin{bmatrix} 0 \\ -\frac{g}{V_a} \end{bmatrix}.$$

Hence, the non-linear system in (3.7) can be written as follows

$$\dot{x} = A_p x + b_p u + \tilde{f}, \quad (3.9)$$

where $\tilde{f}(x, u, t)$ is a nonlinear function that includes the higher order terms of the Taylor series expansion of $f(x, u)$ and the external disturbance $\zeta(t)$.

It is important to underline that the matrix A_p and the vector b_p are uncertain because it not possible in real flight conditions to maintain a constant airspeed V_a , especially in the presence of wind. Therefore, the system in (3.9) can be written as

$$\dot{x} = A_m x + b \omega u + (A_p - A_m)x + \tilde{f}, \quad (3.10)$$

where $A_m = A - b k_p^\top$ is a Hurwitz matrix of the desired dynamics of the system, A is the system dynamics matrix for the nominal airspeed, b is the input vector of the system with the nominal airspeed, $k_p \in \mathbb{R}^2$ is the feedback vector, and $\omega \in \mathbb{R}$ is an unknown gain.

For control design, the following approximation can be used

$$(A_p - A_m)x + \tilde{f} = b(\theta^\top x + \eta_m) + \eta_u, \quad (3.11)$$

where $\theta \in \mathbb{R}^2$ is a vector of unknown parameters, $\eta_m \in \mathbb{R}$ is a matched disturbance and $\eta_u \in \mathbb{R}^2$ is a vector of unmatched disturbances. Consequently, the system in (3.10) leads to

$$\dot{x} = A_m x + b(\omega u + \theta^\top x + \eta_m) + \eta_u. \quad (3.12)$$

3 \mathcal{L}_1 Adaptive Guidance of Fixed-wing UAVs

The resulting model is similar to (2.1), which makes straightforward application of the \mathcal{L}_1 adaptive controller (2.2)-(2.9). The block diagram of fixed-wing UAV path-following in wind, based on \mathcal{L}_1 adaptive control, is illustrated in Fig. 3.2.

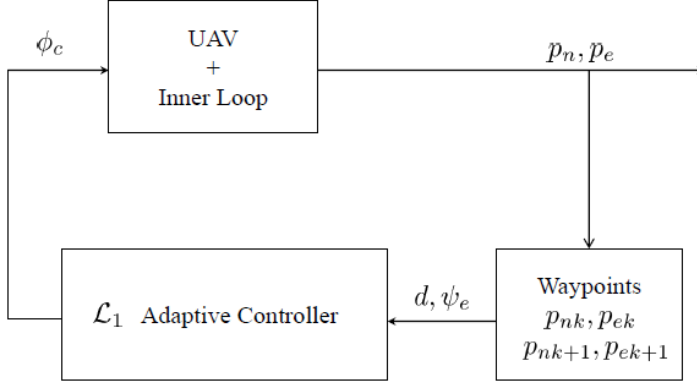


Figure 3.2: \mathcal{L}_1 adaptive path-following.

Remark 3.3 The main advantage of the application of \mathcal{L}_1 adaptive control to UAV path-following in wind is that good performance of the system can be obtained, whether the unknown wind speed is constant or not. This is a direct consequence of what was demonstrated in the previous chapter that the designed \mathcal{L}_1 adaptive controller presents a good compromise between performance and robustness in the presence of disturbances with unknown bounds.

In the following, the design of a linear path-following controller is presented. The objective is to provide a comparison baseline for the performance evaluation of the \mathcal{L}_1 adaptive path-following controller. To provide better robustness against disturbances, the integral of the regulated output error, denoted by e_I , is considered for the linear system in (3.8). The augmented system can be written as follows

$$\begin{bmatrix} \dot{\bar{x}} \\ \dot{e}_I \end{bmatrix} = \begin{bmatrix} A & 0 \\ -c & 0 \end{bmatrix} \begin{bmatrix} \bar{x} \\ e_I \end{bmatrix} + \begin{bmatrix} b \\ 0 \end{bmatrix} \bar{u}. \quad (3.13)$$

The control law of the system is given by

$$\bar{u} = -k_p^\top \bar{x} - k_I e_I, \quad (3.14)$$

3.2 \mathcal{L}_1 Adaptive Straight-Line Path-Following in the Horizontal Plane

where $k_I \in \mathbb{R}$ is the integral gain and $k_p \in \mathbb{R}^2$ is the proportional feedback vector that is designed to obtain the same desired system dynamics matrix as the \mathcal{L}_1 adaptive controller $A_m = A - b k_p^\top$.

3.2.2 Simulation Results

In this section, the simulation results for the \mathcal{L}_1 adaptive and the linear path-following controllers are presented. The performance of the controllers was evaluated in four case scenarios: without wind, in constant wind, in time-varying wind and in a situation where the airspeed of the UAV varies under wind effect.

It was assumed that the nominal airspeed of the UAV is $V_a = 20 \text{ m/s}$. The gravity is $g = 9.81 \text{ m/s}^2$. It was further assumed that the maximum turn angle is $|\phi| = 60^\circ$.

The desired dynamics of the system were chosen with a frequency of 0.7 rad/s and a damping factor of 0.7. The transfer function $D(s)$ of the \mathcal{L}_1 adaptive controller was chosen $D(s) = \frac{1}{s(s+9.8)}$ and $k = 36$, which leads to a filter $C(s) = \frac{36}{s^2+9.6s+36}$. It is important to note that the same desired system dynamics and initialization parameters were used for both controllers in order to provide a fair comparison.

The UAV was commanded to fly a straight-line path, defined by four (4) waypoints, with the cross-track error d required to be zero. The initial position of the UAV was at the origin of the Earth frame.

Performance Analysis without Wind

Simulation results have shown that both controllers present a satisfactory performance when there are no wind disturbances. The trajectories of the UAV, relative to the desired path, are illustrated in Fig. 3.3. It can be observed that, when the UAV moved from the initial location to the desired path, the \mathcal{L}_1 adaptive controller has presented better performance than the linear controller. The cross-track error, the heading error and the commanded roll angle are illustrated versus time in Fig. 3.4. The presence of peaks in the cross-track error is due to the rolling motion of the UAV when turning at the waypoints.

3 \mathcal{L}_1 Adaptive Guidance of Fixed-wing UAVs

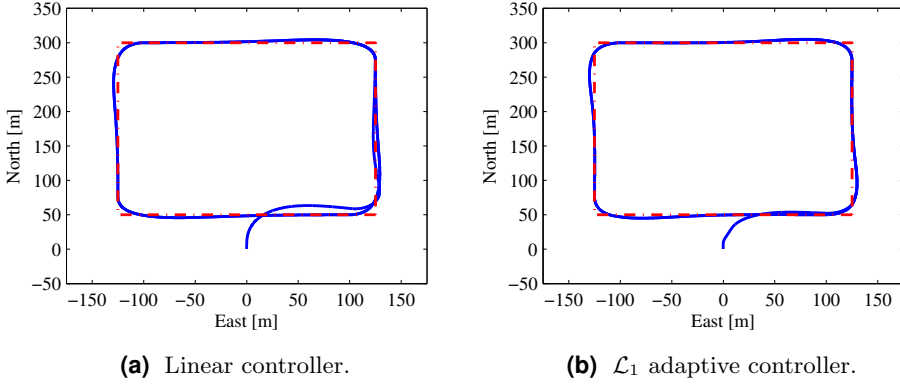


Figure 3.3: Trajectory of the UAV: desired (red) and actual (blue) without wind.

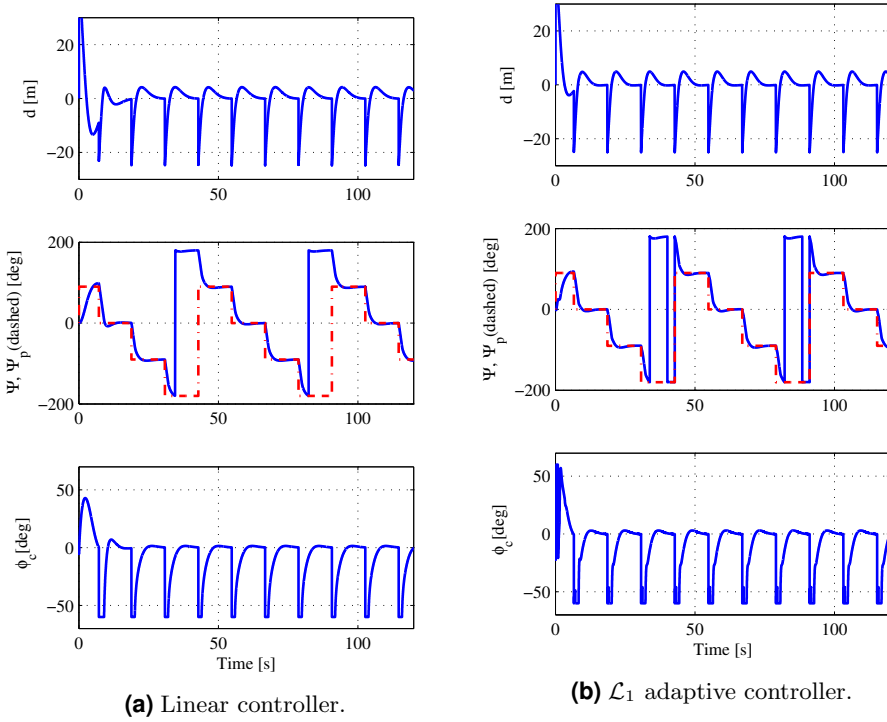


Figure 3.4: Parameters of the controllers without wind.

Performance Analysis in Constant Wind

In a second simulation scenario, a constant crosswind with a speed of 10 m/s , blowing in the easterly direction, was introduced. As observed from Fig. 3.5 and Fig. 3.6, the \mathcal{L}_1 adaptive controller performs better than the linear controller in the same wind conditions. In particular, it can be noted that the trajectory of the UAV is smoother and more precise with the \mathcal{L}_1 adaptive controller. This is especially true when the UAV, moved from the initial location to the desired path. Note that trying to improve the performance of the linear controller, by changing the gain of the integral output error, leads either to instability of the control system or to an even worst transient regime when starting from the initial position.

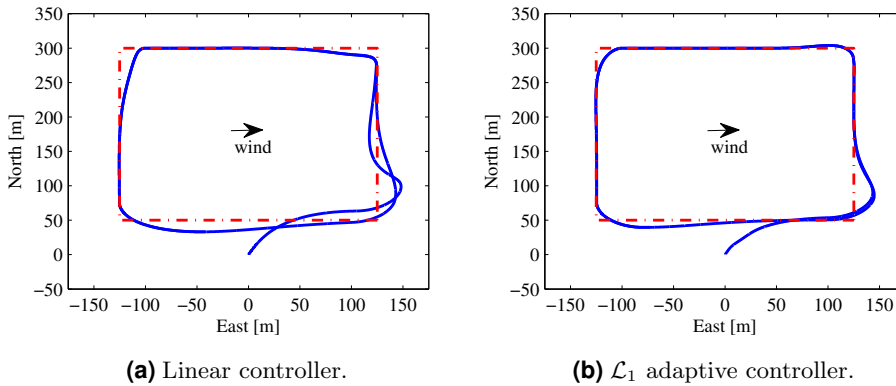


Figure 3.5: Trajectory of the UAV: desired (red) and actual (blue) in constant crosswind.

Performance Analysis in Time-Varying Wind

In the next simulations, a time-varying crosswind was introduced. Its velocity was assumed to be a periodic signal, $W_e(t) = 5 + 5 \sin(2\pi t)$. Simulation results are shown in Fig. 3.7 and Fig. 3.8. It is obvious that the adaptive controller performs better than the linear controller in this wind conditions. Moreover, it is clearly illustrated that the cross-track error is not completely eliminated by the linear controller. Similar to simulations in constant wind, trying to enhance the performance of the linear controller by changing the gain of the integral output error leads either to instability of the control system or to worst transient regimes when starting from the initial position.

3 \mathcal{L}_1 Adaptive Guidance of Fixed-wing UAVs

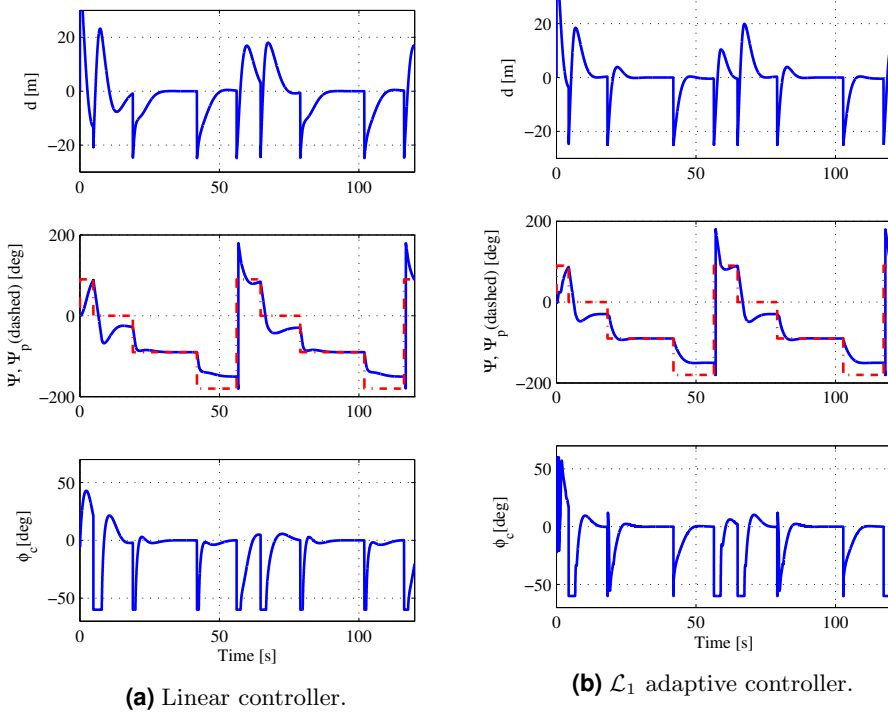


Figure 3.6: Parameters of the controllers in constant crosswind.

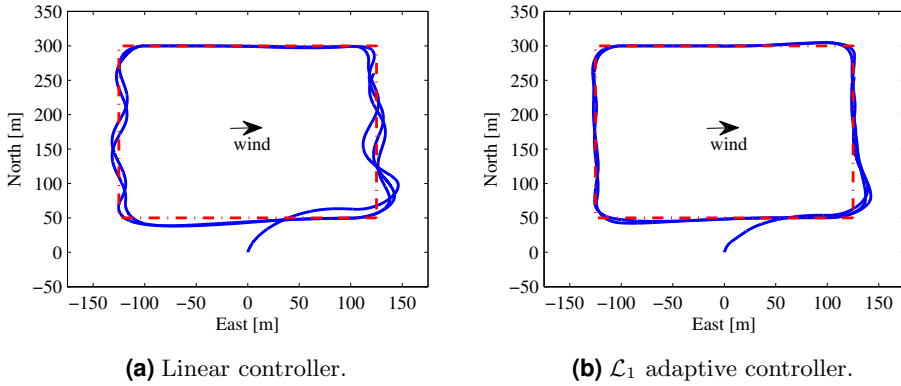


Figure 3.7: Trajectory of the UAV: desired (red) and actual (blue) in time-varying crosswind.

3.2 \mathcal{L}_1 Adaptive Straight-Line Path-Following in the Horizontal Plane

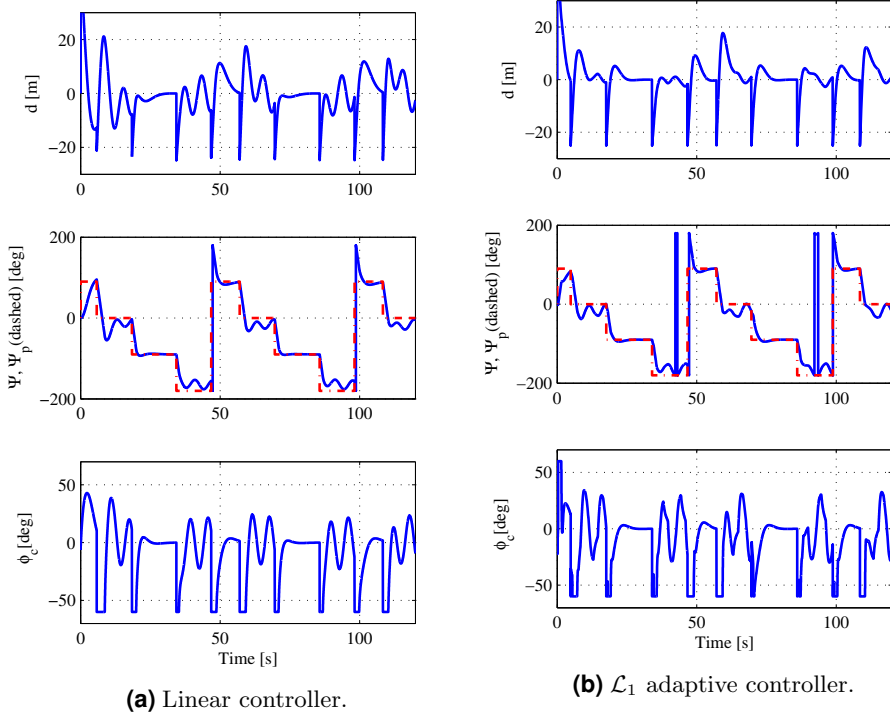


Figure 3.8: Parameters of the controllers in time-varying crosswind.

Performance Analysis in Case of Varying Airspeed

As explained above, maintaining a constant airspeed is not feasible in practice, especially in the presence of wind disturbances. In order to simulate this situation, the previous scenario of a constant wind, with a speed of 10 m/s , blowing in the easterly direction was reproduced. It was furthermore supposed that:

- The airspeed increases by 5 m/s when the UAV is flying downwind.
- The airspeed decreases by 5 m/s when the UAV is flying upwind
- The airspeed decreases by 2 m/s when the UAV is flying crosswind.

This assumption does not have a flight mechanical justification. It is used only for simulation purposes.

3 \mathcal{L}_1 Adaptive Guidance of Fixed-wing UAVs

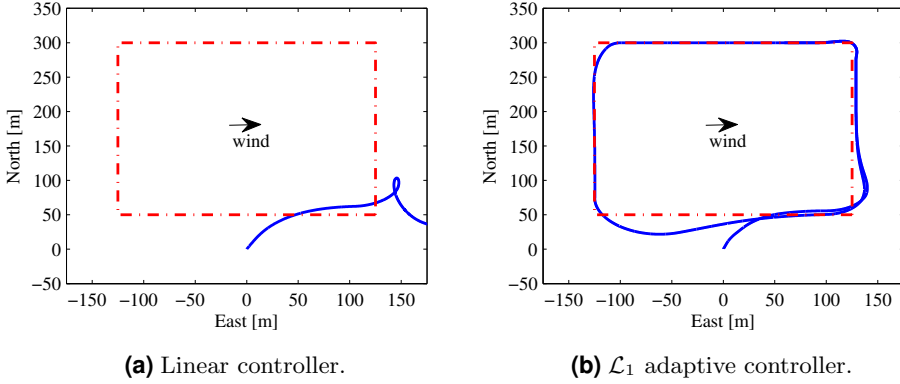


Figure 3.9: Trajectory of the UAV: desired (red) and actual (blue) in varying airspeed.

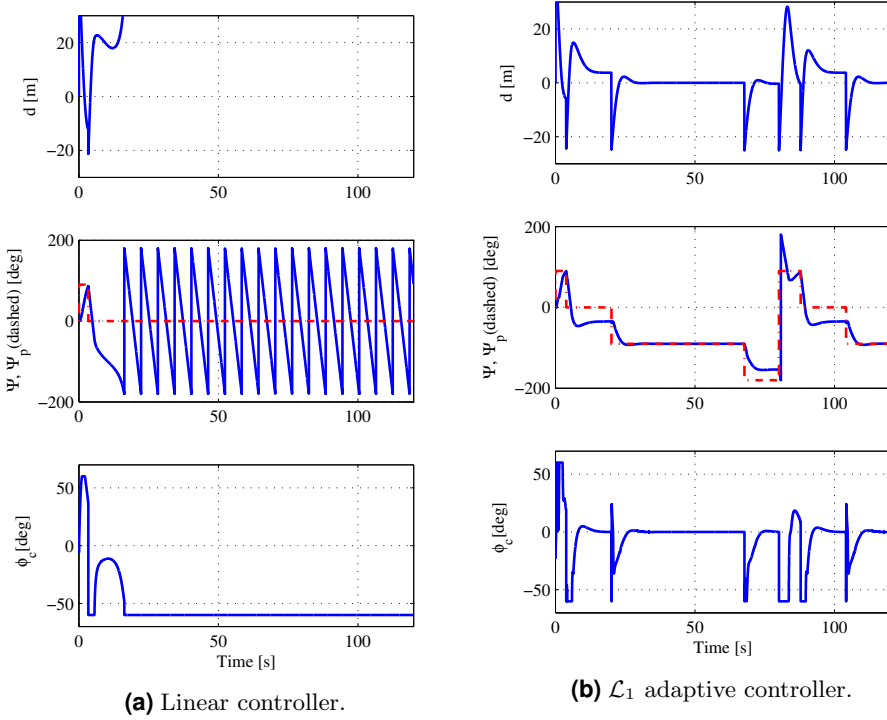


Figure 3.10: Parameters of the controllers in varying airspeed.

It is shown in Fig. 3.9 and Fig. 3.10 that the linear controller was not able to keep the UAV on the desired path under variations of the airspeed, whereas, as expected, the \mathcal{L}_1 adaptive controller has performed well under the same conditions. To explain this, it can be noted from the model in (3.9) that unknown time-varying parameters are introduced in the system when the airspeed of the UAV varies due to wind. The robustness of linear controllers is relatively limited in this situation, while the improved performance of the \mathcal{L}_1 adaptive controller is due to its ability to compensate unknown parameters and external disturbances.

These simulations conclude that the designed \mathcal{L}_1 adaptive path-following was shown to be more performing, in different wind conditions, than the linear controller. This is due to its robustness and fast adaptation in the presence of unknown system parameters and external disturbances.

3.3 \mathcal{L}_1 Adaptive Circular Path-Following

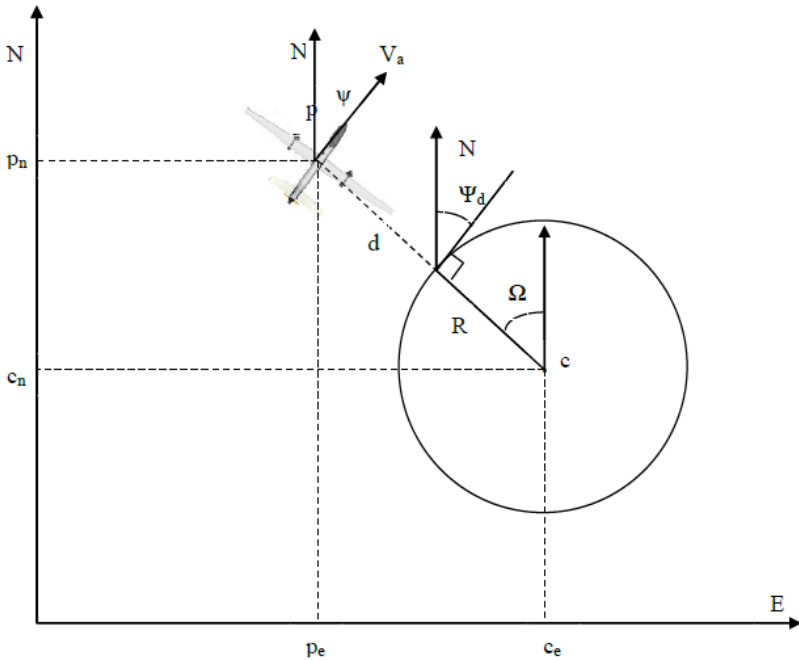


Figure 3.11: Circular path-following design.

3.3.1 Controller Design

A circular path, as it is shown Fig. 3.11, is defined by its radius R and its center with coordinates $(c_n, c_e)^\top$ in the reference frame. The design is based on the formulation of the kinematics of the UAV in polar coordinates as follows

$$\begin{aligned} p_n &= (d + R) \cos(\Omega) + c_n, \\ p_e &= (d + R) \sin(\Omega) + c_e, \end{aligned} \quad (3.15)$$

where d is the shortest distance from the UAV to the circle line and Ω is the phase angle of the relative position of the UAV defined by

$$\Omega = \text{atan2}(p_e - c_e, p_n - c_n). \quad (3.16)$$

Taking time derivative of (3.15) and comparing with (3.3), yields

$$\begin{aligned} \dot{d} \cos(\Omega) - (d + R) \dot{\Omega} \sin(\Omega) &= V_a \cos(\psi) + W_n, \\ \dot{d} \sin(\Omega) + (d + R) \dot{\Omega} \cos(\Omega) &= V_a \sin(\psi) + W_e. \end{aligned} \quad (3.17)$$

Eliminating the term $\dot{\Omega}$ from (3.17) gives

$$\dot{d} = V_a \cos(\psi - \Omega) + d_{w1}, \quad (3.18)$$

where

$$d_{w1} = W_n \cos(\Omega) + W_e \sin(\Omega).$$

Moreover, differentiating (3.16) yields

$$\dot{\Omega} = \frac{V_a}{d + R} \sin(\psi - \Omega) + d_{w2}, \quad (3.19)$$

where

$$d_{w2} = \frac{W_e \sin(\Omega) - W_n \cos(\Omega)}{d + R}.$$

If the planned flight direction is counterclockwise, then the desired heading angle is $\psi_d = \Omega - \pi/2$. Likewise, if the planned flight direction is clockwise, then the desired heading angle is $\psi_d = \Omega + \pi/2$.

3.3 \mathcal{L}_1 Adaptive Circular Path-Following

Without loss of generality, it is assumed that the UAV will fly in the clockwise direction. Recalling that $\psi_e = \psi_d - \psi$, equation (3.19) can be written as follows

$$\dot{\psi}_d = \frac{V_a}{d+R} \cos(\psi_e) + d_{w2} \quad (3.20)$$

Consequently, the system in (3.18) and (3.20) leads to

$$\begin{aligned} \dot{d} &= V_a \sin(\psi_e) + d_{w1}, \\ \dot{\psi}_e &= \frac{V_a}{d+R} \cos(\psi_e) - \frac{g}{V_a} \tan(\phi_c) + d_{w2}. \end{aligned} \quad (3.21)$$

Similar to straight-line path-following, letting $x = [d, \psi_e]^\top$ and $u = \phi_c$, the system leads to the following nonlinear state-space model

$$\dot{x} = f(x, u) + \zeta, \quad (3.22)$$

where

$$f(x, u) = \begin{pmatrix} V_a \sin(x_2) \\ \frac{V_a}{x_1+R} \cos(x_2) - \frac{g}{V_a} \tan(u) \end{pmatrix} \quad \text{and} \quad \zeta(t) = \begin{pmatrix} d_{w1} \\ d_{w2} \end{pmatrix}.$$

For the equilibrium point $x_{eq} = [d_{eq} \ 0]^\top$, $u_{eq} = \text{atan}(V_a^2/(g(R+d_{eq})))$ and $\zeta_e = 0$, the linearized state space model of (3.22) is given by

$$\dot{\bar{x}} = A_p \bar{x} + b_p \bar{u}, \quad (3.23)$$

where

$$A_p = \begin{bmatrix} 0 & V_a \\ -V_a/(d_{eq}+R)^2 & 0 \end{bmatrix}, \quad b_p = \begin{pmatrix} 0 \\ -\bar{g}/V_a \end{pmatrix},$$

with $\bar{g} = g \left(\frac{V^4}{g^2(R+d)^2} + 1 \right)$.

Therefore, the system in (3.22) can be written as follows

$$\dot{x} = A_p x + b_p u + \tilde{f}, \quad (3.24)$$

where $\tilde{f}(x, u, t)$ is a nonlinear function that includes the higher order terms of the Taylor series expansion of $f(x, u)$ and the external disturbance $\zeta(t)$.

The resulting model is similar to the straight-line path-following in (3.9). That is why the \mathcal{L}_1 adaptive controller can be applied.

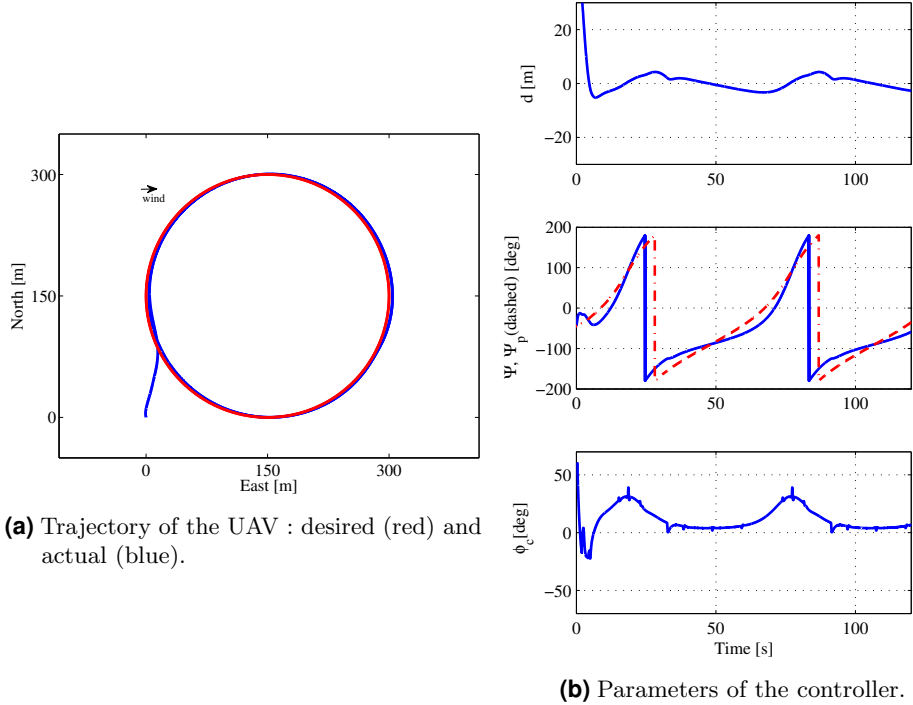


Figure 3.12: Circular path-following with the adaptive controller in constant crosswind.

3.3.2 Simulation Results

The objective of the simulations was to follow a circular path, with a diameter $R = 150\text{ m}$, centered at $c(150\text{ m}, 150\text{ m})$. The initial position of the UAV was at the origin of the Earth frame. The tuning parameters of the controller are similar to those used for straight-line path-following controller. The performance of the controller was evaluated in constant wind and in time-varying wind.

In Fig. 3.12, it is shown that the controller copes well with a constant wind disturbance of 10 m/s of speed. The cross-track error is maintained within a very small range.

Simulation results in time-varying wind, with a velocity that was assumed to be a periodic signal, $W_e(t) = 5 + 5\sin(\pi t)$, are shown in Fig. 3.13. It can be seen that the effect of wind disturbance is compensated by the adaptive controller.

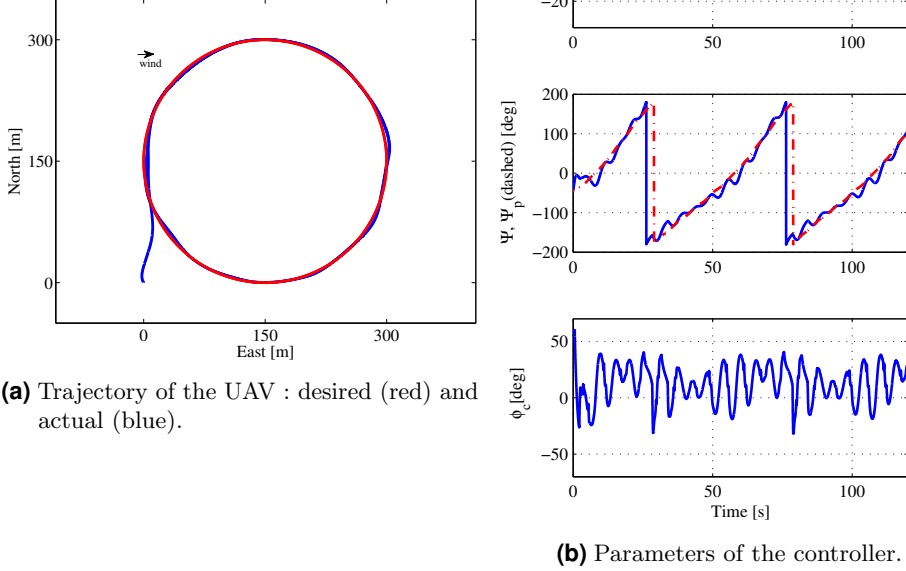


Figure 3.13: Circular path-following with the adaptive controller in time-varying wind.

3.4 Flight Test Results

In this section, the results in the real flight of the proposed \mathcal{L}_1 adaptive path-following controller are presented. Flight experiments were conducted on the Twinstar-II small fixed-wing UAV airframe which is shown in Fig. 1.1. The UAV is equipped with an on-board computer which consists of a Gumstix Overo SBC and an FPGA.

The autopilot system has a cascaded design, composed of path-following (outer-loop) and attitude (inner-loop) controllers. The \mathcal{L}_1 adaptive path-following controller computes the commanded roll angle ϕ_c to achieve desired waypoints. The inner-loop ensures that the states of the UAV track the desired angles using PID based control architecture.

The UAV was commanded to fly a straight-line path, defined by four (4) waypoints, at a constant altitude of 50 m, with the cross-track error d required to be zero. The desired airspeed was set at $V_a = 20$ m/s.

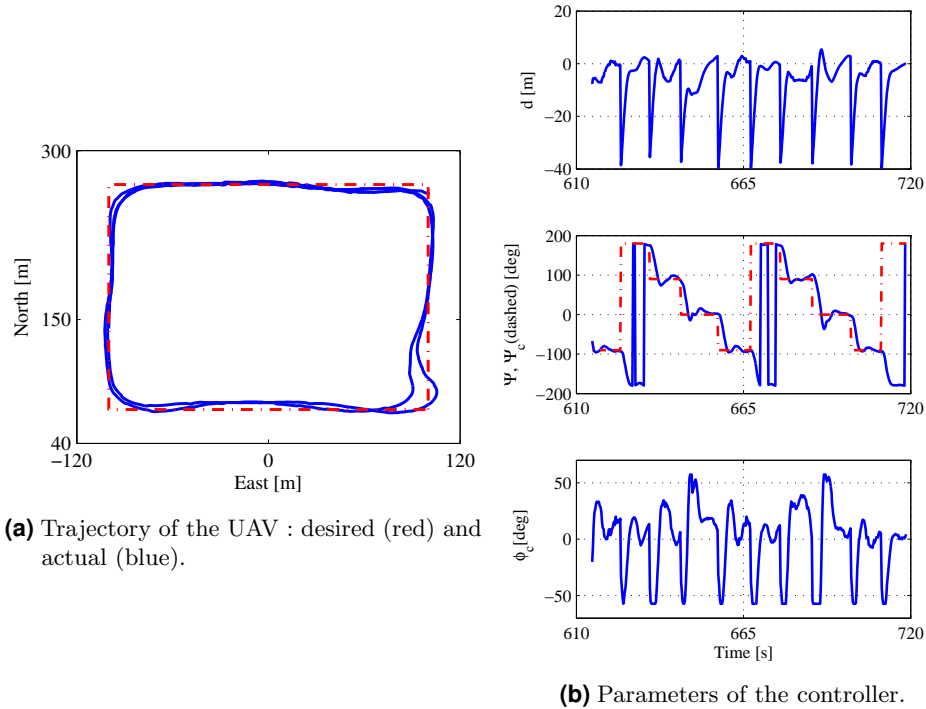


Figure 3.14: Flight test of the \mathcal{L}_1 adaptive controller without wind.

The preliminary tests were carried out without wind; this permitted further testing in real flight conditions. In Fig. 3.14 are shown flight test results of the \mathcal{L}_1 adaptive controller. Similarly to simulation results, the controller has demonstrated good performance when there are no wind disturbances. It can be seen that the cross-track error converges quickly to zero after turns and the UAV follows the desired path with feasible commands.

The next flight tests were performed in wind which was blowing southerly at approximately 5 m/s , with gusts estimated locally up to 10 m/s . Flight test results for the \mathcal{L}_1 adaptive controller in wind are shown in Fig. 3.15. As it can be seen, the cross-track error is maintained within an acceptable range. Furthermore, it can be observed that the UAV produces the commanded roll angle ϕ_c that compensates wind effect.

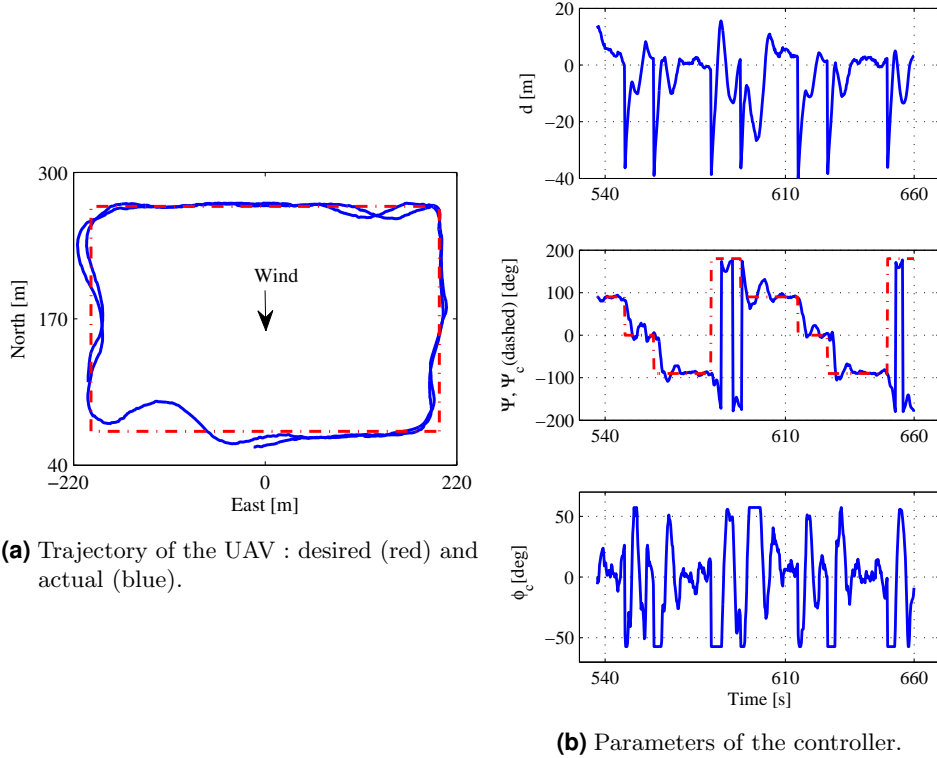


Figure 3.15: Flight test of the \mathcal{L}_1 adaptive controller in wind.

3.5 Summary

This chapter presented an approach for an adaptive path-following of a small fixed-wing UAV. The design was made for 2D straight and circular paths. The proposed approach is based on the \mathcal{L}_1 adaptive control for disturbances of unknown bounds. The adaptive controller has shown better behavior in simulations compared to an LQR controller with integral action. The controller was demonstrated in real flight under winds up to 10 m/s , representing 50% of the airspeed of the UAV. Even though the framework developed in this chapter has been demonstrated in practice, it needs to be extended to 3D path-following, which should show better robustness, because it takes into account the synergy of the UAV motion in the horizontal and vertical planes. This is true especially in the presence of wind.

Chapter 4

4 \mathcal{L}_1 Adaptive Guidance of Fixed-wing UAVs for 3D Curved Paths

4.1	Problem Formulation	52
4.2	\mathcal{L}_1 Adaptive Path-Following of Three Dimensional Curved Paths	57
4.3	Simulation Results	58
	4.3.1 Simulation Results for a Dubins Path	59
	4.3.2 Simulation Results for a Helix Path	64
4.4	Summary	65

In the previous chapter the \mathcal{L}_1 adaptive guidance was presented assuming that the motion of the plant is decoupled within the horizontal and the vertical planes. However, considering a three dimensional (3D) guidance through general paths is more appropriate. This is particularly true when taking atmospheric disturbances into account.

Research in mobile robots was the precursor of curved paths tracking. The most notable result was presented by [73]. This approach was based on the introduction of a virtual target, which moves on the path. This virtual target is represented by a Serret-Frenet frame [40, 92]. The position of the virtual target is defined by the projection of the mobile robot on the desired path. The projection of the vehicle on the reference path is basically similar to what is commonly used in straight-line and circle path-following. The drawback of this approach is that the initial position of the robot has to be

inside a confined pipe, depending on the curvature of the path.

This problem was solved in [94], by introducing a Lyapunov-based control law for the virtual target speed, which showed the convergence of the vehicle to the desired path within a finite time, completely independent of the initial conditions. This result was extended to the 3D path-following of fixed-wing UAVs in [59]. The work in [69] takes into consideration the presence of steady wind. Test results of [69] observed that the controller is also robust against time-varying wind, but no clear theoretical proof was provided.

In this chapter, the formulation of the path-following of fixed-wing UAVs as guidance towards a virtual moving target is the basis of the proposed approach. The idea, similar to the 2D path-following in the previous chapter, is based on the formulation of the path-following as a control design problem of systems in the presence of uncertainties and external disturbances. The \mathcal{L}_1 adaptive control of Multi-Input Multi-Output (MIMO) systems with disturbances of unknown bounds is applied in this case.

4.1 Problem Formulation

In Fig. 4.1, the position of the center of gravity of the UAV is defined as point Q , with coordinates $q_i = [x_q, y_q, z_q]^\top$ in the inertial frame \mathcal{I} . The moving orthonormal frame \mathcal{M} , is referenced by the speed vector of the virtual target [14]. This frame is completely different from the Serret-Frenet frame. The position of the virtual target, moving on the desired path, which is the origin of \mathcal{M} , is defined as point P , with coordinates $p_i = [x_p, y_p, z_p]^\top$ in the inertial frame \mathcal{I} .

The objective is to minimize the position error of the UAV relative to the virtual target, which permits to maintain the UAV on the reference path despite the presence of wind disturbances.

Assumption 4.1 Similar to the previous chapter, it is assumed that the low-level controller commands the attitude angles instead of the rates, based on the bank to turn strategy.

In the following, the mathematical model of the three-dimensional curved path-following is derived.

The orientation of the desired path at position p_i can be characterized by its heading angle ψ_p and flight path angle γ_p , defined as follows [14]

$$\begin{aligned}\psi_p &= \arctan(\dot{y}_p/\dot{x}_p), \\ \gamma_p &= \arctan(\dot{z}_p/\sqrt{\dot{x}_p^2 + \dot{y}_p^2}),\end{aligned}\tag{4.1}$$

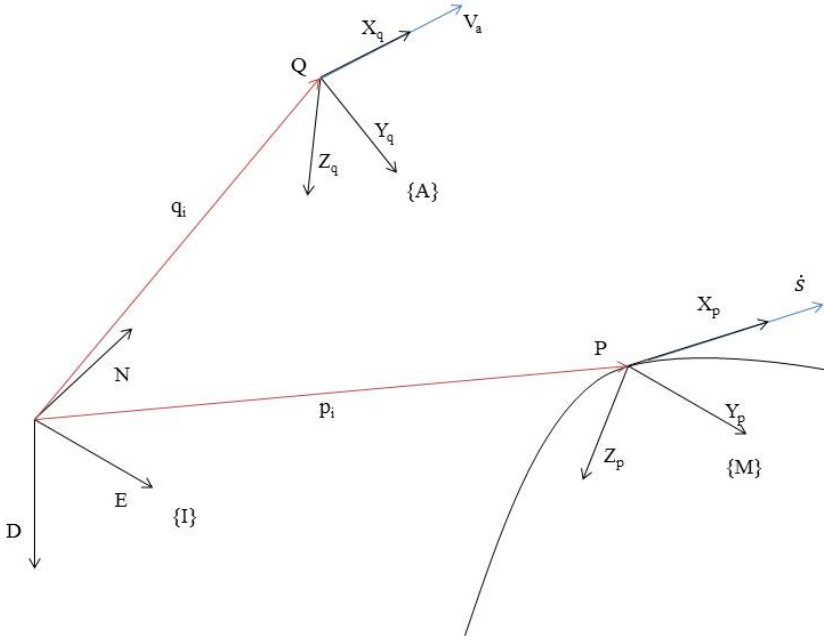


Figure 4.1: Curved Path-Following Frames.

where $[\dot{x}_p, \dot{y}_p, \dot{z}_p]$ are the coordinates of the velocity vector \dot{p}_i in the inertial frame \mathcal{I} .

Consequently, the position error e_m of the UAV expressed in the moving frame \mathcal{M} , can be written as follows

$$e_m = T_{mi}(q_i - p_i), \quad (4.2)$$

where p_i q_i are, respectively, the position vector of the UAV and the virtual target expressed in the inertial frame \mathcal{I} , and $T_{mi} = T_2(\gamma_p)T_3(\psi_p)$ is the transformation matrix from the inertial frame \mathcal{I} , to the moving frame \mathcal{M} , given by

$$T_{mi} = \begin{bmatrix} \cos\gamma_p \cos\psi_p & \cos\gamma_p \sin\psi_p & -\sin\gamma_p \\ -\sin\psi_p & \cos\psi_p & 0 \\ \sin\gamma_p \cos\psi_p & \sin\gamma_p \sin\psi_p & \cos\gamma_p \end{bmatrix}.$$

Taking time derivative of equation (4.2), yields

$$\dot{e}_m = T_{mi}(\dot{q}_i - \dot{p}_i) - \omega_{mi}^m \times T_{mi}(q_i - p_i), \quad (4.3)$$

where \times denotes the cross product, and ω_{mi}^m is the angular rate of the moving frame \mathcal{M} with respect to the inertial frame \mathcal{I} resolved in the moving frame \mathcal{M} .

Hence

$$\dot{e}_m = T_{mi}\dot{q}_i - \dot{p}_m - \omega_{mi}^m \times e_m, \quad (4.4)$$

where \dot{p}_m is the velocity vector of the virtual target in the moving frame \mathcal{M} defined by

$$\dot{p}_m = \begin{bmatrix} \dot{s} \\ 0 \\ 0 \end{bmatrix}, \quad (4.5)$$

with \dot{s} is the speed of the virtual target and s is the length of the path.

In order to expand equation (4.4), the expression of the angular rate ω_{mi}^m can be written as follows

$$\omega_{mi}^m = \begin{bmatrix} 0 \\ \dot{\gamma}_p \\ 0 \end{bmatrix} + \begin{bmatrix} \cos\gamma_p & 0 & -\sin\gamma_p \\ 0 & 1 & 0 \\ \sin\gamma_p & 0 & \cos\gamma_p \end{bmatrix} \begin{bmatrix} 0 \\ 0 \\ \dot{\psi}_p \end{bmatrix} = \begin{bmatrix} -\dot{\psi}_p \sin\gamma_p \\ \dot{\gamma}_p \\ \dot{\psi}_p \cos\gamma_p \end{bmatrix}. \quad (4.6)$$

We also have

$$\dot{\psi}_p = \frac{ds}{dt} \frac{d\psi_p}{ds}. \quad (4.7)$$

Using (4.1), it can be written

$$\psi_p = \arctan(y'_p/x'_p), \quad (4.8)$$

where $x'_p = \frac{dx_p(s)}{ds}$ and $y'_p = \frac{dy_p(s)}{ds}$.

Hence

$$\begin{aligned}\dot{\psi}_p &= \dot{s} \frac{d}{ds} \left(\arctan(y'_p/x'_p) \right), \\ &= \dot{s} c_1(s),\end{aligned}\tag{4.9}$$

where $c_1(s) = (x'_p y''_p - y'_p x''_p) / (x_p'^2 + y_p'^2)$.

By proceeding similarly, it can be shown that

$$\dot{\gamma}_p = \dot{s} c_2(s),\tag{4.10}$$

where $c_2(s) = (z_p''(x_p'^2 + y_p'^2) - z_p'(x_p'x_p'' + y_p'y_p'')) / ((x_p'^2 + y_p'^2 + z_p'^2)(x_p'^2 + y_p'^2)^{1/2})$.

Consequently, the system in (4.4) can be expanded as follows

$$\begin{aligned}\begin{bmatrix} \dot{x}_e \\ \dot{y}_e \\ \dot{z}_e \end{bmatrix} &= T_{mi} \begin{bmatrix} \dot{x}_q \\ \dot{y}_q \\ \dot{z}_q \end{bmatrix} - \begin{bmatrix} \dot{s} \\ 0 \\ 0 \end{bmatrix} \\ &- \begin{bmatrix} 0 & -\dot{s} c_1(s) \cos \gamma_p & \dot{s} c_2(s) \\ \dot{s} c_1(s) \cos \gamma_p & 0 & \dot{s} c_1(s) \sin \gamma_p \\ -\dot{s} c_2(s) & -\dot{s} c_1(s) \sin \gamma_p & 0 \end{bmatrix} \begin{bmatrix} x_e \\ y_e \\ z_e \end{bmatrix},\end{aligned}\tag{4.11}$$

where (x_e, y_e, z_e) are the coordinates of e_m .

Recalling from (3.1), the 3D kinematic model of a fixed-wing UAV is given by

$$\begin{bmatrix} \dot{x}_q \\ \dot{y}_q \\ \dot{z}_q \end{bmatrix} = T_{ia} \begin{bmatrix} V_a \\ 0 \\ 0 \end{bmatrix} + \begin{bmatrix} W_n \\ W_e \\ W_d \end{bmatrix},\tag{4.12}$$

where $T_{ia} = T_3(-\psi) T_2(-\gamma_a)$ is the transformation matrix from the airspeed referenced frame \mathcal{A} to the inertial frame \mathcal{I} given by

$$T_{ia} = \begin{bmatrix} \cos \gamma_a \cos \psi & -\sin \psi & \sin \gamma_a \cos \psi \\ \cos \gamma_a \sin \psi & \cos \psi & \sin \gamma_a \sin \psi \\ -\sin \gamma_a & 0 & \cos \gamma_a \end{bmatrix}.$$

Hence

$$T_{mi} \begin{bmatrix} \dot{x}_q \\ \dot{y}_q \\ \dot{z}_q \end{bmatrix} = T_{ma} \begin{bmatrix} V_a \\ 0 \\ 0 \end{bmatrix} + \begin{bmatrix} V_x \\ V_y \\ V_z \end{bmatrix},\tag{4.13}$$

where

$$\begin{bmatrix} V_x \\ V_y \\ V_z \end{bmatrix} = T_{mi} \begin{bmatrix} W_n \\ W_e \\ W_d \end{bmatrix},$$

and $T_{ma} = T_{mi} T_{ia}$ is the transformation matrix from the airspeed referenced frame \mathcal{A} to the moving frame \mathcal{M} defined by

$$\begin{aligned} T_{ma} &= T_2(\gamma_p) T_3(\psi_p) T_3(-\psi) T_2(-\gamma_a) \\ &= T_2(\gamma_p) T_3(-\psi_e) T_2(-\gamma_a) \\ &= \begin{bmatrix} C\gamma_p C\gamma_a C\psi_e + S\gamma_p S\gamma_a & -C\gamma_p C\psi_e & C\gamma_p S\gamma_a C\psi_e - S\gamma_p C\gamma_a \\ & C\gamma_a S\psi_e & C\psi_e & S\gamma_a S\psi_e \\ S\gamma_p C\gamma_a C\psi_e - C\gamma_p S\gamma_a & -C\gamma_p S\psi_e & S\gamma_p S\gamma_a C\psi_e + C\gamma_p C\gamma_a \end{bmatrix}, \end{aligned}$$

with $\psi_e = \psi - \psi_p$, $C \triangleq \cos$ and $S \triangleq \sin$.

Recalling the expression of coordinated turn from (3.2) and using (4.7), it can be written

$$\dot{\psi}_e = \frac{g}{V_a} \tan\phi - c_1(s)\dot{s}. \quad (4.14)$$

Substituting (4.13) in (4.11) and including (4.14), it follows that

$$\begin{aligned} \dot{x}_e &= V_a C\gamma_p C\psi_e C\gamma_a + V_a S\gamma_p S\gamma_a - (1 - c_1(s) C\gamma_p y_e + c_2(s) z_e)\dot{s} + V_x, \\ \dot{y}_e &= V_a S\psi_e C\gamma_a - (c_1(s) C\gamma_p x_e + c_1(s) S\gamma_p z_e)\dot{s} + V_y, \\ \dot{z}_e &= V_a S\gamma_p C\psi_e C\gamma_a - V_a C\gamma_p S\gamma_a + (c_2(s) x_e + c_1(s) S\gamma_p y_e)\dot{s} + V_z \\ \dot{\psi}_e &= \frac{g}{V_a} \tan\phi - c_1(s)\dot{s}. \end{aligned} \quad (4.15)$$

The objective is to compute the desired speed of the virtual target \dot{s} , the commanded roll angle $\phi_c = \phi$ and air referenced flight path angle $\gamma_c = \gamma_a$ that maintain the UAV on the desired path, despite the presence of wind. The proposed method is based on \mathcal{L}_1 adaptive control.

Remark 4.1 The use of the notations ϕ_c and γ_c is justified by the fact that, in practice, these angles are the reference inputs for the low-level controller.

4.2 \mathcal{L}_1 Adaptive Path-Following of Three Dimensional Curved Paths

Letting $x = [x_e, y_e, z_e, \psi_e]^\top$ and $u = [\phi_c, \gamma_c, \dot{s}]^\top$, equation (4.15) can be written in a compact form as follows

$$\dot{x} = f(x, u) + \zeta(t), \quad (4.16)$$

where

$$f(x, u) = \begin{bmatrix} V_a C \gamma_p C x_4 C u_2 + V_a S \gamma_p S u_2 - (1 - c_1(s) C \gamma_p x_2 + c_2(s) x_3) u_3 \\ V_a S x_4 C u_2 - (c_1(s) C \gamma_p x_1 + c_1(s) S \gamma_p x_3) u_3 \\ V_a S \gamma_p C x_4 C u_2 - V_a C \gamma_p S u_2 + (c_2(s) x_1 + c_1(s) S \gamma_p x_2) u_3 \\ \frac{g}{V_a} \tan u_1 - c_1(s) u_3 \end{bmatrix}$$

and

$$\zeta(t) = \begin{bmatrix} V_x(t) \\ V_y(t) \\ V_z(t) \\ 0 \end{bmatrix}.$$

The aim is to design the control law $u(t)$ that stabilizes the system, and consequently, steers the position of the UAV towards the desired path. To this end, a linearized model is first derived. For control design, it is assumed that a curved path can be approximated by an infinite number of waypoints (a set of waypoints with very small spacing).

This assumption leads to

$$x_p'' = y_p'' = z_p'' = 0,$$

which implies that

$$c_1(s) = c_2(s) = 0.$$

So, for the equilibrium point $x_{eq} = [x_{1eq} \ x_{2eq} \ x_{3eq} \ 0]^\top$, $u_{eq} = [0 \ \gamma_p \ V_a]^\top$ and $\zeta_{eq} = 0$, where x_{1eq} , x_{2eq} and x_{3eq} are arbitrary, the linearized state space model of (4.16) is given by

$$\dot{\bar{x}} = A_p \bar{x} + B_p \bar{u}, \quad (4.17)$$

where

$$A_p = \begin{bmatrix} 0 & 0 & 0 & 0 \\ 0 & 0 & 0 & V_a \\ 0 & 0 & 0 & 0 \\ 0 & 0 & 0 & 0 \end{bmatrix}$$

and

$$B_p = \begin{bmatrix} 0 & 0 & -1 \\ 0 & 0 & 0 \\ 0 & -V_a & 0 \\ \frac{g}{V_a} & 0 & 0 \end{bmatrix}.$$

Hence, the non-linear system in (4.16) can be written as follows

$$\dot{x} = A_p x + B_p u + \tilde{f}, \quad (4.18)$$

where $\tilde{f}(x, u, t)$ is a nonlinear function that includes the higher order terms of the Taylor series expansion of $f(x, u)$ and the external disturbance $\zeta(t)$.

Similarly, to what it was argued in the previous chapter, the system in (4.18) can be written as

$$\dot{x} = A_m x + B \omega u + (A_p - A_m)x + \tilde{f}, \quad (4.19)$$

where $A_m = A - B K_p$ is a Hurwitz matrix of the desired dynamics of the system, A is the system dynamics matrix for the nominal airspeed, B is the input matrix of the system with the nominal airspeed, $K_p \in \mathbb{R}^{3 \times 4}$ is the feedback matrix, and $\omega \in \mathbb{R}$ is an unknown gain.

For control design, the following approximation can be used

$$(A_p - A_m)x + \tilde{f} = B(\theta^\top x + \eta_m) + \eta_u, \quad (4.20)$$

where $\theta \in \mathbb{R}^{4 \times 3}$ is a matrix of unknown parameters, $\eta_m(t) \in \mathbb{R}^3$ is a vector of matched disturbances, and $\eta_u(t, x) \in \mathbb{R}^4$ is a vector of unmatched disturbances.

Consequently, the system in (4.19) leads to

$$\dot{x} = A_m x + B(\omega u + \theta^\top x + \eta_m) + \eta_u. \quad (4.21)$$

The resulting model is similar to (2.49), which makes straightforward application of the \mathcal{L}_1 adaptive controller defined in equations (2.50) to (2.57).

4.3 Simulation Results

The \mathcal{L}_1 adaptive controller was demonstrated through simulations of 3D path-following by a small fixed-wing UAV. The airspeed V_a was assumed to be regulated at $20m/s$. Gravity was $g = 9.81m/s^2$. It was further assumed that the maximum turn angle is $|\phi| = 60^\circ$.

The preceding cases, presented in 3 three, were considered, i.e., without wind, in the presence of steady wind, in time-varying wind, and in the situation where the airspeed of the UAV varies under wind effect.

In the first scenario, the objective was to follow a Dubins path, composed of a sequence of circular arcs and straight lines. In the second scenario, the objective was to show the controller performance on a helix path, which is a conventional benchmark for 3D path-following [16, 26, 36].

4.3.1 Simulation Results for a Dubins Path

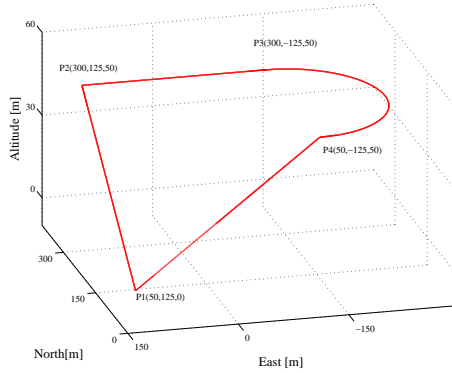


Figure 4.2: Desired 3D trajectory.

The desired path, shown on Fig. 4.2, is represented by three straight lines and a circular arc. The objective was that the UAV did a takeoff from P_1 , reached the altitude of $50m$ at P_2 , followed a straight-line until P_3 and made a circle turn at this altitude, until P_4 , it then performed a landing.

Performance Analysis without Wind

In Fig. 4.3a, it can be seen that the trajectory of the UAV is smooth and precise. The presence of peaks is due to the rolling motion of the UAV when turning at the waypoints. This can be confirmed by looking at Fig. 4.3b.

Performance Analysis in Constant Wind

In the second test, a constant wind was introduced, blowing with a velocity vector of $[0, 5, 5]^T m/s$. In Fig. 4.4a, it can be seen that the UAV follows

4 \mathcal{L}_1 Adaptive Guidance of Fixed-wing UAVs for 3D Curved Paths

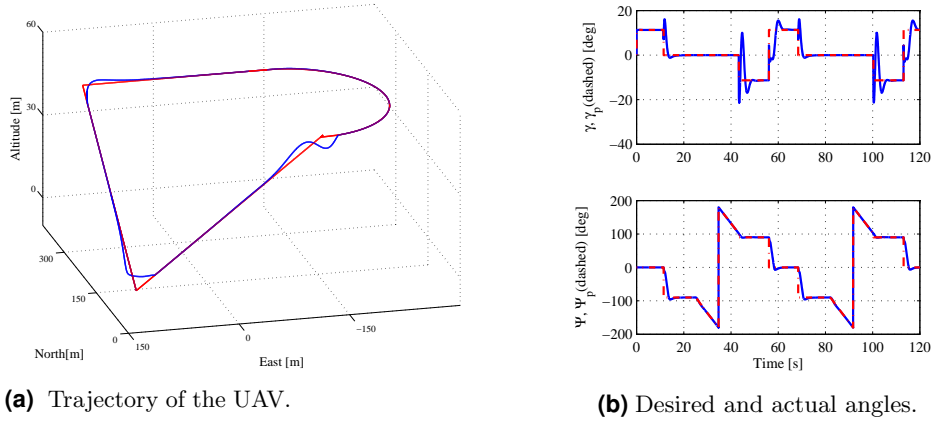


Figure 4.3: Dubins path-following without wind.

the desired path under these wind conditions. The trajectory of the UAV is smooth and precise in these relatively extreme wind conditions.

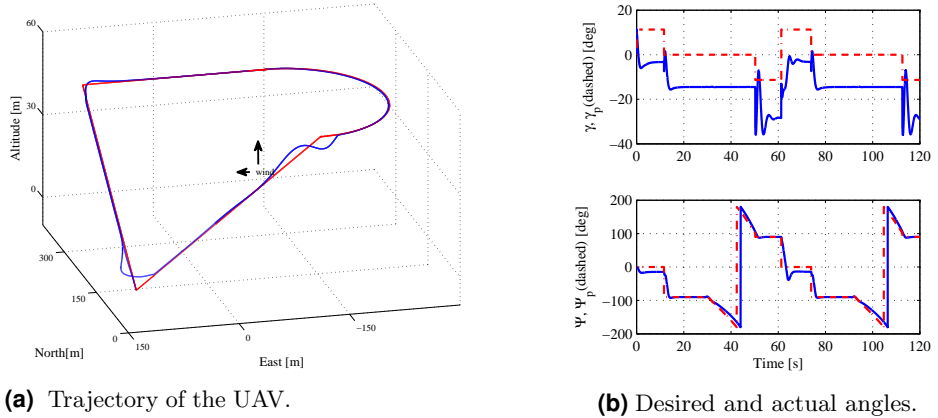


Figure 4.4: Dubins path-following in constant wind.

It can be also observed in Fig. 4.4b that the UAV produced the necessary deviation (crab) angles that compensated wind effect. It should be noted that the maximum value of the deviation angles is approximately equal to 15° which is reasonable in this situation.

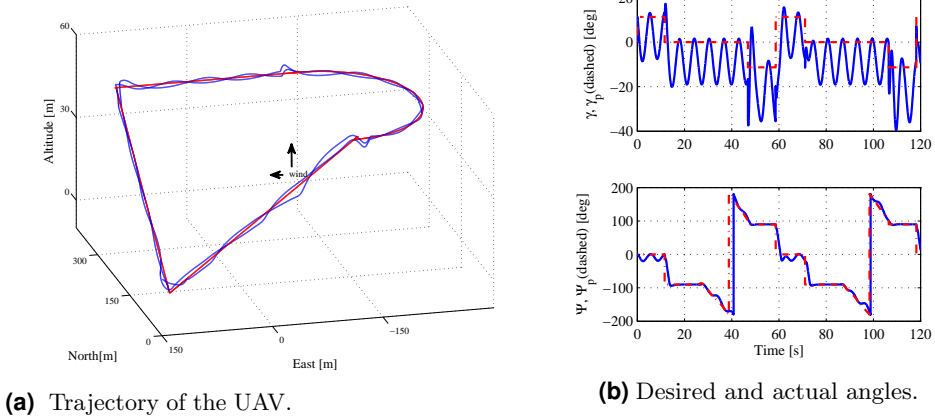


Figure 4.5: Dubins path-following in time-varying wind.

Performance Analysis in Time-Varying Wind

In the third test, a time-varying cross-wind was introduced, with a velocity that was assumed to be a periodic signal $[0, 3 + 3\sin(2\pi t), 3 + 3\sin(2\pi t)]^T m/s$.

As it can be observed in Fig. 4.5a, the controller performs well in the presence of time-varying wind disturbances. Moreover, it can be seen in Fig. 4.5b that the UAV produced the necessary sinusoidal crab angles that compensated wind effect.

Performance Analysis in Case of Varying Airspeed

In the next simulations, the situation where the UAV airspeed varies in the presence of wind was reproduced. Airspeed variations due to wind were created in a similar way as in chapter 3. The previous scenario of a constant wind, with a speed vector of $[0, 5, 5]^T m/s$, was considered.

It can be observed in Fig. 4.6a and Fig. 4.6b that the controller has maintained good performance in the presence of airspeed variations, resulting from flying in relatively strong wind. This confirms the results obtained in the previous chapter.

Furthermore, it can be observed in Fig. 4.7a, Fig. 4.8a, Fig. 4.9a, and Fig. 4.10a, that the necessary commands of the bank angle ϕ_c and path angle γ_c were produced to counteract wind disturbance. As shown in Fig. 4.7b, Fig. 4.8b, Fig. 4.9b, and Fig. 4.10b, the maximal long-track error x_e , cross-track error y_e and altitude error z_e , are within reasonable limits, considering

4 \mathcal{L}_1 Adaptive Guidance of Fixed-wing UAVs for 3D Curved Paths

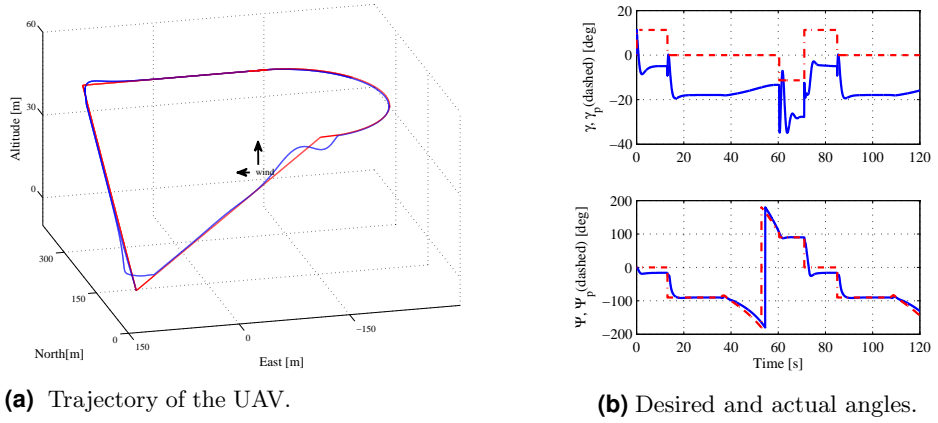


Figure 4.6: Dubins path-following with varying airspeed.

that this wind condition is extreme for such a small UAV. It can also be noted that the speed of the virtual target is accelerated or slowed as necessary.

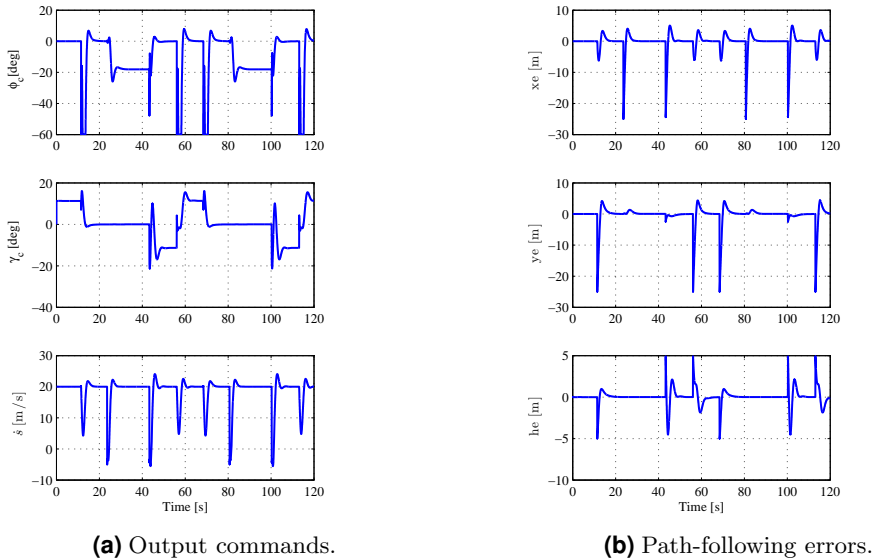
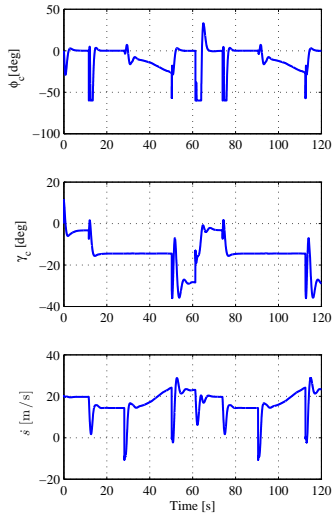
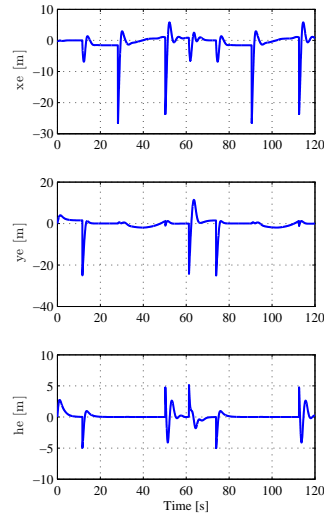


Figure 4.7: System parameters for Dubins path-following without wind.

4.3 Simulation Results

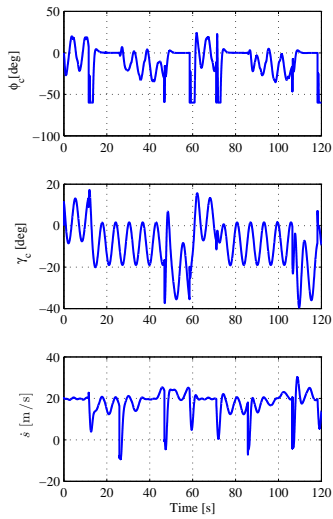


(a) Output commands.

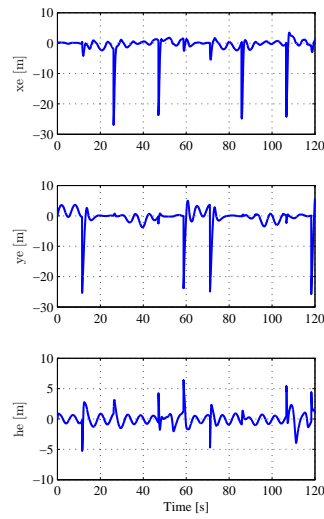


(b) Path-following errors.

Figure 4.8: System parameters for Dubins path-following in constant wind.

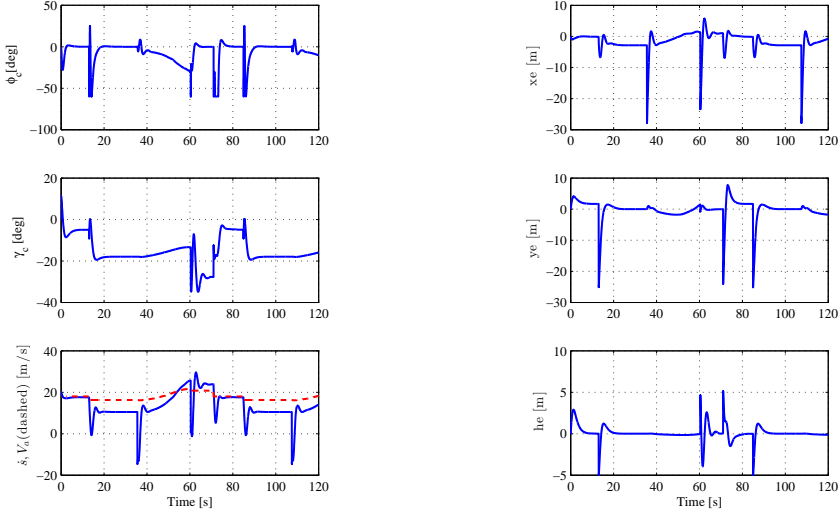


(a) Output commands.



(b) Path-following errors.

Figure 4.9: System parameters for Dubins path-following in time-varying wind.



(a) Output commands.

(b) Path-following errors.

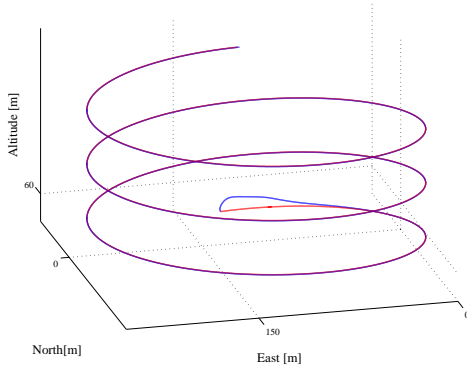
Figure 4.10: System parameters for Dubins path-following with time-varying airspeed.

4.3.2 Simulation Results for a Helix Path

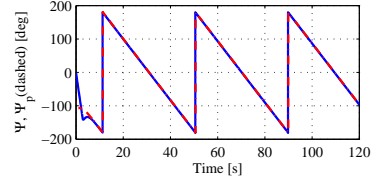
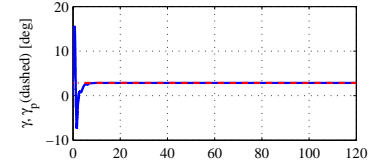
Simulation results for helix path-following were conducted with the same tuning parameters as for the previously designed controller. The preceding cases were considered, i.e., without wind, in the presence of steady wind, in time-varying wind, and in the situation where the airspeed of the UAV varies under wind effect.

As it is shown in Fig. 4.11, Fig. 4.12, Fig. 4.13, and Fig. 4.14, the designed controller performed well when following a helix path. The UAV follows the desired path in the different cases, and its trajectory is smooth and precise. The maximum values of deviation angles are reasonable while taking into account these relatively extreme wind conditions.

Furthermore, it can be seen in Fig. 4.15, Fig. 4.16, Fig. 4.17, and Fig. 4.18 that the controller was able to produce the necessary commands of the bank angle ϕ_c and path angle γ_c counteract wind disturbance. The maximal long-track error x_e , cross-track error y_e and altitude error z_e are within reasonable limits, and the speed of the virtual target is accelerated or slowed as necessary.

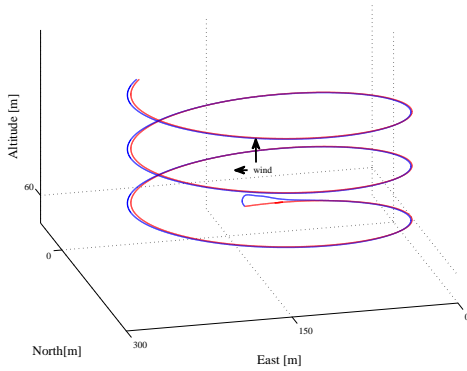


(a) Trajectory of the UAV.

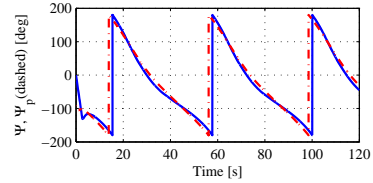
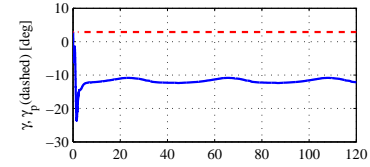


(b) Desired and actual angles.

Figure 4.11: Helix path-following without wind.



(a) Trajectory of the UAV.



(b) Desired and actual angles.

Figure 4.12: Helix path-following in constant wind.

4.4 Summary

In this chapter, an approach for adaptive 3D path-following by a small fixed-wing UAV was presented. General curved paths were considered here. Similar to the 2D path-following, the proposed approach was based on \mathcal{L}_1 adaptive control for disturbances of unknown bounds. The considered model for control was the error of the position of the UAV relative to a virtual target that moved on the desired path. The speed of the moving target was considered as a control input for the system.

4 \mathcal{L}_1 Adaptive Guidance of Fixed-wing UAVs for 3D Curved Paths

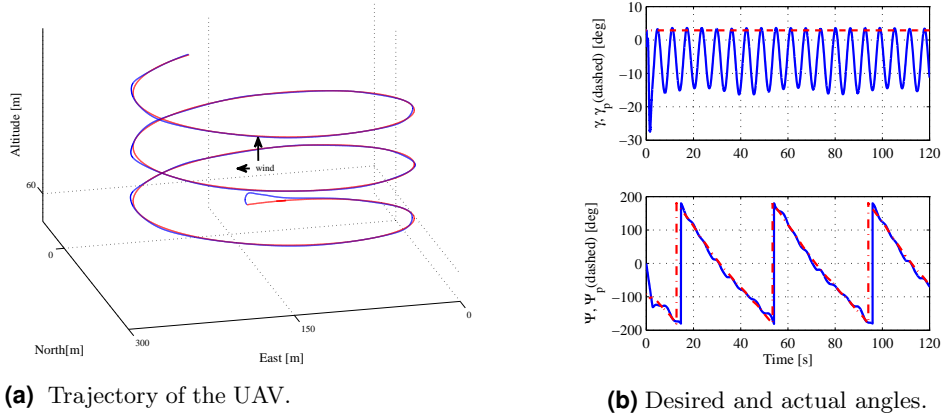


Figure 4.13: Helix path-following in time-varying wind.

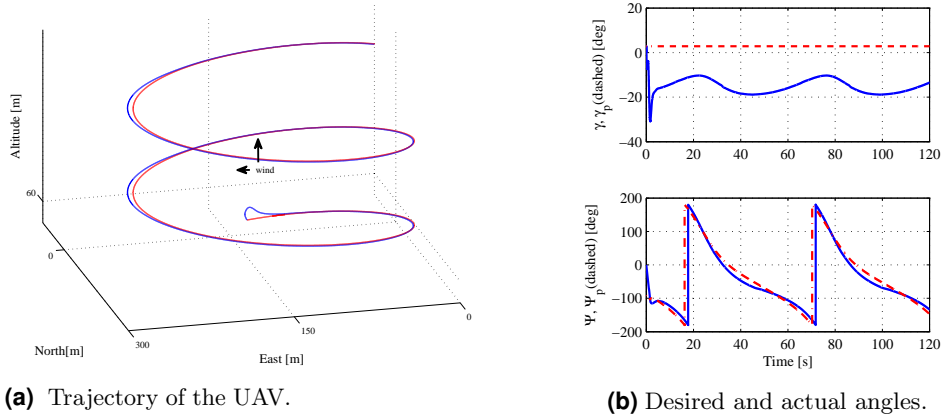
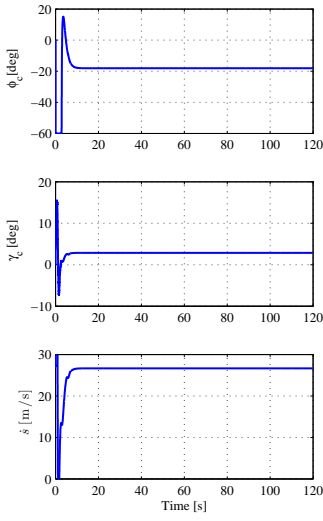
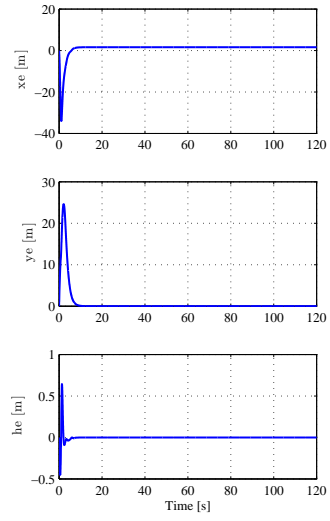


Figure 4.14: Helix path-following with time-varying airspeed.

Compared with previous approaches for path-following based on a moving target, this method relaxes what is commonly assumed namely that wind speed is constant.

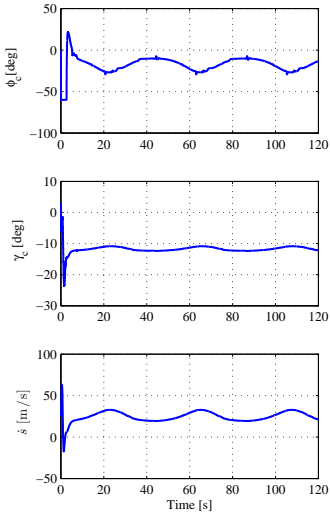


(a) Output commands.

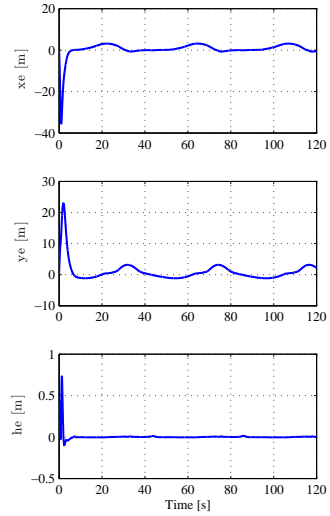


(b) Path-following errors.

Figure 4.15: System parameters for helix path-following without wind.



(a) Output commands.



(b) Path-following errors.

Figure 4.16: System parameters for helix path-following in constant wind.

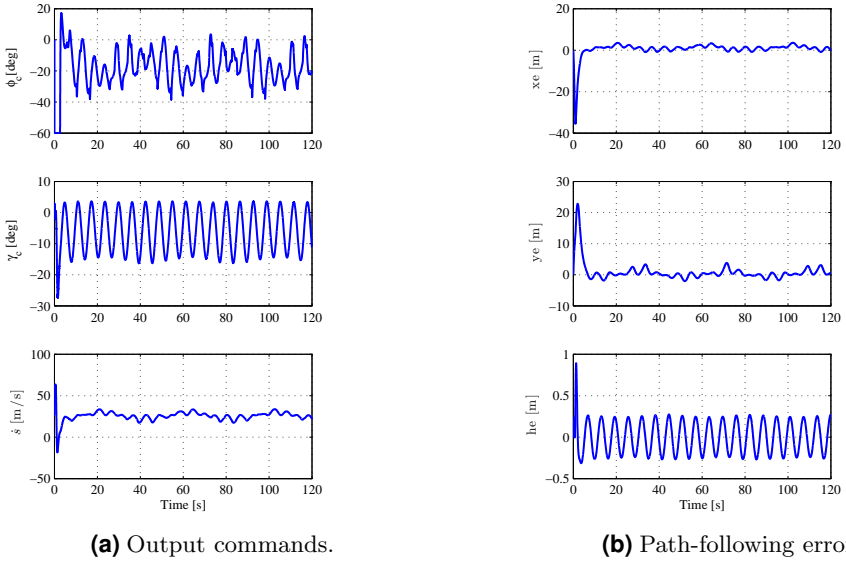


Figure 4.17: System parameters for helix path-following in time-varying wind.

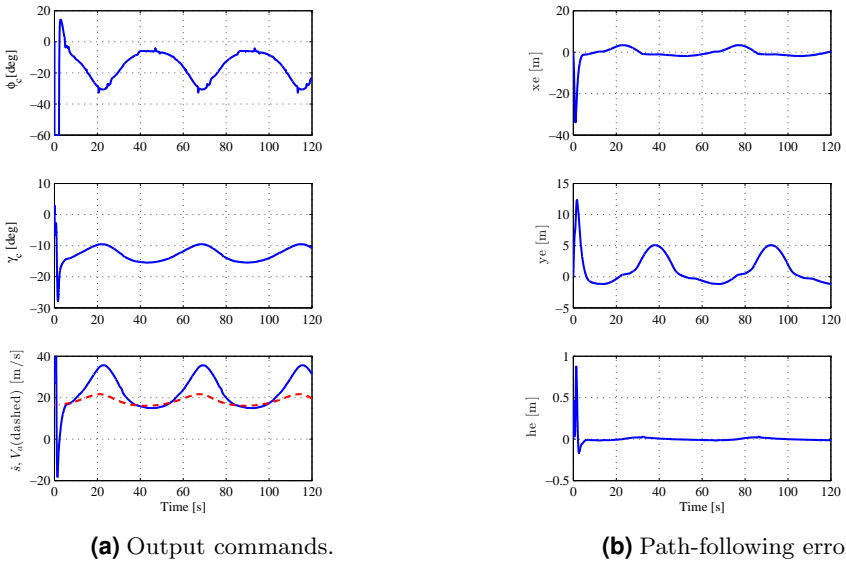


Figure 4.18: System parameters for helix path-following with time-varying airspeed.

Chapter 5

5 Fault-Tolerant \mathcal{L}_1 Adaptive Control Based on Multiple Models

5.1	Multiple Model \mathcal{L}_1 Adaptive Control of SISO Systems	70
5.1.1	Controller Design	71
5.1.2	The Switching Logic	73
5.1.3	Controller Analysis	74
5.2	Control of a Small UAV in Case of Inversion of the Elevator Command	76
5.2.1	Controller Design	76
5.2.2	Simulation Results	77
5.3	Multiple Model \mathcal{L}_1 Adaptive Control of MIMO Systems	79
5.4	UAV Lateral-Directional Control in Case of Inversion of the Commands	82
5.4.1	Controller Design	82
5.4.2	Simulation Results	83
5.5	Summary	85

Despite the excellent performance of \mathcal{L}_1 adaptive control, for fault-tolerant control [29, 28, 81], it is still true that when the uncertainties induced by disturbances, faults or failures are too large, they may reduce the performance of the controller or even make the system unstable. Actually, if a fault or failure occurs on the system, the unknown parameters may go outside

the predefined sets of the control design, which may lead to poor system performance or more critically to system instability.

This chapter, based on [98], proposes a solution to this problem, which uses a multiple model \mathcal{L}_1 adaptive controller. The key idea is to design an \mathcal{L}_1 adaptive controller with a nominal reference model and a set of degraded reference models. The nominal model is the model with desired dynamics that are optimal regarding some specific criteria. A degraded model does not necessarily verify these specifications. It is designed to ensure system robustness in the presence of large uncertainties.

The objectives of this chapter are:

- Introducing a new approach for fault-tolerant control based on performance degradation of the nominal \mathcal{L}_1 adaptive controller.
- Proving the performance bounds of the architecture for both system input and output.
- Extending the obtained results for SISO systems to MIMO systems.
- Applying the design to the control of a small UAV in case of inversion of the control direction, and showing, with simulation results, that the multiple model \mathcal{L}_1 adaptive controller outperforms the classical controller with one nominal model.

5.1 Multiple Model \mathcal{L}_1 Adaptive Control of SISO Systems

Given the following class of nonlinear systems

$$\dot{x}(t) = A_p x(t) + b_p u(t) + f(t, x), \quad x(0) = x_0, \quad (5.1)$$

where $A_p \in \mathbb{R}^{n \times n}$ is an unknown matrix, $b_p \in \mathbb{R}^n$ is an unknown vector, $x(t) \in \mathbb{R}^n$ is the state vector, $u(t) \in \mathbb{R}$ is the control input, and $f(t, x) \in \mathbb{R}$ is an unknown nonlinear function.

The system, with its nominal desired dynamics for \mathcal{L}_1 adaptive control design, can be parameterized to become similar with the class of SISO systems considered in chapter 2 equation (2.1), defined by

$$\dot{x}(t) = A_{m(0)} x(t) + b_0 (\omega_0 u(t) + \theta_0^\top x(t) + \eta_{m(0)}(t)) + \eta_{u(0)}(t, x), \quad (5.2)$$

where $A_{m(0)} \in \mathbb{R}^{n \times n}$ is a known Hurwitz matrix that defines the desired dynamics of the system, $b_0 \in \mathbb{R}^n$ is the desired input vector, $\omega_0 \in \mathbb{R}$ is an unknown constant with known sign that represents the model input uncertainties, $\theta_0 \in \mathbb{R}^n$ is a vector of unknown constant parameters that represents the model uncertainties, $\eta_{m(0)} \in \mathbb{R}$ is an unknown matched disturbance, and $\eta_{u(0)} \in \mathbb{R}^n$ is an unknown unmatched disturbance.

Assumption 5.1 The unknown parameters are bounded, i.e., $\theta_0 \in \Theta_0$, where Θ_0 is a known compact convex set and $0 < \omega_{l(0)} \leq \omega_0 \leq \omega_{u(0)}$. Furthermore, the non-linear functions $\eta_{m(0)}$ and $\eta_{u(0)}$ are uniformly bounded, i.e., there exist unknown real constants $L_{m(0)} > 0$ and $L_{u(0)} > 0$, such that for all $t \geq 0$ $|\eta_{m(0)}(t)| \leq L_{m(0)}$ and $\|\eta_{u(0)}(t, x)\| \leq L_{u(0)}$.

Considering probable faults scenarios, a set of plant parameterizations, based on degraded models, is arranged, and the objective is that the adequate controller is selected automatically to deal with every situation. This means that the model which is the best match of the plant is selected.

The desired performance of each model is made through the design of the pair $(A_{m(i)}, b_i)$, for $i = 0 \dots M$, where M is the number of the degraded models. The system in (5.1) can, consequently, be parameterized as follows

$$\dot{x}(t) = A_{m(i)}x(t) + b_i(\omega_i u(t) + \theta_i^\top x(t) + \eta_{m(i)}(t)) + \eta_{u(i)}(t, x). \quad (5.3)$$

Assumption 5.2 The unknown parameters are within different known bounds, i.e., $\theta_i \in \Theta_i$ where Θ_i is a known compact convex set, and $0 < \omega_{l(i)} \leq \omega_i \leq \omega_{u(i)}$. Furthermore, the nonlinear functions $\eta_{m(i)}(t)$, and $\eta_{u(i)}(t, x)$ are uniformly bounded, i.e., there exists unknown real constants $L_{m(i)} > 0$ and $L_{u(i)} > 0$ such that for all $t \geq 0$ the following bounds hold

$$|\eta_{m(i)}(t)| \leq L_{m(i)} \text{ and } \|\eta_{u(i)}(t, x)\| \leq L_{u(i)}.$$

5.1.1 Controller Design

The multiple model \mathcal{L}_1 adaptive controller, as shown in Fig. 5.1, is composed of a set of state predictors, a set of adaptation laws, a set of control laws and a control input selector (switching system).

The state predictors are given by

$$\dot{\hat{x}}_i(t) = A_{m(i)}\hat{x}_i(t) + b_i(\hat{\omega}_i(t)u(t) + \hat{\theta}_i^\top(t)x(t) + \hat{\eta}_{m(i)}(t)) + \hat{\eta}_{u(i)}(t), \quad (5.4)$$

where $\hat{x}_i(t)$ are the predicted states, and $\hat{\theta}_i(t)$, $\hat{\omega}_i(t)$, $\hat{\eta}_{m(i)}(t)$, and $\hat{\eta}_{u(i)}(t)$ are the estimates of the unknown parameters and external disturbances.

5 Fault-Tolerant \mathcal{L}_1 Adaptive Control Based on Multiple Models

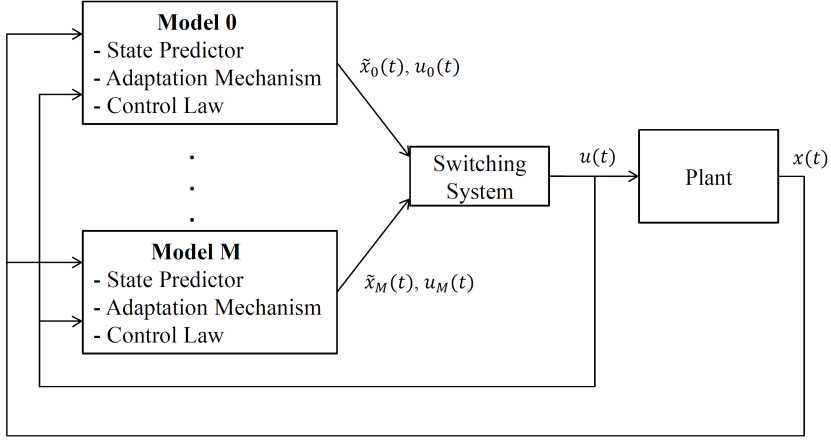


Figure 5.1: Block diagram of the multiple model \mathcal{L}_1 adaptive controller.

The sliding surfaces are defined by

$$\sigma_i(t) = \lambda_i \tilde{x}_i(t), \quad (5.5)$$

where $\tilde{x}_i(t) = \hat{x}_i(t) - x(t)$ are the state estimation errors and $\lambda_i \in \mathbb{R}^{1 \times n}$ are constant row vectors, chosen such that $\lambda_i b_i \neq 0$ and the coefficients of the vectors form stable manifolds.

The adaptation laws are given by

$$\begin{aligned} \dot{\hat{\omega}}_i(t) &= -\Gamma_i \text{Proj}(\hat{\omega}_i(t), \lambda_i b_i \sigma_i(t) u(t)), \\ \dot{\hat{\theta}}_i(t) &= -\Gamma_i \text{Proj}(\hat{\theta}_i(t), \lambda_i b_i \sigma_i(t) x(t)), \\ \hat{\eta}_{m(i)}(t) &= -(\lambda_i b_i)^{-1} (\lambda_i A_{m(i)} \tilde{x}_i(t) + \rho_i \sigma_i(t)) - \hat{L}_{m(i)}(t) \frac{\lambda_i b_i \sigma_i(t)}{|\lambda_i b_i \sigma_i(t)|}, \\ \hat{\eta}_{u(i)}(t) &= -\hat{L}_{u(i)}(t) \frac{(\lambda_i \sigma_i(t))^\top}{\|\lambda_i \sigma_i(t)\|}, \\ \dot{\hat{L}}_{m(i)}(t) &= \Gamma_i |\lambda_i b_i \sigma_i(t)|, \\ \dot{\hat{L}}_{u(i)}(t) &= \Gamma_i \|\lambda_i \sigma_i(t)\|, \end{aligned} \quad (5.6)$$

where $\rho_i > 0$ are arbitrary and $\Gamma_i \in \mathbb{R}^+$ are the adaptation rates.

The control laws are given by

$$u_i(s) = k_i D_i(s) \left(k_{g(i)} r(s) - \hat{v}_i(s) - \phi_i(s) \hat{\eta}_{u(i)}(s) \right), \quad (5.7)$$

where $\hat{v}_i(s)$ are the Laplace transformations of the terms $\hat{\theta}_i^\top(t)x(t) + \hat{\omega}_i(t)u_i(t) + \hat{\eta}_{m(i)}(t)$, $\phi_i(s) = c^\top(sI - A_{m(i)})^{-1}H_{m(i)}^{-1}$ with $H_{m(i)} = c^\top(A_{m(i)})^{-1}b_i$, $\hat{\eta}_{u(i)}(s)$ are the Laplace transformations of $\hat{\eta}_{u(i)}(t)$, $k_{g(i)}$ are the static gains, $k_i > 0$, and $D_i(s)$ are transfer functions that lead to strictly proper stable filters $C_i(s) = \omega k_i D_i(s)/(1 + \omega k_i D_i(s))$ with $C_i(0) = 1$.

5.1.2 The Switching Logic

The quadratic criterion with forgetting factor is used to select the adequate controller for the plant. It is given from [76] by

$$\min_{i=0..M} \left\{ J_i(t) = c_1 \|\tilde{x}_i(t)\|^2 + c_2 \int_0^t e^{-c_3(t-\tau)} \|\tilde{x}_i(\tau)\|^2 d\tau \right\}, \quad (5.8)$$

where c_1 , c_2 and c_3 are arbitrary positive reals.

The \mathcal{L}_1 adaptive controller which minimizes the criterion in (5.8) is the best match for the system in (5.1). As a consequence, its control output is selected by the switching logic and becomes the control law $u(t)$ to be applied to the plant.

It was shown in [4] that the switching does not result in an unstable closed-loop for multiple model reference adaptive controllers (MRAC). This result is, consequently, valid for the \mathcal{L}_1 adaptive controller as well.

The system, with the selected \mathcal{L}_1 adaptive controller, can be parameterized as follows

$$\dot{x}(t) = A_{m(*)}x(t) + b_*(\omega_*u(t) + \theta_*^\top x(t) + \eta_{m(*)}(t)) + \eta_{u(*)}(t, x). \quad (5.9)$$

The selected control law can be written as follows

$$u(s) = k_* D_*(s) \left(k_{g(*)} r(s) - \hat{v}_*(s) - \phi_*(s) \hat{\eta}_{u(*)}(s) \right), \quad (5.10)$$

where $\hat{v}_*(s)$ is the Laplace transformation of the term $\hat{\theta}_*^\top(t)x(t) + \hat{\omega}_*(t)u(t) + \hat{\eta}_{m(*)}(t)$, $\phi_*(s) = c^\top(sI - A_{m(*)})^{-1}H_{m(*)}^{-1}$ with $H_{m(*)} = c^\top(A_{m(*)})^{-1}b_*$, $\hat{\eta}_{u(*)}(s)$ is the Laplace transformation of $\hat{\eta}_{u(*)}(t)$, $k_{g(*)}$ is the static gain of the selected controller, $k_* > 0$ is arbitrary, and $D_*(s)$ is a transfer function that leads to a strictly proper stable filter $C_*(s) = \omega k_* D_*(s)/(1 + \omega k_* D_*(s))$ with $C_*(0) = 1$.

5.1.3 Controller Analysis

Let

$$L_* = \max_{\theta_* \in \Theta_*} \|\theta_*\|_1, \quad H_*(s) = (sI - A_{m(*)})^{-1}b_*, \quad G_*(s) = (1 - C_*(s))H_*(s).$$

The selected \mathcal{L}_1 adaptive controller defined by equations (5.9) and (5.10) is subject to the following \mathcal{L}_1 -norm condition

$$\|G_*(s)\|_{\mathcal{L}_1} L_* < 1. \quad (5.11)$$

Moreover, the design of k_* and $D_*(s)$ needs to ensure that

$$G_{u*}(s) = (s\mathbb{I} - A_{m(*)})^{-1} - C_*(s)H_*(s)\phi_*(s), \quad (5.12)$$

is proper and stable.

Closed-Loop Reference System

The selected controller with the nominal parameters of the system is the reference model, defined by

$$\begin{aligned} \dot{x}_r(t) &= A_{m(*)}x_r(t) + b_*(\omega_*u_r(t) + \theta_*^\top x_r(t) + \eta_{m(*)}(t)) + \eta_{u(*)}(t, x_r), \\ y_r(t) &= c^\top x_r(t), \end{aligned} \quad (5.13)$$

where ω_* , θ_* , $\eta_{m(*)}(t)$ and $\eta_{u(*)}(t, x_r)$ are the nominal parameters of the selected model.

The control law for the reference system is given by

$$u_r(s) = \frac{C_*(s)}{\omega_*} \left(k_{g(*)}r(s) - \theta_*^\top x_r(s) - \eta_{m(*)}(s) - \phi_*(s)\eta_{u(*)}(s) \right), \quad (5.14)$$

where $\eta_{m(*)}(s)$ and $\eta_{u(*)}(s)$ are the Laplace transformations of $\eta_{m(*)}(t)$ and $\eta_{u(*)}(t, x_r)$ respectively.

The stability of the closed-loop reference system is stated through the following Lemma.

Lemma 5.1 If the filter $C_*(s)$ is designed such that it verifies the \mathcal{L}_1 -norm condition in (5.11) and the requirement in (5.12), then the closed-loop reference system in (5.13) and (5.14) is BIBS stable with respect to the reference input and initial conditions.

The proof is similar to Lemma 2.1 and is omitted here.

Transient and Steady-State Performance

In the following Lemma, it is stated that the prediction errors $\tilde{x}_i(t)$ and the estimation errors of the unknown parameters are bounded for $i = 0 \dots M$.

Lemma 5.2 The following bounds hold for the norm of the prediction errors

$$\|\tilde{x}_i\|_{\mathcal{L}_\infty} \leq \rho_i, \quad (5.15)$$

where $\rho_i > 0$ are arbitrary small reals.

Furthermore, if the closed-loop system is stable then the prediction errors $\tilde{x}_i(t)$ converge to zero, i.e.,

$$\lim_{t \rightarrow \infty} \tilde{x}_i(t) = 0. \quad (5.16)$$

The proof is similar to Lemma 2.2 and is omitted here.

In the following Theorem, it is shown that the performance bounds of closed-loop system, generated by the selected model, are bounded.

Theorem 5.1 Given the system (5.9), the reference system (5.13), (5.14) and the selected \mathcal{L}_1 adaptive model (5.9) and (5.10), we have

$$\|x_r - x_*\|_{\mathcal{L}_\infty} \leq \gamma_{1*}, \quad (5.17)$$

and

$$\|u_r - u_*\|_{\mathcal{L}_\infty} \leq \gamma_{2*}, \quad (5.18)$$

where

$$\begin{aligned} \gamma_{1*} = & 2 \frac{\|G_*(s)\|_{\mathcal{L}_1}}{1 - \|G_*(s)\|_{\mathcal{L}_1} L_*} L_{m(*)} + 2 \frac{\|G_{u(*)}\|_{\mathcal{L}_1}}{1 - \|G_*(s)\|_{\mathcal{L}_1} L_*} L_{u(*)} \\ & + \frac{\|H_*(s)C_*(s)H_{m(*)}^{-1}(s)c^\top\|_{\mathcal{L}_1}}{1 - \|G_*(s)\|_{\mathcal{L}_1} L} \rho_*, \end{aligned}$$

and

$$\gamma_{2*} = \left\| \frac{C_*(s)}{\omega} \right\|_{\mathcal{L}_1} \left(L_* \gamma_{1*} + 2(L_{m(*)} + \|\phi_*(s)\|_{\mathcal{L}_1} L_{u(*)}) \right) + \left\| \frac{H_{1(*)}c^\top}{\omega} \right\|_{\mathcal{L}_1} \rho_*.$$

The proof is similar to Theorem 2.1 and is omitted here.

In the following, the multiple model \mathcal{L}_1 adaptive controller is applied to the control of the pitch rate of a small fixed-wing UAV under a critical failure of the elevator.

5.2 Control of a Small UAV in Case of Inversion of the Elevator Command

A critical situation in flight control systems is that in case of structural damage of the aircraft, the control direction can be inverted. Actually, if an aircraft suffer damage, a control surface may generate a totally opposite angular acceleration, which means the actuation signs will be changed [70, 103]. For this reason control systems of UAVs, subject to possible damage, such as those employed in battlefields, have to take into account this situation. The inversion of the sign of the control direction can also result from hardware or software faults.

This situation cannot be handled by an \mathcal{L}_1 adaptive controller with only one model. Actually, a conservative condition in adaptive control is that the sign of the input vector must be known and should not change [53]. The proposed solution is the application of the multiple model \mathcal{L}_1 adaptive controller.

5.2.1 Controller Design

The model of the short-period dynamics of a fixed-wing aircraft is described by the set of states (α, q) , where α is the angle of attack and q is the pitch rate. The control input is the elevator deflection δ_e .

The objective is to design a control input $u(t) = \delta_e$ to enable tracking of the pitch rate command $q_c(t)$.

From [100], the model of the short-period dynamics of a fixed-wing aircraft can be written in matrix form as follows

$$\underbrace{\begin{bmatrix} \dot{\alpha} \\ \dot{q} \end{bmatrix}}_{\dot{x}} = \underbrace{\begin{bmatrix} \frac{Z_\alpha}{V_a} & 1 + \frac{Z_q}{V_a} \\ M_\alpha & M_q \end{bmatrix}}_{A_p} \underbrace{\begin{bmatrix} \alpha \\ q \end{bmatrix}}_x + \underbrace{\begin{bmatrix} \frac{Z_{\delta_e}}{V_a} \\ M_{\delta_e} \end{bmatrix}}_{b_p} \underbrace{\delta_e}_u, \quad (5.19)$$

where V_a is the trimmed airspeed, $(Z_\alpha, Z_q, Z_{\delta_e})$ and $(M_\alpha, M_q, M_{\delta_e})$ are fixed-wing aircrafts stability derivatives. It should be noted that the stability derivatives can not be measured, and they vary depending on flight conditions [100].

Taking into account the model uncertainties and the external disturbances, the system in (5.19) can be extended as follows

$$\dot{x}(t) = A_p x(t) + b_p u(t) + f(t, x). \quad (5.20)$$

5.2 Control of a Small UAV in Case of Inversion of the Elevator Command

The system with its nominal desired dynamics can be parameterized to become similar to the class of SISO systems in (5.2) defined by

$$\dot{x}(t) = A_{m(0)}x(t) + b_0(\omega_0 u(t) + \theta_0^\top x(t) + \eta_{m(0)}(t)) + \eta_{u(0)}(t, x). \quad (5.21)$$

A second model for the case of inversion of the elevator direction is given by

$$\dot{x}(t) = A_{m(1)}x(t) - b_0(\omega_1 u(t) + \theta_1^\top x(t) + \eta_{m(1)}(t)) + \eta_{u(1)}(t, x). \quad (5.22)$$

The input vector b_0 was taken to be the same for both models.

5.2.2 Simulation Results

For the nominal controller, the eigenvalues of the desired dynamics matrix $A_{m(0)}$ were chosen $\lambda_{1,2} = -5.6 \pm 4.2j$, i. e., a pulsation $\omega_n = 7 \text{ rad/s}$ and a damping $\xi = 0.8$. The compact set of the unknown parameters was $\Theta_0 = [-5, 5]$. The unknown input gain was within the interval $[0.25, 1.75]$. The filter parameters were $D_0(s) = 1/s$, and $k_0 = 350$. The adaptation rate was $\Gamma_0 = 1000$.

To show the efficiency of the designed control scheme in a "standard" failure situation, the following uncertainties were added to the system at simulation time $t = 7s$:

- Linear-in-state uncertainty representing 50% decrease in static stability M_α and loose of margin stability $M_q = 0$;
- Control loss of effectiveness $\omega = 0.5$;
- Matched disturbance $\eta_m(t) = \sin(2\pi t)$ deg;
- Unmatched disturbance $\eta_u(t) = [0, \quad 1]^\top$.

The simulations were made using only the nominal controller.

As seen in Fig. 5.2, the \mathcal{L}_1 adaptive controller copes well with large parameter uncertainties and shows good tracking performance in steady state. Moreover, the elevator command is within acceptable limits.

In the second scenario, the previous parametric uncertainties were introduced, but it was assumed that the control loss of effectiveness is $\omega = -0.5$, which means that the sign of the control input has changed. As it can be

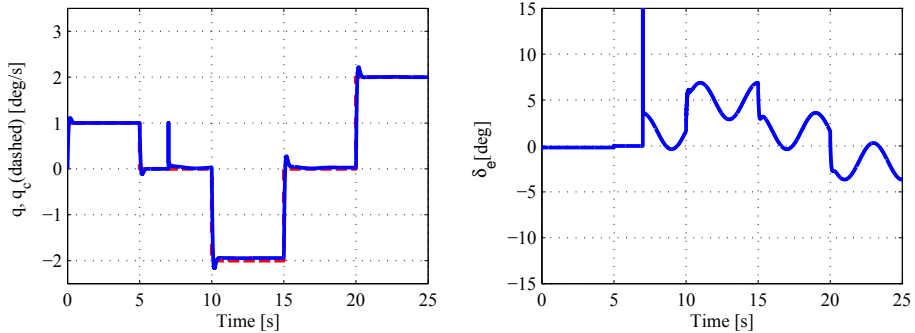


Figure 5.2: Closed-loop tracking performance of the nominal controller in a "standard" failure situation.

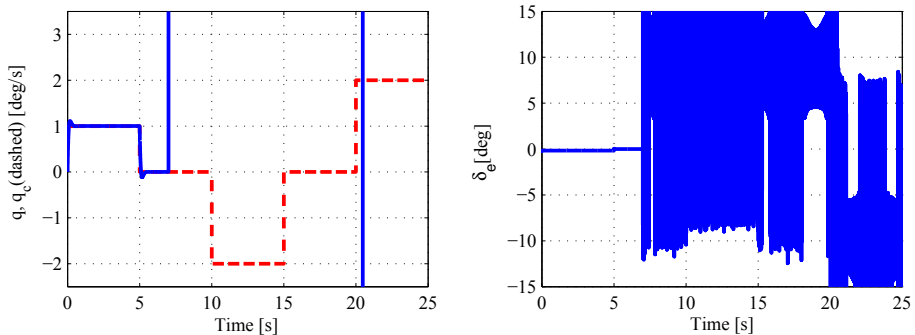


Figure 5.3: Closed-loop tracking performance of the nominal controller in case of inversion of the sign.

observed in Fig. 5.3, the control system with only the nominal controller has become unstable.

Next, the multiple model controller was applied. The tuning parameters and the desired dynamics of the degraded controller were the same as the nominal controller. It can be observed in Fig. 5.4 that the multiple model controller has maintained stability and good tracking performance of the system in a situation where the system with only one nominal model has failed. Furthermore, it is shown in Fig. 5.5 that before the inversion of the control input at simulation time $t = 7$ s, the system was controlled by the nominal model, and it switches to the degraded model immediately after the occurrence of the failure.

These simulations conclude that the multiple model \mathcal{L}_1 adaptive controller

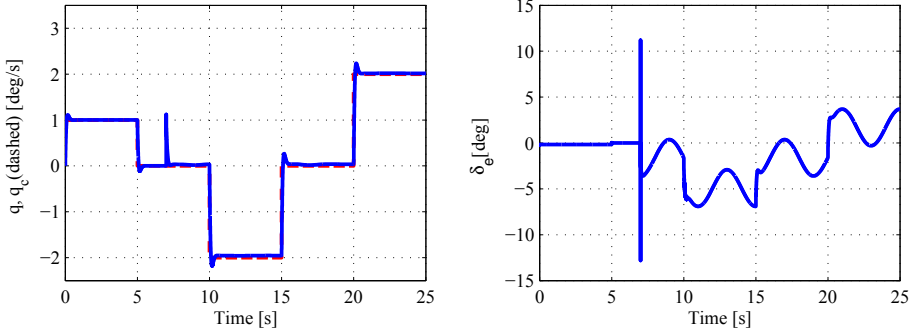


Figure 5.4: Closed-loop tracking performance of the multiple model controller in case of inversion of the sign.

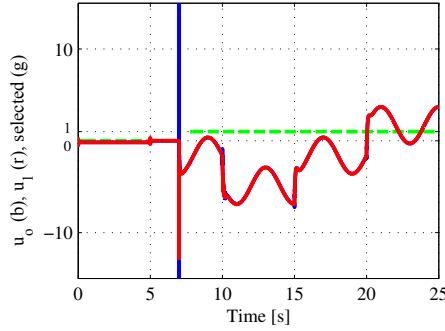


Figure 5.5: Switching of the output commands of the multiple model controller.

is better performing, in case of hard failures, such as the inversion of the direction of the input vector, than the controller with one model. So, its application in the control of safety-critical systems is justified.

5.3 Multiple Model \mathcal{L}_1 Adaptive Control of MIMO Systems

In the following, the proposed approach is extended to the control of Multi-Input Multi-Output systems.

Given the the following class of nonlinear systems

$$\dot{x}(t) = A_p x(t) + B_p u(t) + f(t, x), \quad x(0) = x_0, \quad (5.23)$$

5 Fault-Tolerant \mathcal{L}_1 Adaptive Control Based on Multiple Models

where $A_p \in \mathbb{R}^{n \times n}$ is an unknown matrix, $B_p \in \mathbb{R}^{n \times m}$ is an unknown matrix, $x(t) \in \mathbb{R}^n$ is the state vector which is assumed to be available through measurement, $u(t) \in \mathbb{R}^m$ is the control input vector and $f(t, x) \in \mathbb{R}^n$ is a vector of unknown nonlinear functions.

The desired performance of each model is made through the design of the pair $(A_{m(i)}, B_i)$, for $i = 0 \dots M$, where M is the number of the degraded models.

The system in (5.23) can, consequently, be parameterized as follows

$$\dot{x}(t) = A_{m(i)}x(t) + B_i(\omega_i u(t) + \theta_i^\top x(t) + \eta_{m(i)}(t)) + \eta_{u(i)}(t, x), \quad (5.24)$$

where $A_{m(i)} \in \mathbb{R}^{n \times n}$ are known Hurwitz matrices that define the desired dynamics of the system $B_i \in \mathbb{R}^{n \times m}$ are the desired input matrices, $\omega_i \in \mathbb{R}^{m \times m}$ are unknown constant matrices representing the system input gain, $\theta_i^\top \in \mathbb{R}^{m \times n}$ are matrices of constant unknown parameters representing model uncertainties, $\eta_{m(i)}(t) \in \mathbb{R}^m$ are unknown matched disturbances, and $\eta_{u(i)}(t, x) \in \mathbb{R}^n$ are unknown unmatched disturbances.

Assumption 5.3 The system input gain matrices ω_i are assumed to be unknown (non-singular) strictly row-diagonally dominant matrices with known signs of diagonals. Also, it is assumed that the unknown parameters are bounded, i.e., $\theta_i \in \Theta_i$, where Θ_i are known compact convex sets. Furthermore, the functions $\eta_{m(i)}$ and $\eta_{u(i)}$ are uniformly bounded, i.e., there exist unknown real constants $L_{m(i)} > 0$ and $L_{u(i)} > 0$, such that for all $t \geq 0$ $|\eta_{m(i)}(t)| \leq L_{m(i)}$ and $\|\eta_{u(i)}(t, x)\| \leq L_{u(i)}$.

Similar to SISO systems, the multiple model \mathcal{L}_1 adaptive controller of MIMO systems is composed of a set of state predictors, a set of adaptation laws, a set of control laws and a control signal selector.

The state predictors are defined by

$$\dot{\hat{x}}_i(t) = A_{m(i)}\hat{x}_i(t) + B_i(\hat{\omega}_i(t)u(t) + \hat{\theta}_i^\top(t)x(t) + \hat{\eta}_{m(i)}(t)) + \hat{\eta}_{u(i)}(t), \quad (5.25)$$

where $\hat{x}_i(t)$ are the predicted states and, $\hat{\theta}_i(t)$, $\hat{\omega}_i(t)$, $\hat{\eta}_{m(i)}(t)$, and $\hat{\eta}_{u(i)}(t)$ are the estimates of the unknown system parameters and external disturbances.

The sliding surfaces are given by

$$\sigma_i(t) = \lambda_i \tilde{x}_i(t), \quad (5.26)$$

where $\tilde{x}_i(t) = \hat{x}_i(t) - x(t)$ are the state estimation errors and $\lambda_i \in \mathbb{R}^{m \times n}$ are constant arbitrary matrices, chosen such that $\lambda_i B_i$ are non-singular and the coefficients $\lambda_i(k, j) : k = 1 \dots n; j = 1 \dots m$ form a stable hyperplane.

The adaptation laws are given by

$$\begin{aligned}
 \dot{\hat{\omega}}_i(t) &= -\Gamma_i \text{Proj}(u(t) \sigma_i^\top(t) \lambda_i B_i)^\top, \\
 \dot{\hat{\theta}}_i(t) &= -\Gamma_i \text{Proj}(x(t) \sigma_i^\top(t) \lambda_i B_i), \\
 \hat{\eta}_{m(i)}(t) &= -(\lambda_i B_i)^{-1} (\lambda_i A_{m(i)} \tilde{x}_i(t) + \rho_i \sigma_i(t)) - \hat{L}_{m(i)}(t) \frac{B_i^\top \lambda_i^\top \sigma_i(t)}{\|B_i^\top \lambda_i^\top \sigma_i(t)\|}, \\
 \hat{\eta}_{u(i)}(t) &= -\hat{L}_{u(i)}(t) \frac{\lambda_i^\top \sigma_i(t)}{\|\lambda_i^\top \sigma_i(t)\|}, \\
 \dot{\hat{L}}_{m(i)}(t) &= \Gamma_i \|\sigma_i^\top(t) \lambda_i B_i\|, \\
 \dot{\hat{L}}_{u(i)}(t) &= \Gamma_i \|\sigma_i^\top(t) \lambda_i\|,
 \end{aligned} \tag{5.27}$$

where $\rho_i > 0$ are arbitrary and $\Gamma_i \in \mathbb{R}^+$ are the adaptation rates.

Let $H_{m(i)}(s) = C_i(s\mathbb{I} - A_{m(i)})^{-1} B_i$, $H_{0(i)}(s) = C_i(s\mathbb{I} - A_{m(i)})^{-1}$.

The control laws are given by

$$u_i(s) = K_i D_i(s) \left(K_{g(i)} r_i(s) - \hat{\nu}_{1(i)}(s) - \hat{\nu}_{2(i)}(s) \right), \tag{5.28}$$

where $\hat{\nu}_{1(i)}(s)$ are the Laplace transformations of $\hat{\nu}_{1(i)}(t) = \hat{\theta}_i^\top(t)x(t) + \hat{\omega}_i(t)u_i(t) + \hat{\eta}_{m(i)}(t)$, $\hat{\nu}_2 = H_{m(i)}^{-1}(s)H_{0(i)}(s)\hat{\eta}_{u(i)}(s)$, $K_{g(i)} = -(C_i A_{m(i)}^{-1} B_i)^{-1}$ are the pre-filters of the MIMO control laws, $D_i(s)$ are $m \times m$ strictly proper transfer matrices and $K_i \in \mathbb{R}^{m \times m}$.

The design of $D_i(s)$ and K_i should lead to a strictly proper and stable filter transfer matrices

$$C_i(s) = \omega_i K_i D_i(s) (\mathbb{I} + \omega_i K_i D_i(s))^{-1},$$

with DC gain $C_i(0) = \mathbb{I}$.

Similarly to SISO systems, the switching logic is defined by

$$\min_{i=0..M} \left\{ J_i(t) = c_1 \|\tilde{x}_i(t)\|^2 + c_2 \int_0^t e^{-c_3(t-\tau)} \|\tilde{x}_i(\tau)\|^2 d\tau \right\}, \tag{5.29}$$

where c_1 , c_2 and c_3 are arbitrary positive reals.

The model that minimizes the criterion in (5.29) becomes the selected model, and the system in (5.23) can, consequently, be parametrized as follows

$$\dot{x}(t) = A_{m(*)}x(t) + B_*(\omega_*u(t) + \theta_*^\top x(t) + \eta_{m(*)}(t)) + \eta_{u(*)}(t, x). \tag{5.30}$$

The selected control law can be written as follows

$$u(s) = K_* D_*(s) \left(K_{g(*)} r_i(s) - \hat{v}_{1(*)}(s) - \hat{v}_{2(*)}(s) \hat{\eta}_{u(*)}(s) \right). \quad (5.31)$$

Remark 5.1 Controller analysis is straightforward from section 5.2 and section 2.2, and is omitted here.

5.4 UAV Lateral-Directional Control in Case of Inversion of the Commands

The lateral-directional equations of motion of a fixed-wing aircraft are described by the set of states (β, p, r, ϕ) , where β is the sideslip angle, p is the roll rate, r is the yaw rate and ϕ is the roll angle. The control inputs are the aileron deflection δ_a and the rudder deflection δ_r .

The objective is to design a control input $u(t) = [\delta_a, \delta_r]^\top$ to enable tracking of the roll command $\phi_c(t)$ and the sideslip angle command $\beta_c(t)$.

5.4.1 Controller Design

From [100], the linearized model of the lateral-directional dynamics of a fixed-wing aircraft can be written in matrix form as follows

$$\underbrace{\begin{bmatrix} \dot{\beta} \\ \dot{p} \\ \dot{r} \\ \dot{\phi} \end{bmatrix}}_{\dot{x}} = \underbrace{\begin{bmatrix} \frac{Y_\beta}{V_a} & \frac{Y_p}{V_a} & \frac{Y_r}{V_a} - 1 & \frac{g}{V_a} \\ L_\beta & L_p & L_r & 0 \\ N_\beta & N_p & N_r & 0 \\ 0 & 1 & 0 & 0 \end{bmatrix}}_{A_p} \underbrace{\begin{bmatrix} \beta \\ p \\ r \\ \phi \end{bmatrix}}_x + \underbrace{\begin{bmatrix} \frac{Y_{\delta_a}}{V_a} & \frac{Y_{\delta_r}}{V_a} \\ L_{\delta_a} & L_{\delta_r} \\ N_{\delta_a} & N_{\delta_r} \\ 0 & 0 \end{bmatrix}}_{B_p} \underbrace{\begin{bmatrix} \delta_a \\ \delta_r \end{bmatrix}}_u, \quad (5.32)$$

where $(Y_\beta, Y_p, Y_r, Y_{\delta_a}, Y_{\delta_r})$, $(L_\beta, L_p, L_r, L_{\delta_a}, L_{\delta_r})$ and $(N_\beta, N_p, N_r, N_{\delta_a}, N_{\delta_r})$ are the lateral-directional stability derivatives, V_a is the trimmed airspeed and g is the gravity. It should be recalled that the stability derivatives can not be measured, and they vary depending on flight conditions [100].

Taking the external disturbances and the model uncertainties into account, the system in (5.32) can be extended as follows

$$\dot{x}(t) = A_p x(t) + B_p u(t) + f(t, x). \quad (5.33)$$

5.4 UAV Lateral-Directional Control in Case of Inversion of the Commands

The system with its nominal desired dynamics can be parameterized to become similar to the class of MIMO systems in (5.24) defined by

$$\dot{x}(t) = A_{m(0)}x(t) + B_0(\omega_0 u(t) + \theta_0^\top x(t) + \eta_{m(0)}(t)) + \eta_{u(0)}(t, x). \quad (5.34)$$

A second model for the case of inversion of the sign of the aileron command is given by

$$\dot{x}(t) = A_{m(1)}x(t) + B_0\beta_1(\omega_1 u(t) + \theta_1^\top x(t) + \eta_{m(1)}(t)) + \eta_{u(1)}(t, x), \quad (5.35)$$

where $\beta_1 = \begin{bmatrix} -1 & 0 \\ 0 & 1 \end{bmatrix}$.

A third model for the case of inversion of the sign of the rudder command is given by

$$\dot{x}(t) = A_{m(2)}x(t) + B_0\beta_2(\omega_2 u(t) + \theta_2^\top x(t) + \eta_{m(2)}(t)) + \eta_{u(2)}(t, x), \quad (5.36)$$

where $\beta_2 = \begin{bmatrix} 1 & 0 \\ 0 & -1 \end{bmatrix}$.

A fourth model for the case of inversion of both the signs of the aileron and the rudder commands is given by

$$\dot{x}(t) = A_{m(3)}x(t) + B_0\beta_3(\omega_3 u(t) + \theta_3^\top x(t) + \eta_{m(3)}(t)) + \eta_{u(3)}(t, x), \quad (5.37)$$

where $\beta_3 = \begin{bmatrix} -1 & 0 \\ 0 & -1 \end{bmatrix}$.

The input matrix B_0 was taken to be the same for both models.

5.4.2 Simulation Results

Four situations were considered in simulations:

1. Loss of effectiveness of 50% without the inversion of the commands;
2. Loss of effectiveness of 50% with the inversion of the sign of the aileron command;
3. Loss of effectiveness of 50% with the inversion of the sign of the rudder command;
4. Loss of effectiveness of 50% with the of both the signs of the aileron and the rudder commands.

5 Fault-Tolerant \mathcal{L}_1 Adaptive Control Based on Multiple Models

Furthermore, the following uncertainties were added to the plant:

- Linear-in-state unknown parameters;
- Matched disturbance $d_m(t) = \sin(2\pi t)$ deg .

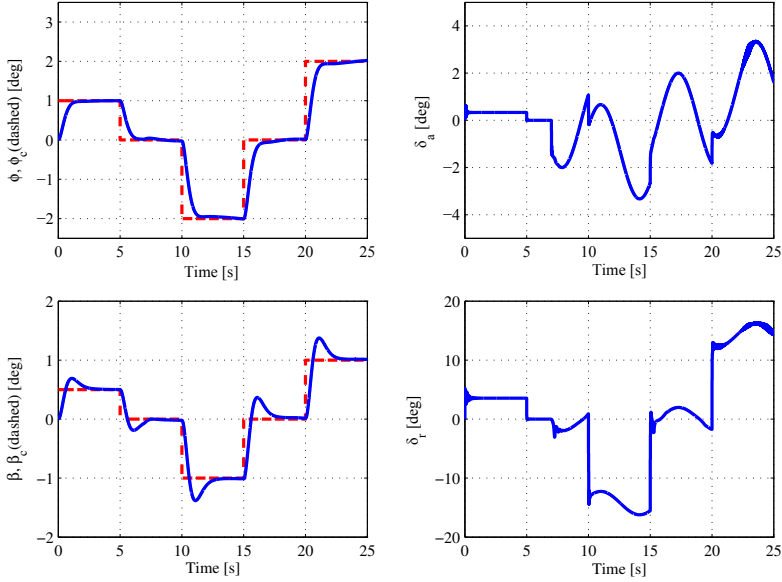


Figure 5.6: Closed-loop tracking performance of the controller without inversion of the sign of the commands.

The failures were introduced at simulation time $t = 7$ s. The tuning parameters of the fourth controllers were chosen to be the same.

Simulation results for the nominal \mathcal{L}_1 adaptive controller, without inversion of actuation signs, are shown in Fig. 5.6. As expected, the system has good performance in the presence of uncertainties. The aileron command δ_a and the rudder command δ_r are within acceptable limits.

In the second simulation scenario, uncertainties were introduced to the plant in the case of change of the sign of the aileron command. It can be observed in Fig. 5.7 that the system has switched to the first degraded controller that manages sign change in the aileron actuation. It can be clearly seen that the system shows a good tracking performance. The aileron command δ_a and the rudder command δ_r are within acceptable limits.

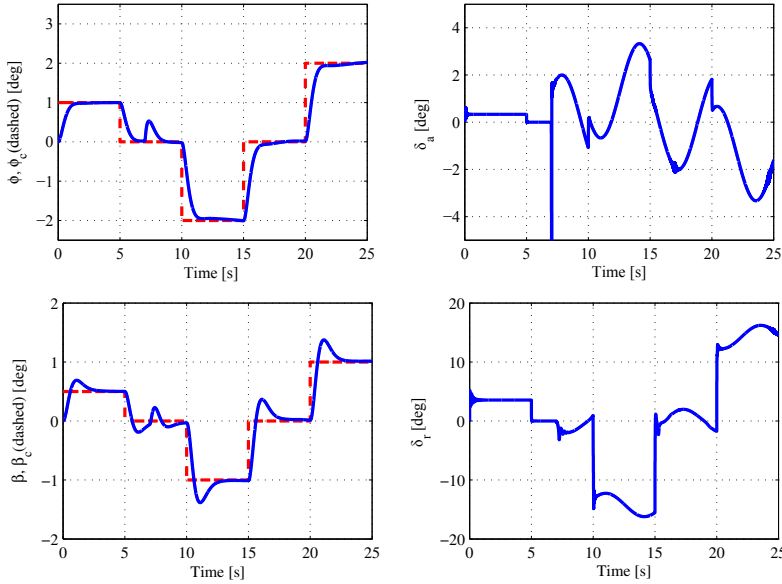


Figure 5.7: Closed-loop tracking performance of the controller with inversion of the sign of the aileron.

The simulation results in case of inversion of the sign of the rudder command, and both the ailerons and the rudder commands, are shown in Fig. 5.8 and Fig. 5.9, respectively.

These simulations conclude that the application of the multiple model \mathcal{L}_1 adaptive controller is justified in case of structural damages or faults that lead to inversion of the sign of the control input of flight systems.

5.5 Summary

In this chapter, an approach for \mathcal{L}_1 adaptive fault-tolerant control was presented for both SISO and MIMO systems. The design is based on a nominal model for a fault-free plant and a set of degraded models for the plant under failures. The switching between the models is based on a simple quadratic criterion.

The main advantage of this approach is that it allows a larger class of uncertainties and faults to be considered and can achieve better accommodation and preserve system integrity.

5 Fault-Tolerant \mathcal{L}_1 Adaptive Control Based on Multiple Models

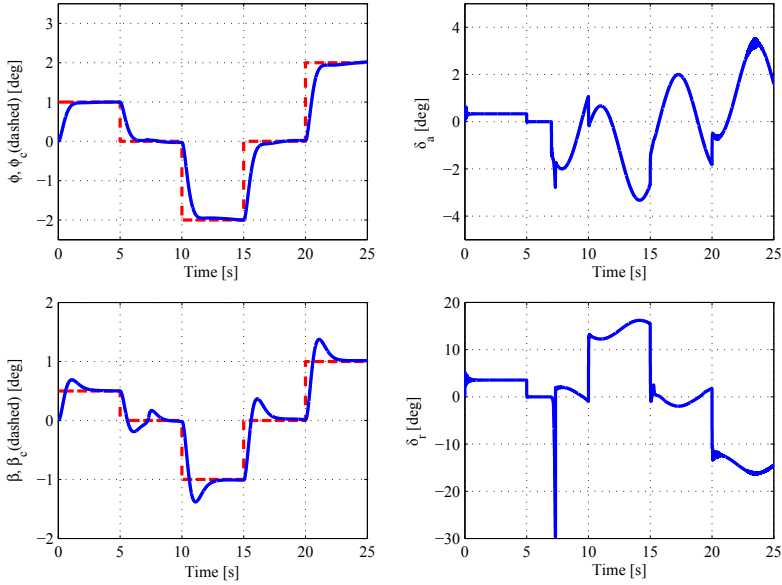


Figure 5.8: Closed-loop tracking performance of the controller with inversion of the sign of the rudder.

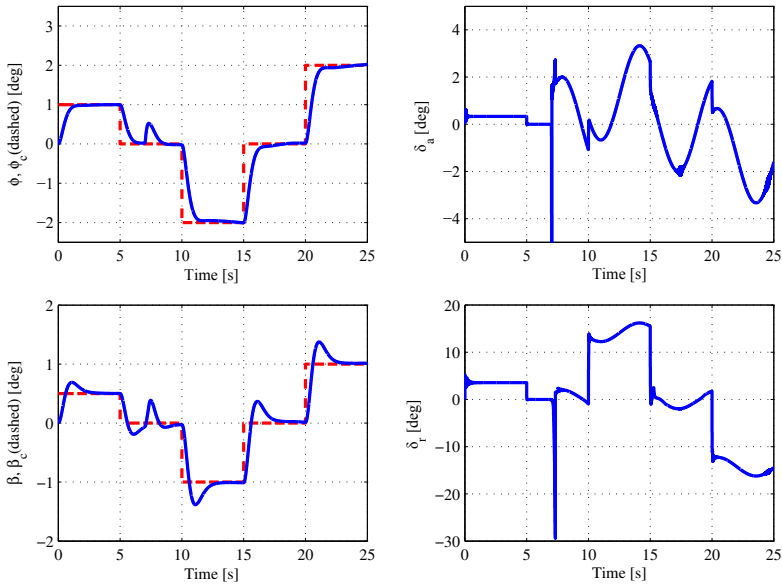


Figure 5.9: Closed-loop tracking performance of the controller with inversion of the sign of both the aileron and the rudder.

6

Chapter 6

Output Feedback Fault-Tolerant \mathcal{L}_1 Adaptive Control

6.1	Observer-based \mathcal{L}_1 Adaptive Control	88
6.1.1	Controller Design	88
6.1.2	Controller analysis	90
6.1.3	Flight Test Results	94
6.2	Multiple Model Output Feedback \mathcal{L}_1 Adaptive Control.	97
6.2.1	Controller Design	97
6.2.2	Controller analysis	99
6.2.3	Flight Test Results	101
6.3	Summary.	103

In this chapter, an approach for output feedback \mathcal{L}_1 adaptive control is designed and analyzed. It is based on the use of a Luenberger observer instead of the state predictor.

Since a state space description is maintained, the system performance can be specified with physical insight. Actually, the previous approaches for output feedback \mathcal{L}_1 adaptive control [18, 19] were based on transfer function formulation which makes the definition of uncertainties and the definition of reference models less intuitive compared to a formulation with a state-space model.

The proposed design was initially introduced in [97], where an output-feedback \mathcal{L}_1 adaptive controller that combines the use of an estimated state feedback with a switching adaptation law was presented.

The objectives of this chapter are:

- Introducing an approach for output feedback \mathcal{L}_1 adaptive control based on the Luenberger observer instead of the state predictor.
- Extending the obtained results to the multiple model \mathcal{L}_1 adaptive controller.
- Showing the flight test results of the approach on a Twinstar II small fixed-wing UAV.

6.1 Observer-based \mathcal{L}_1 Adaptive Control

Recall the class of systems defined in chapter 2, equation (2.1), as follows

$$\begin{aligned} \dot{x}(t) &= A_m x(t) + b(\omega u(t) + \theta^\top x(t) + \eta_m(t)) + \eta_u(t, x), \\ y(t) &= c^\top x(t), \quad x(0) = x_0. \end{aligned} \quad (6.1)$$

The objective is to design an output feedback adaptive controller to ensure that the system output $y(t)$ tracks a given bounded reference signal $r(t)$.

Assumption 6.1 The pair (A_m, c) is observable.

Assumption 6.2 The system is minimum phase of relative degree one, i.e., $c^\top b \neq 0$. This assumption is quite common in adaptive output feedback control, because direct adaptive controllers employ high gain feedback that can drive the system to instability [112]. This assumption, is not conservative in flight control systems [65].

Assumption 6.3 The unknown parameters are bounded, i.e., $\theta \in \Theta$, where Θ is a known compact convex set and $0 < \omega_{l(0)} \leq \omega \leq \omega_{u(0)}$. Furthermore, the non-linear functions $\eta_m(t)$ and $\eta_u(t, x)$ are uniformly bounded, i.e., there exists unknown real constants $L_m > 0$ and $L_u > 0$, such that for all $t \geq 0$ $\|\eta_m(t)\| \leq L_m$ and $\|\eta_u(t, x)\| \leq L_u$.

6.1.1 Controller Design

The state observer is defined as follows

$$\begin{aligned} \dot{\hat{x}}(t) &= A_m \hat{x}(t) + b(\hat{\omega}(t)u(t) + \hat{\theta}^\top(t)\hat{x}(t) + \hat{\eta}_m(t)) + \hat{\eta}_u(t) - L_v \tilde{y}(t), \\ \hat{y}(t) &= c^\top \hat{x}(t), \quad \hat{x}(0) = \hat{x}_0, \end{aligned} \quad (6.2)$$

where \hat{x} is the predicted state and, $\hat{\theta}(t)$, $\hat{\omega}(t)$, $\hat{\eta}_m(t)$, and $\hat{\eta}_u(t)$ are the estimates of the unknown system parameters and disturbances, $L_v \in \mathbb{R}^n$ is chosen such that $A_c = A_m - L_v c^\top$ is Hurwitz, $\tilde{y}(t) = \hat{y}(t) - y(t)$ is the output estimation error, and $\hat{x}(0)$ is initialized arbitrarily.

Remark 6.1 When compared with the state observer, a state predictor is designed while assuming that the full system state is measurable, whereas the state observer is based on the measured output of the system. A particular case is the use of an open-loop observer by choosing $L_v = 0$ [97].

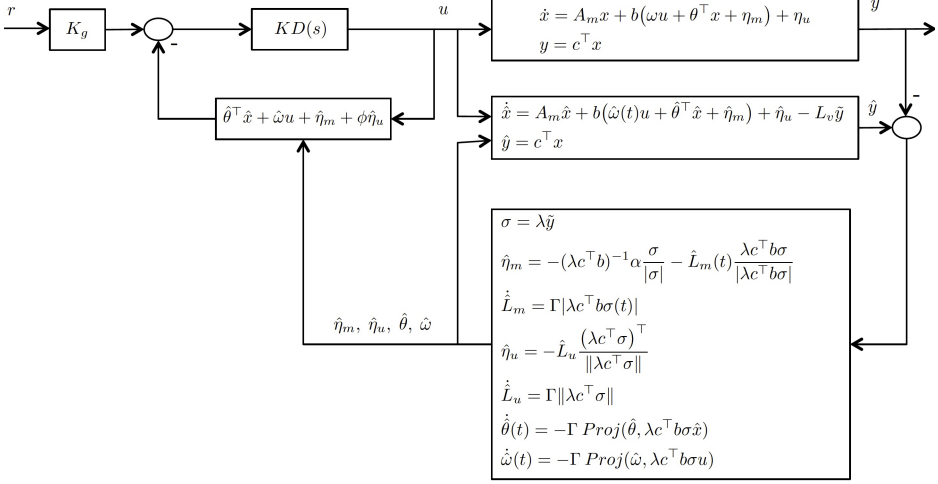


Figure 6.1: Block diagram of the observer-based \mathcal{L}_1 adaptive controller.

The sliding surface is given by

$$\sigma(t) = \lambda \tilde{y}(t), \quad (6.3)$$

where $\lambda \in \mathbb{R}^*$ is an arbitrary real.

The estimation of the matched disturbance $\eta_m(t)$ is defined by

$$\hat{\eta}_m(t) = -(\lambda c^\top b)^{-1} \alpha \frac{\sigma(t)}{|\sigma(t)|} - \hat{L}_m(t) \frac{\lambda c^\top b \sigma(t)}{|\lambda c^\top b \sigma(t)|}, \quad (6.4)$$

where $\alpha \in \mathbb{R}^+$ is arbitrary, and the estimated bound $\hat{L}_m(t)$ of the unmatched disturbance $\eta_u(t)$ is given by

$$\dot{\hat{L}}_m(t) = \Gamma |\lambda c^\top b \sigma(t)|, \quad L_{m0} = \hat{L}_m(0), \quad (6.5)$$

6 Output Feedback Fault-Tolerant \mathcal{L}_1 Adaptive Control

where $\Gamma \in \mathbb{R}^+$ is the adaptation rate.

The estimation of the unmatched disturbance $\eta_u(t, x)$ is given by

$$\hat{\eta}_u(t) = -\hat{L}_u(t) \frac{(\lambda c^\top \sigma(t))^\top}{\|\lambda c^\top \sigma(t)\|}, \quad (6.6)$$

where the estimated bound $\hat{L}_u(t)$ of the unmatched disturbance $\eta_u(t, x)$ is computed by

$$\dot{\hat{L}}_u(t) = \Gamma \|\lambda c^\top \sigma(t)\|, \quad L_{u0} = \hat{L}_u(0). \quad (6.7)$$

The estimation of the unknown parameter θ and the input gain ω are defined by

$$\begin{aligned} \dot{\hat{\theta}}(t) &= -\Gamma \text{Proj}(\hat{\theta}(t), \lambda c^\top b \sigma(t) \hat{x}(t)), \\ \dot{\hat{\omega}}(t) &= -\Gamma \text{Proj}(\hat{\omega}(t), \lambda c^\top b \sigma(t) u(t)). \end{aligned} \quad (6.8)$$

The control law is given by

$$u(s) = kD(s) \left(k_g r(s) - \hat{v}(s) - \phi(s) \hat{\eta}_u(s) \right), \quad (6.9)$$

where $k > 0$ is arbitrary, $D(s)$ is a transfer function that leads to a strictly proper stable filter $C(s) = \omega k D(s) / (1 + \omega k D(s))$ with $C(0) = 1$, the static gain is chosen as $k_g = -1 / (c^\top A_m^{-1} b)$, $\hat{v}(s)$ is the Laplace transformation of the term $\hat{\theta}^\top(t) \hat{x}(t) + \hat{\omega}(t) u(t) + \hat{\eta}_m(t)$, $\phi(s) = c^\top (sI - A_m)^{-1} / H_m(s)$, $H_m(s) = c^\top (s\mathbb{I} - A_m)^{-1} b$, and $\hat{\eta}_u(s)$ is the Laplace transform of $\hat{\eta}_u(t)$.

6.1.2 Controller analysis

Let

$$L = \max_{\theta \in \Theta} \|\theta\|_1, \quad H(s) = (s\mathbb{I} - A_m)^{-1} b, \quad G(s) = (1 - C(s)) H(s).$$

The \mathcal{L}_1 adaptive controller is defined via equations (6.2) to (6.9), and is subject to the \mathcal{L}_1 -norm condition

$$\|G(s)\|_{\mathcal{L}_1} L < 1. \quad (6.10)$$

Moreover, the design of k and $D(s)$ needs to ensure that

$$G_u(s) = (s\mathbb{I} - A_m)^{-1} - C(s) H(s) \phi(s), \quad (6.11)$$

is proper and stable.

Closed-Loop Reference System

The reference system in this case is the same as in all previous \mathcal{L}_1 adaptive control architectures. The reference system is defined by

$$\begin{aligned} \dot{x}_r(t) &= A_c x_r(t) + b(\omega u_r(t) + \theta^\top x_r(t) + \eta_m(t)) + \eta_u(t, x_r), \\ y_r(t) &= c^\top x_r(t), \quad x_r(0) = x_0. \end{aligned} \quad (6.12)$$

The reference control law is given by

$$u_r(s) = \frac{C(s)}{\omega} \left(k_g r(s) - \theta^\top x_r(s) - \eta_m(s) - \phi(s) \eta_u(s) \right). \quad (6.13)$$

Lemma 6.1 If the filter $C(s)$ is designed such that it verifies the \mathcal{L}_1 -norm condition in (6.10) and the requirement in (6.11), then the closed-loop reference system in (6.12) and (6.13) is Bounded-Input Bounded-State (BIBS) stable with respect to the reference input and initial conditions.

The proof is similar to Lemma 2.1 and is omitted here.

Transient and Steady-State Performance

In the following Lemma, it is stated that the prediction error $\tilde{x}(t) = \hat{x}(t) - x(t)$ and the estimation errors of the unknown parameters are bounded.

Lemma 6.2 The following uniform bound holds for the prediction error

$$\|\tilde{x}\|_{\mathcal{L}_\infty} < \rho = \frac{\alpha}{|\lambda| \|c\| (\|A_c\| + \|b\| \theta_m)}, \quad (6.14)$$

where $\theta_m = \max_{\theta \in \Theta} \|\theta\|$.

Proof. From (6.1) and (6.2), the prediction error dynamics can be written as follows

$$\dot{\tilde{x}} = A_c \tilde{x} + b(\tilde{\omega} u + \theta^\top \tilde{x} + \tilde{\theta}^\top \hat{x} + \tilde{\eta}_m) + \tilde{\eta}_u, \quad (6.15)$$

where $\tilde{\theta} = \hat{\theta} - \theta$, $\tilde{\omega} = \hat{\omega} - \omega$, $\tilde{\eta}_m = \hat{\eta}_m - \eta_m$ and $\tilde{\eta}_u = \hat{\eta}_u - \eta_u$. We define also $\tilde{L}_m = \hat{L}_m - L_m$ and $\tilde{L}_u = \hat{L}_u - L_u$.

Consider the Lyapunov function candidate

$$V = \frac{1}{2} \sigma^2 + \frac{1}{2} \Gamma^{-1} (\tilde{\theta}^\top \tilde{\theta} + \tilde{\omega}^2 + \tilde{L}_m^2 + \tilde{L}_u^2). \quad (6.16)$$

The derivative of the Lyapunov function is given by

$$\dot{V} = \sigma \dot{\sigma} + \Gamma^{-1} (\tilde{\theta}^\top \dot{\tilde{\theta}} + \tilde{\omega} \dot{\tilde{\omega}} + \tilde{L}_m \dot{\tilde{L}}_m + \tilde{L}_u \dot{\tilde{L}}_u). \quad (6.17)$$

From (6.3), the derivative of the sliding surface can be written as follows

$$\dot{\sigma} = \lambda c^\top A_c \tilde{x} + \lambda c^\top b (\theta^\top \tilde{x} + \tilde{\theta}^\top \hat{x} + \tilde{\omega} u + \tilde{\eta}_m) + \lambda c^\top \tilde{\eta}_u. \quad (6.18)$$

Replacing (6.18) in (6.17), it follows that

$$\begin{aligned} \dot{V} &= \sigma \left(\lambda c^\top A_c \tilde{x} + \lambda c^\top b (\theta^\top \tilde{x} + \tilde{\theta}^\top \hat{x} + \tilde{\omega} u + (\hat{\eta}_m - \eta_m)) + \lambda c^\top (\hat{\eta}_u - \eta_u) \right) \\ &\quad + \Gamma^{-1} (\tilde{\theta}^\top \dot{\hat{\theta}} + \tilde{\omega} \dot{\hat{\omega}} + \tilde{L}_m \dot{\hat{L}}_m + \tilde{L}_u \dot{\hat{L}}_u) \\ &= \sigma \lambda c^\top A_c \tilde{x} + \sigma \lambda c^\top b \theta^\top \tilde{x} + \sigma \lambda c^\top b \tilde{\theta}^\top \hat{x} + \sigma \lambda c^\top b \tilde{\omega} u + \sigma \lambda c^\top b (\hat{\eta}_m - \eta_m) \\ &\quad + \sigma \lambda c^\top (\hat{\eta}_u - \eta_u) + \Gamma^{-1} (\tilde{\theta}^\top \dot{\hat{\theta}} + \tilde{\omega} \dot{\hat{\omega}} + \tilde{L}_m \dot{\hat{L}}_m + \tilde{L}_u \dot{\hat{L}}_u) \\ &= \sigma \lambda c^\top A_c \tilde{x} + \sigma \lambda c^\top b \theta^\top \tilde{x} + \sigma \lambda c^\top b \hat{\eta}_m - \sigma \lambda c^\top b \eta_m + \sigma \lambda c^\top \hat{\eta}_u - \sigma \lambda c^\top \eta_u \\ &\quad + \tilde{\theta}^\top \hat{x} \sigma \lambda c^\top b + \tilde{\omega} u \sigma \lambda c^\top b + \Gamma^{-1} (\tilde{\theta}^\top \dot{\hat{\theta}} + \tilde{\omega} \dot{\hat{\omega}} + \tilde{L}_m \dot{\hat{L}}_m + \tilde{L}_u \dot{\hat{L}}_u). \end{aligned}$$

Given $\hat{\eta}_m$ and $\hat{\eta}_u$ from (6.4) and (6.6) and the adaptation law (6.8) it can be written

$$\begin{aligned} \dot{V} &= -\alpha |\sigma| + \sigma \lambda c^\top A_c \tilde{x} + \sigma \lambda c^\top b \theta^\top \tilde{x} - \sigma \lambda c^\top b \eta_m - \sigma \lambda c^\top \eta_u \\ &\quad - |\sigma \lambda c^\top b| \hat{L}_m - \|\sigma \lambda c^\top\| \hat{L}_u + \Gamma^{-1} (\tilde{L}_m \dot{\hat{L}}_m + \tilde{L}_u \dot{\hat{L}}_u). \end{aligned} \quad (6.19)$$

Hence, the following upper bound can be derived

$$\begin{aligned} \dot{V} &\leq -\alpha |\sigma| + \sigma \lambda c^\top A_c \tilde{x} + \sigma \lambda c^\top b \theta^\top \tilde{x} + |\lambda c^\top b \sigma| |\eta_m| + \|\lambda c^\top \sigma\| \|\eta_u\| \\ &\quad - |\sigma \lambda c^\top b| \hat{L}_m - \|\sigma \lambda c^\top\| \hat{L}_u + \Gamma^{-1} (\tilde{L}_m \dot{\hat{L}}_m + \tilde{L}_u \dot{\hat{L}}_u). \end{aligned} \quad (6.20)$$

From assumption 6.3, it can be written

$$\begin{aligned} \dot{V} &\leq -\alpha |\sigma| + \sigma \lambda c^\top A_c \tilde{x} + \sigma \lambda c^\top b \theta^\top \tilde{x} \\ &\quad - |\sigma \lambda c^\top b| \tilde{L}_m - \sigma \|\lambda c^\top\| \tilde{L}_u + \Gamma^{-1} (\tilde{L}_m \dot{\hat{L}}_m + \tilde{L}_u \dot{\hat{L}}_u). \end{aligned} \quad (6.21)$$

Considering the adaptation laws from (6.5) and (6.7), it follows that

$$\dot{V} \leq -\alpha |\sigma| + \sigma \lambda c^\top A_c \tilde{x} + \sigma \lambda c^\top b \theta^\top \tilde{x}. \quad (6.22)$$

Given that $\sigma \leq |\sigma|$, $\lambda c^\top A_c \tilde{x} \leq |\lambda| \|c\| \|A_c\| \|\tilde{x}\|$, $\lambda c^\top b \theta^\top \tilde{x} \leq |\lambda| \|c\| \|b\| \|\theta\| \|\tilde{x}\|$ and since the projection law insures $\|\theta\| \leq \theta_m$, then the following bound holds for (6.22)

$$\dot{V} \leq |\sigma| \left(-\alpha + |\lambda| \|c\| (\|A_c\| + \|b\| \theta_m) \|\tilde{x}\| \right). \quad (6.23)$$

If α is chosen arbitrarily large so that it verifies $\forall t > 0$

$$\alpha > |\lambda| \|c\| (\|A_c\| + \|b\| \theta_m) \|\tilde{x}\|, \quad (6.24)$$

then

$$\dot{V} < 0. \quad (6.25)$$

It follows that the sliding surface σ , the estimation errors of $\tilde{\theta}$, $\tilde{\omega}$, \tilde{L}_m and \tilde{L}_u are uniformly bounded. Consequently, the following bound holds for \tilde{x}

$$\|\tilde{x}\| < \rho = \frac{\alpha}{|\lambda| \|c\| (\|A_c\| + \|b\| \theta_m)}. \quad (6.26)$$

Recalling, that $\|\cdot\|_{\mathcal{L}_\infty} \leq \|\cdot\|$ this completes the proof. \square

Remark 6.2 From the previous lemma, it can be stated that the bound of the prediction error can be made arbitrarily small by choosing large values of λ .

Next, in the following theorem, the performance bounds of the \mathcal{L}_1 adaptive controller are shown.

Theorem 6.1 Given the system (6.1), the reference system (6.12), (6.13) and the \mathcal{L}_1 adaptive controller (6.2), (6.5), (6.8) and (6.9) we have

$$\|x_r - x\|_{\mathcal{L}_\infty} \leq \gamma_1, \quad (6.27)$$

and

$$\|u_r - u\|_{\mathcal{L}_\infty} \leq \gamma_2, \quad (6.28)$$

where

$$\gamma_1 = 2 \frac{\|G(s)\|_{\mathcal{L}_1}}{1 - \|G(s)\|_{\mathcal{L}_1} L} L_m + 2 \frac{\|G_u(s)\|_{\mathcal{L}_1}}{1 - \|G(s)\|_{\mathcal{L}_1} L} L_u + \frac{\|H(s)C(s)H_m^{-1}(s)c^\top\|_{\mathcal{L}_1}}{1 - \|G(s)\|_{\mathcal{L}_1} L} \rho,$$

and

$$\gamma_2 = \left\| \frac{C(s)}{\omega} \right\|_{\mathcal{L}_1} (L\gamma_1 + 2(L_m + \|\phi(s)\|_{\mathcal{L}_1} L_u)) + \left\| \frac{C(s)}{\omega} H_m^{-1}(s)c^\top \right\|_{\mathcal{L}_1} \rho.$$

The proof is similar to the proof of Theorem 2.1, and is omitted here.

6.1.3 Flight Test Results

Similar to the path-following controller, flight tests were conducted on the Twinstar-II fixed-wing UAV. The objective was to apply the proposed controller to the design of an altitude hold system. To this end, the controller was implemented to stabilize the pitch rate loop defined in (5.19). The avionic suite available on the UAV does not include a sensor to measure the angle of attack α .

The control architecture was based on the augmentation, by the adaptive controller, of the existing baseline PI controller as it is shown in Fig. 6.2. The total deflection of the elevator $\delta_e(t) = u_b(t) + u(t)$ is the sum of the commands from the baseline linear controller $u_b(t)$ and the adaptive controller $u(t)$.

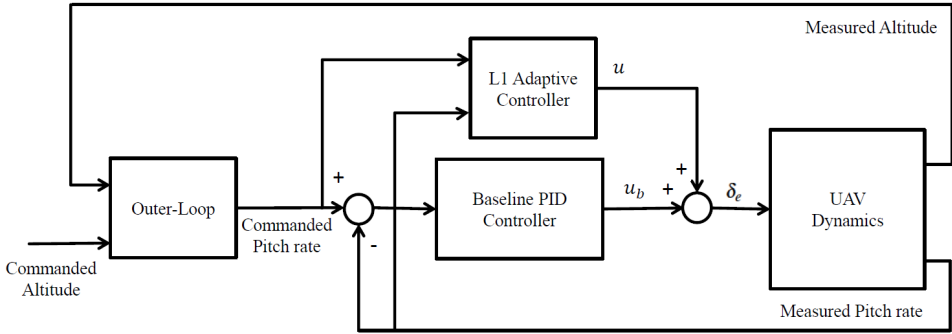


Figure 6.2: The augmented controller.

The desired eigenvalues of the system were chosen $\lambda_{1,2} = -5.6 \pm 4.2j$, i. e., a pulsation $\omega_n = 7 \text{ rad/s}$ and a damping $\xi = 0.8$. The controller was designed to be robust against model uncertainties within the compact sets $\Theta = [-1, 1]$ and $\Omega = [0.25, 1.25]$. The \mathcal{L}_1 adaptive controller parameters were set $\Gamma = 500$, $D(s) = 1/s$, $k = 150$.

The first challenge was to perform a flight while the input commands are from the pilot using the remote control. In Fig. 6.3, it is shown that the pilot was able to land the UAV under a loss of effectiveness of 50% of the elevator command, introduced from $t = 355\text{s}$.

The next scenario was that the UAV follows, autonomously, a path defined by four waypoints at a fixed altitude $h = 70\text{m}$. The robustness of the designed controller was tested in the presence of the following faults:

- A loss of actuator effectiveness $\omega = 0.5$;

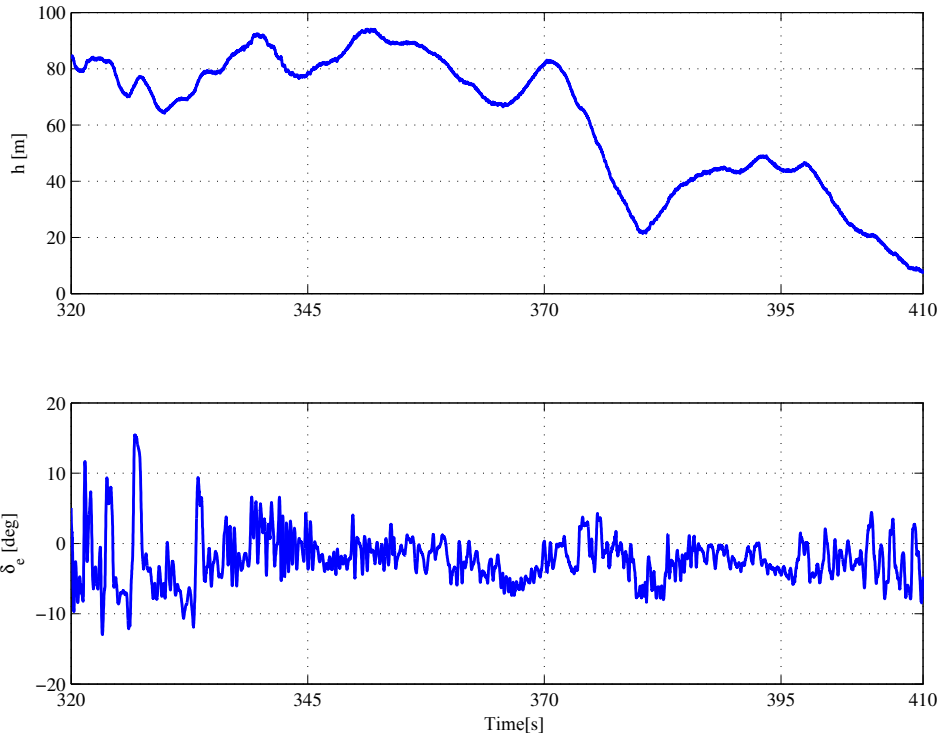


Figure 6.3: Manual landing of the UAV with the \mathcal{L}_1 adaptive controller under loss of effectiveness of the elevator command.

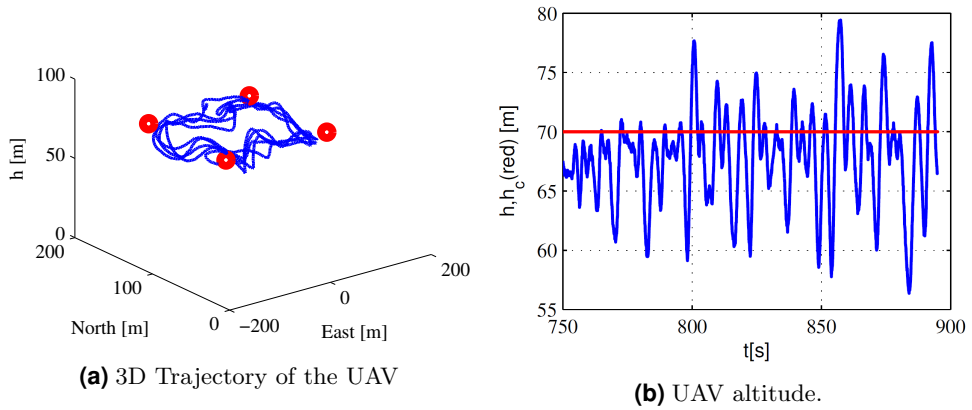
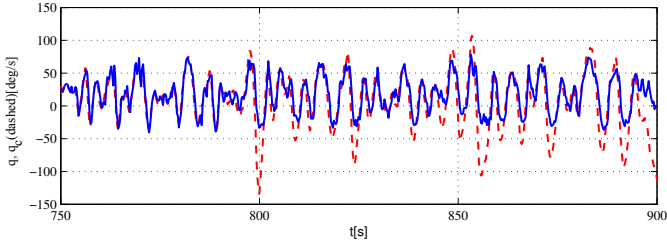


Figure 6.4: Performance of the adaptive controller under large uncertainties.

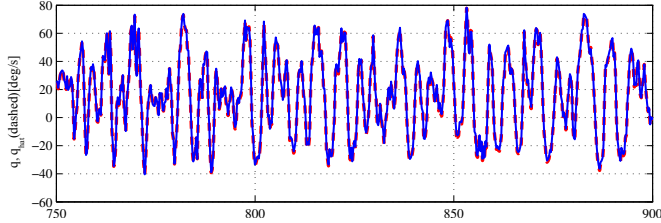
6 Output Feedback Fault-Tolerant \mathcal{L}_1 Adaptive Control

- A constant control bias $\eta_m(t) = -0.10$ rad.

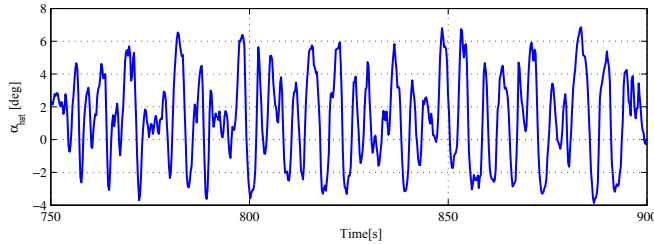
As it is shown in Fig. 6.4, the adaptive controller, without any retuning, maintains the altitude of the UAV under those uncertainties, introduced at flight time $t = 792s$. Note the presence of peaks due to the rolling motion of the UAV when turning.



(a) Tracking performance



(b) Pitch rate estimation



(c) Angle of attack estimation

Figure 6.5: Tracking and estimation performance of the \mathcal{L}_1 adaptive controller under large uncertainties.

Additionally, good tracking and estimation performances for the pitch rate q are demonstrated in Fig. 6.5. It can, also, be noted that the estimated angle of attack α is within a reasonable interval.

In contrast, as it appears in Fig. 6.6, when the adaptive controller was turned off, at time $t = 896s$, the baseline PI controller was not able to hold

the altitude of the UAV under the same uncertainties.

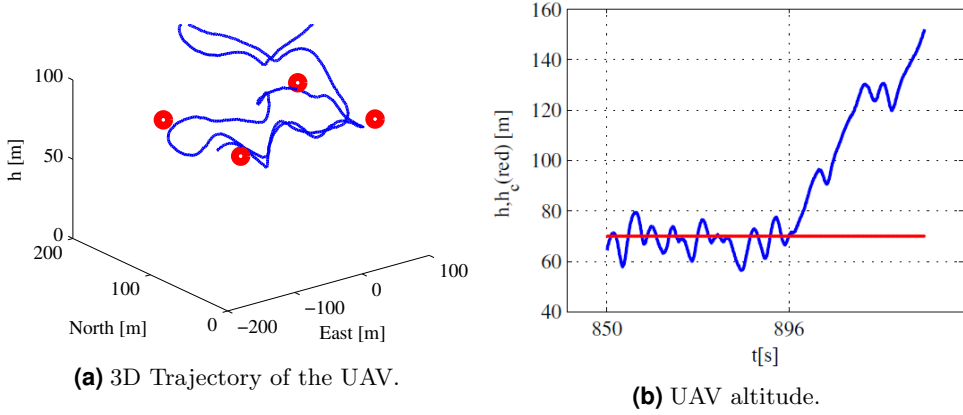


Figure 6.6: Performance of the baseline controller under failures.

These flight tests conclude that the output feedback \mathcal{L}_1 adaptive controller shows good tracking and estimation performance in the presence of faults and uncertainties.

6.2 Multiple Model Output Feedback \mathcal{L}_1 Adaptive Control

In the following, the proposed approach for output feedback \mathcal{L}_1 adaptive control is extended to multiple model systems.

6.2.1 Controller Design

The controller is a straightforward combination of the multiple model \mathcal{L}_1 adaptive controller presented in Chapter 5, and the output feedback \mathcal{L}_1 adaptive controller based on sliding mode adaptation law introduced in this chapter.

For the design of the multiple model output feedback \mathcal{L}_1 adaptive controller, the system in (5.1) can be parametrized, for $i = 0 \dots M$, as follows

$$\begin{aligned} \dot{x}(t) &= A_{m(i)}x(t) + b_i(\omega_i u(t) + \theta_i^\top x(t) + \eta_{m(i)}(t)) + \eta_{u(i)}(t, x), \\ y(t) &= c^\top x(t), \quad x(0) = x_0, \end{aligned} \quad (6.29)$$

where, $i = 0$ is the nominal model and M is the number of degraded models.

The output-feedback multiple model \mathcal{L}_1 adaptive controller is composed of a set of observers, adaptation laws, a control law and a switching logic.

The state observers are defined by

$$\begin{aligned}\dot{\hat{x}}_i(t) &= A_{m(i)}\hat{x}_i(t) + b_i(\hat{\omega}_i(t)u(t) + \hat{\theta}_i^\top(t)\hat{x}_i(t) + \hat{\eta}_{m(i)}(t)) \\ &\quad + \hat{\eta}_{u(i)}(t) - L_{v(i)}\tilde{y}_i(t), \\ \hat{y}_i(t) &= c^\top \hat{x}_i(t), \quad \hat{x}_i(0) = x_{0(i)},\end{aligned}\tag{6.30}$$

where $\hat{x}_i(t)$ are the predicted states and, $\hat{\theta}_i(t)$, $\hat{\omega}_i(t)$, $\hat{\eta}_{m(i)}(t)$, and $\hat{\eta}_{u(i)}(t)$ are the estimates of the unknown system parameters and disturbances, $L_{v(i)} \in \mathbb{R}^n$ are chosen such that $A_{c(i)} = A_{m(i)} - L_{v(i)}c^\top$ are Hurwitz, $\tilde{y}_i(t) = \hat{y}_i(t) - y(t)$ are the output estimation errors, and $\hat{x}_i(0)$ are initialized arbitrarily.

The sliding surfaces are defined by

$$\sigma_i(t) = \lambda_i \tilde{y}_i(t),\tag{6.31}$$

where $\lambda_i \in \mathbb{R}$ are arbitrary reals.

The adaptation laws are given by

$$\begin{aligned}\dot{\hat{\eta}}_{m(i)}(t) &= -(\lambda c^\top b_i)^{-1} \alpha_i \frac{|\sigma_i(t)|}{\sigma_i(t)} - \hat{L}_{m(i)}(t) \frac{\lambda_i c^\top b_i \sigma_i(t)}{|\lambda_i c^\top b_i \sigma_i(t)|}, \\ \dot{\hat{\eta}}_{u(i)}(t) &= -\hat{L}_{u(i)}(t) \frac{(\lambda_i c^\top \sigma_i(t))^\top}{\|\lambda_i c^\top \sigma_i(t)\|}, \\ \dot{\hat{L}}_{m(i)}(t) &= \Gamma_i |\lambda_i c^\top b_i \sigma_i(t)|, \\ \dot{\hat{L}}_{u(i)}(t) &= \Gamma_i \|\lambda_i c^\top \sigma_i(t)\|, \\ \dot{\hat{\omega}}_i(t) &= -\Gamma_i \text{Proj}(\hat{\omega}_i(t), \lambda_i c^\top b_i \sigma_i(t) u(t)), \\ \dot{\hat{\theta}}_i(t) &= -\Gamma_i \text{Proj}(\hat{\theta}_i(t), \lambda_i c^\top b_i \sigma_i(t) \hat{x}_i(t)),\end{aligned}\tag{6.32}$$

where $\Gamma_i \in \mathbb{R}^+$ are the adaptation rates.

The Switching Logic

Similarly to the state feedback case, a quadratic criterion with forgetting factor is used to select the model that matches the system in the presence of faults. It is given by

$$\min_{i=0..M} \left\{ J_i(t) = c_1 \|\tilde{x}_i(t)\|^2 + c_2 \int_0^t e^{-c_3(t-\tau)} \|\tilde{y}_i(\tau)\|^2 d\tau \right\}, \quad (6.33)$$

where $c_1 > 0$, $c_2 > 0$ and $c_3 > 0$ are arbitrary reals.

The plant with the selected controller can be parameterized as follows

$$\dot{x}_*(t) = A_{m(*)}x(t) + b_*(\omega_*u(t) + \theta_*^\top x(t) + \eta_{m(*)}(t)) + \eta_{u(*)}(t, x). \quad (6.34)$$

The control law acting on the system is defined by

$$u(s) = k_* D_*(s) \left(k_{g(*)} r(s) - \hat{v}_*(s) - \phi_*(s) \hat{\eta}_{u(*)}(s) \right), \quad (6.35)$$

where $\hat{v}_*(s)$ is the Laplace transformation of the term $\hat{\theta}_*^\top(t)\hat{x}_*(t) + \hat{\omega}_*(t)u(t) + \hat{\eta}_{m(*)}(t)$, $\phi_*(s) = c^\top (sI - A_{m(*)})^{-1} / c^\top (s\mathbb{I} - A_{m(*)})^{-1} b$, and $\hat{\eta}_{u(*)}(s)$ is the Laplace transform of $\hat{\eta}_{u(*)}(t)$, $k_{g(*)}$ is the static gain of the selected controller; $k_* > 0$ is arbitrary, $D_*(s)$ is a transfer function that leads to a strictly proper stable filter $C_*(s) = \omega k_* D_*(s) / (1 + \omega k_* D_*(s))$ with $C_*(0) = 1$.

6.2.2 Controller analysis

Let

$$L_* = \max_{\theta_* \in \Theta_*} \|\theta_*\|_1, \quad H_*(s) = (sI - A_{m(*)})^{-1} b_*, \quad G_*(s) = (1 - C_*(s)) H_*(s).$$

The selected \mathcal{L}_1 adaptive controller defined by equations (6.34) and (6.35) is subject to the following \mathcal{L}_1 -norm condition

$$\|G_*(s)\|_{\mathcal{L}_1} L_* < 1. \quad (6.36)$$

Moreover, the design of k_* and $D_*(s)$ needs to ensure that

$$G_{u*}(s) = (s\mathbb{I} - A_{m(*)})^{-1} - C_*(s) H_*(s) \phi_*(s), \quad (6.37)$$

is proper and stable.

Closed-Loop Reference System

If a controller is selected by the switching logic, it becomes the reference model defined by

$$\begin{aligned} \dot{x}_r(t) &= A_{m(*)}x_r(t) + b_*(\omega_*u_r(t) + \theta_*^\top x_r(t) + \eta_{m(*)}(t)) + \eta_{u(*)}(t, x_r), \\ y_r(t) &= c^\top x_r(t), \quad x_r(0) = x_0, \end{aligned} \quad (6.38)$$

where ω_* , θ_* , $\eta_{m(*)}(t)$ and $\eta_{u(*)}(t, x^r)$ are the nominal parameters of the selected model.

The control law for the reference system is given by

$$u_r(s) = \frac{C_*(s)}{\omega_*} \left(k_{g(*)}r(s) - \theta_*^\top x_r(s) + \eta_{m(*)}(s) - \phi_*(s)\eta_{u(*)}(s) \right), \quad (6.39)$$

where $\eta_{m(*)}(s)$, $\eta_{u(*)}(s)$ are the Laplace transforms of $\eta_{m(*)}(t)$, $\eta_{u(*)}(t, x_r)$ respectively.

Lemma 6.3 If the filter $C_*(s)$ is designed such that it verifies the \mathcal{L}_1 -norm condition

$$\|G_*(s)\|_{\mathcal{L}_1} L_* < 1, \quad (6.40)$$

then the closed-loop reference system in (6.38) and (6.39) is BIBS stable with respect to the reference input and initial conditions.

The proof is similar to Lemma 2.1, and is omitted here.

Transient and Steady-State Performance

In the following Lemma, is stated that the prediction errors, of the state predictors, $\tilde{x}_i(t)$ and the estimation errors of the unknown parameters are bounded.

Lemma 6.4 The following uniform bounds hold for the prediction errors

$$\|\tilde{x}_i\|_{\mathcal{L}_\infty} < \rho_i = \frac{\alpha_i}{|\lambda_i| \|c\| (\|A_{c(i)}\| + \|b_i\| \theta_{m(i)})}, \quad (6.41)$$

where $\theta_{m(i)} = \max_{\theta_i \in \Theta_i} \|\theta_i\|$.

The proof is straightforward from Lemma 5.2 and Lemma 6.2 and is omitted here.

Theorem 6.2 Given the system (6.29), the reference system (6.38), (6.39) and the selected \mathcal{L}_1 adaptive model (6.34) and (6.35) we have

$$\|x_r - x_*\|_{\mathcal{L}_\infty} \leq \gamma_{1*}, \quad (6.42)$$

and

$$\|u_r - u_*\|_{\mathcal{L}_\infty} \leq \gamma_{2*}, \quad (6.43)$$

where

$$\begin{aligned} \gamma_{1*} = & 2 \frac{\|G_*(s)\|_{\mathcal{L}_1}}{1 - \|G_*(s)\|_{\mathcal{L}_1} L_*} L_m + 2 \frac{\|G_{u(*)}\|_{\mathcal{L}_1}}{1 - \|G_*(s)\|_{\mathcal{L}_1} L_*} L_u \\ & + \frac{\|H_*(s)C_*(s)H_{m(*)}^{-1}(s)c^\top\|_{\mathcal{L}_1}}{1 - \|G_*(s)\|_{\mathcal{L}_1} L} \rho_*, \end{aligned}$$

and

$$\gamma_{2*} = \left\| \frac{C_*(s)}{\omega} \right\|_{\mathcal{L}_1} (L_* \gamma_{1*} + 2(L_m + \|\phi_*(s)\|_{\mathcal{L}_1} L_u)) + \left\| \frac{C_*(s)}{\omega} H_{m(*)}^{-1}(s)c^\top \right\|_{\mathcal{L}_1} \rho_*.$$

The proof is straightforward from Theorems 2.1 and 5.1, and is omitted here.

6.2.3 Flight Test Results

Same as the previous flight test, the control approach was based on the augmentation of a baseline linear controller by the \mathcal{L}_1 adaptive controller. The total deflection of the elevator $\delta_e(t) = u_l(t) + u(t)$ is the sum of the commands from the baseline linear controller $u_l(t)$ and the nominal adaptive controller $u(t)$.

For the nominal controller the system takes the form defined in equation (6.29) for $i = 0$

$$\begin{aligned} \dot{x}(t) &= A_{m(0)}x(t) + b_0(\omega_0 u(t) + \theta_0^\top x(t) + \eta_{m(0)}) + \eta_{u(0)}(t), \\ y(t) &= c^\top x(t). \end{aligned} \quad (6.44)$$

The desired eigenvalues were chosen $\lambda_{1,2} = -5.6 \pm 4.2j$, i. e., a pulsation $\omega_n = 7 \text{ rad/s}$ and a damping $\xi = 0.8$. The controller was designed to be robust against model uncertainties within the compact sets $\Theta_0 = [-1, 1]$,

6 Output Feedback Fault-Tolerant \mathcal{L}_1 Adaptive Control

$\Omega_0 = [0.25, 1.25]$. The \mathcal{L}_1 adaptive controller parameters were set as $\Gamma_0 = 500$, $D_0(s) = 1/s$, $k_0 = 150$.

To show the necessity of a multiple model design, a soft failure was introduced during the flight tests:

- linear-in-state uncertainty $\theta = [0.75, -0.1]^\top$,
- 50% of loss of the actuator effectiveness,
- A constant control bias $\eta_m(t) = -0.10$ rad,

A hard failure was introduced as:

- linear-in-state uncertainty $\theta = [2, -0.2]^\top$,
- 75% of loss of the actuator effectiveness,
- A constant control bias $\eta_m(t) = -0.15$ rad.

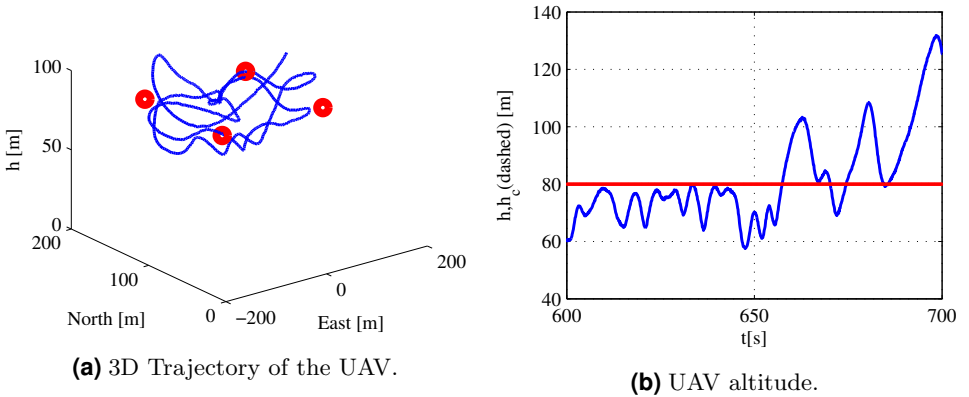


Figure 6.7: Performance of the nominal adaptive controller under hard failures.

It is shown in Fig. 6.7 that the design with only the nominal controller is robust to the soft failure, which was introduced at flight time $t=600s$, but it becomes unstable under the hard failure introduced at flight time $t=650s$.

With the degraded controller, the system takes the form defined in equation (6.29) for $i = 1$

$$\begin{aligned} \dot{x}(t) &= A_{m(1)}x(t) + b_0(\omega_1 u(t) + \theta_1^\top x(t) + \eta_{m(1)}(t)) + \eta_{u(1)}(t), \\ y(t) &= c^\top x(t). \end{aligned} \quad (6.45)$$

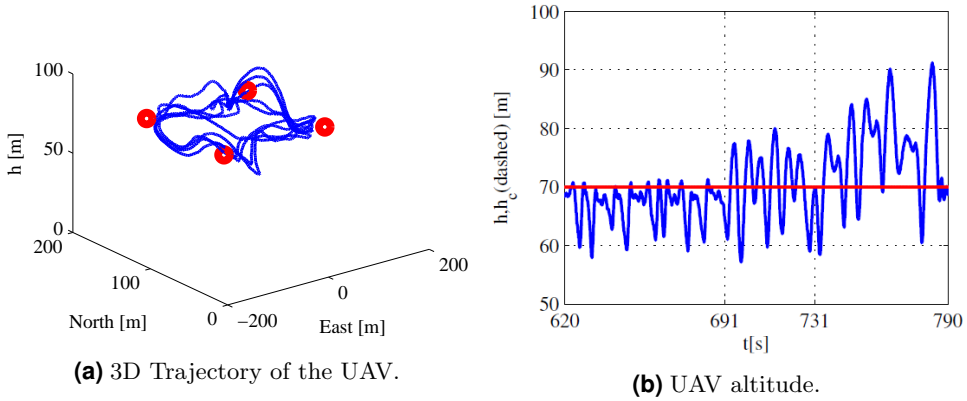


Figure 6.8: Performance of the multiple model adaptive controller under hard failures.

The desired eigenvalues were chosen to obtain slower dynamics of the degraded model, $\lambda_{1,2} = -2.8 \pm 3.1j$, i. e., a pulsation $\omega_n = 4.18 \text{ rad/s}$ and a damping $\zeta = 0.67$. The input vector b_0 was taken to be the same for both models. The controller was designed to be robust against model uncertainties within the compact sets $\Theta_1 = [-2, 2]$, $\Omega_1 = [0.15, 2]$. The \mathcal{L}_1 adaptive controller parameters were set $\Gamma_1 = 500$, $D_1(s) = 1/s$, $k_1 = 250$.

In Fig. 6.8, it is shown that the multiple model controller is robust against the hard disturbance introduced at flight time $t = 731 \text{ s}$. Furthermore, the switching logic in equation (6.33) operates, at $t = 705 \text{ s}$, some time after the introduction of the soft failure at $t = 691 \text{ s}$ (Fig. 6.9).

It can be concluded that the design based on multiple models presents a better compromise between performance in nominal conditions, and robustness against hard failures.

6.3 Summary

It was shown in this chapter that an \mathcal{L}_1 adaptive control law can be formulated on the basis of a state space formulation, using only output measurements rather than full state knowledge. The approach was applied to the \mathcal{L}_1 adaptive control based on sliding mode adaptation. The controller was tested in a real flight, along with the presence of disturbances and actuator loss of effectiveness. Compared to a classic PID controller, the proposed scheme shows satisfactory performance. The proposed technique is an alternative

6 Output Feedback Fault-Tolerant \mathcal{L}_1 Adaptive Control

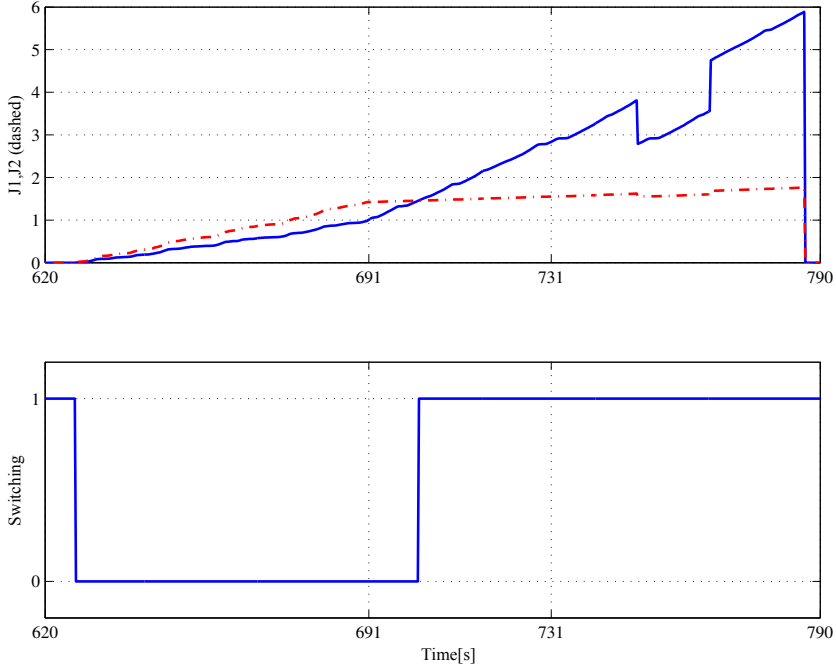


Figure 6.9: Switching logic of the multiple model controller

approach for systems that are not fully instrumented with sensors, such as small UAVs.

Next, the design was extended to the fault tolerant control design based on performance degradation. To this end, the output feedback multiple model \mathcal{L}_1 adaptive controller was intended and implemented towards real flight testing on a small fixed-wing UAV. The controller was verified in flight. It was shown that the design based on multiple models is more robust in the presence of large uncertainties than were not taken into account for the design of the nominal controller.

7

Chapter 7

Conclusions and Outlook

7.1	Conclusions	105
7.2	Outlook	106

7.1 Conclusions

This thesis is involved with the guidance and the control of small fixed-wing UAVs in the presence of wind, unknown dynamics and faults or failures. The adopted methodology is based on \mathcal{L}_1 adaptive control for disturbances of unknown bounds. Elaborating an adaptation law based on the bounding of the external disturbances by the use of a sliding surface relaxed what is commonly assumed in \mathcal{L}_1 adaptive control that external disturbances are within known bounds.

The main idea of this dissertation was to formulate the path-following for fixed-wing UAVs as a control design for systems in the presence of parametric uncertainties and external disturbances. For that purpose, the motion of the UAV was linearized assuming trim conditions. Such a formulation permits the application of the \mathcal{L}_1 adaptive control to the guidance of UAVs in the presence of the wind. As a result, the proposed solution allows to specify clear performance statements in the presence of wind that can be time varying.

The path-following problem was first formulated in 2D as a standard state space model in the presence of unknown parameters and external

disturbances. It was assumed that the desired paths are either straight lines or circular. Next, the architecture was extended to the 3D path-following of general curved paths. The design was based on the control of the motion of the UAV towards a virtual target. The linearization of the motion of the UAV with the virtual target has permitted the formulation of the whole problem as a \mathcal{L}_1 adaptive control for Multi-Input-Multi-Output systems that provides at the same time the desired vehicle attitude and the commanded speed of the virtual target.

The second main topic of this work was the design of a fault tolerant \mathcal{L}_1 adaptive controller. The proposed method is based on a nominal model for a fault-free plant and a set of degraded models for the plant under failures or large disturbances. The switching between the models is based on a simple quadratic criterion. The main advantage of this approach is that it allows a larger class of uncertainties and faults because it permits the improvement of stability margins.

Finally, towards real time implementation, an approach for output feedback \mathcal{L}_1 adaptive control based on the Luenberger observer instead of the state predictor. The main motivation is that the entire states are not always accessible for measurement on small UAVs. Such a design permits to maintain a physical representation of parameters, which supports uncertainty specification and the definition of the reference dynamics.

7.2 Outlook

The formulation of the path-following for small UAVs as a problem of control in the presence of uncertainties and external disturbances opens a gap for the introduction of a large panel of control methodologies for the development of robust path-following in the presence of wind.

Another application to the proposed approach is formation control of small UAVs in the presence of wind, unknown dynamics and faults or failures. Numerous studies were carried out on UAVs formation control. Various nonlinear methods are adopted in this application. All these approaches, however, do not consider wind. Actually, if the formation control system does not account for wind, the trajectory tracking ability of the follower UAVs will be reduced. Therefore, there is a need to design formation control methods that are robust against wind disturbances.

Furthermore, a more realistic approach to the problem of path following under wind disturbance is to consider that in the real world, wind speed is

completely unpredictable, i.e., it is a stochastic phenomenon [31]. Therefore, such an approach needs to borrow tools from stochastic analysis. A solution has been presented in [99] where results were shown for stochastic disturbance accommodation, based on \mathcal{L}_1 adaptive control. This approach could be applied to this problem of path-following in stochastic wind disturbance.

Another challenging problem is the application of the integrated guidance and control to the design of the automatic landing of airplanes or big UAVs in the presence of wind-shear or ground effect where the dynamics of the aircraft cannot be analyzed precisely.

A Appendix A

Appendix

A.1	Comments on \mathcal{L}_1 Stability Condition	109
A.1.1	\mathcal{L}_1 Adaptive Stability Condition	109
A.1.2	Simulation Results	112
A.1.3	Conclusion	112
A.2	\mathcal{L}_1 -Spaces and \mathcal{L}_1 -Norms.	113

A.1 Comments on \mathcal{L}_1 Stability Condition

In a paper by [79], some comments were made on \mathcal{L}_1 adaptive control [49], and the primary result was that "the condition of stability suggested in the literature can not be verified." The objective here is to show that this statement is based on an assumption that artificially restricts the potential of \mathcal{L}_1 adaptive control.

A.1.1 \mathcal{L}_1 Adaptive Stability Condition

Proposition 4 in [79] states that the stability condition of \mathcal{L}_1 adaptive control cannot be ensured for all plants and reference models. The main assumption of this statement is that the bandwidth of the filter must be smaller than the bandwidth of the reference model.

In \mathcal{L}_1 adaptive control, the filter acts as an additional actuator, and if its dynamics are slower than the plant, this will limit both the performance

A Appendix

and the robustness of the closed-loop system.

Actually, the role of the filter is to limit the high-frequency oscillations within a range which must be greater than the bandwidth of the reference model. Furthermore, the filter bandwidth should be small enough to eliminate the effect of high adaptation gain.

However, the allowed bandwidth of the filter is limited by robustness considerations. Indeed, indefinitely increasing the bandwidth of the filter leads to high gain control with a reduced time-delay margin [49]. Nonetheless, this does not justify the assumption in [79] stipulating that the filter bandwidth should be smaller than the model bandwidth.

To further illustrate this point, we use the unstable scalar system defined in [79]

$$\dot{y}(t) = ay(t) + bu(t), \quad y(0) = y_0, \quad (\text{A.1})$$

where $a > 0$ is unknown and $b > 0$ is assumed to be known. The plant model can be written

$$\dot{y}(t) = -a_m y(t) + b\theta y(t) + bu(t), \quad (\text{A.2})$$

where a_m is the reference model dynamics and

$$\theta = \frac{a + a_m}{b}, \quad (\text{A.3})$$

is an unknown parameter, within a known set.

The predictor is defined by

$$\dot{\hat{y}}(t) = -a_m \hat{y}(t) + b\hat{\theta}(t)y(t) + bu(t), \quad \hat{y}(0) = y_0, \quad (\text{A.4})$$

with the adaptation law

$$\dot{\hat{\theta}}(t) = -\gamma \tilde{y}(t)y(t), \quad (\text{A.5})$$

where $\gamma > 0$ is the adaptation rate and $\tilde{y}(t) = \hat{y}(t) - y(t)$ is the prediction error.

The control law is given by

$$u(t) = D(s)\eta(s), \quad (\text{A.6})$$

where $\eta(s)$ is the Laplace transform of the term $\frac{a_m}{b}r(t) - \hat{\theta}(t)y(t)$ and $D(s) = \frac{c}{c+s}$ with $c > 0$.

A.1 Comments on \mathcal{L}_1 Stability Condition

The expression of stability condition in [79] equation (10) is written

$$c > a. \quad (\text{A.7})$$

Hence

$$c > -a_m + b\theta, \quad (\text{A.8})$$

and consequently the stability condition is written

$$\theta < \frac{c + a_m}{b}. \quad (\text{A.9})$$

The restrictive assumption in [79] equation (7)

$$c < a_m, \quad (\text{A.10})$$

means that there exists $\epsilon \in \mathbb{R}^+$ verifying

$$c = a_m + \epsilon. \quad (\text{A.11})$$

It follows from (A.9) the system is stable only if the unknown parameter θ is bounded by

$$\theta < \frac{2a_m + \epsilon}{b}. \quad (\text{A.12})$$

This result is equivalent to proposition (P4) of [79], stipulating that "the stability of the reference model cannot be ensured for all plants and reference models".

As we have mentioned above, by setting faster dynamics for the filter, one can show that the stability of the system can be verified independently of the desired model and plant parameters.

This assumption can be written as

$$c > a_m, \quad (\text{A.13})$$

and the stability condition in equation (A.9) leads to

$$\theta < \frac{c + a_m}{b} < \infty. \quad (\text{A.14})$$

It follows that the system is stable independently of the desired model or of the plant, only by an appropriate choice of the filter bandwidth. Hence, the assumption $c < a_m$ that give rise to propositions (P3) and (P4) of [79] is not justified.

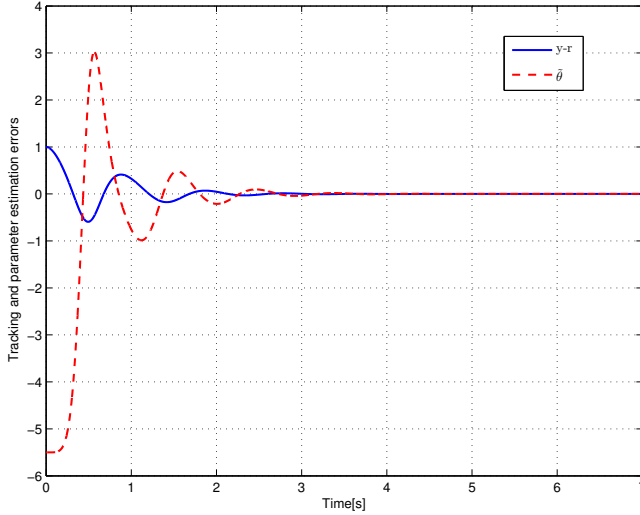


Figure A.1: Time behavior of the tracking error $y(t) - r(t)$ and the parameter estimation error $\hat{\theta}(t)$.

A.1.2 Simulation Results

The same model found in [79] is reproduced here. The plant parameters are $a = 2$, $b = 1$, and $y(0) = 1$. The controller parameters are chosen as $a_m = 3.5$, $\gamma = 50$, and $\hat{y}(0) = 1$. The reference signal is $r(t) = 1$.

By setting $c = 10$, this ensures the stability condition without the restrictive assumption in (A.10), and in Figure A.1, it is shown that the system is stable.

Thus, the discussion in example 2.2 of [79] is negated while choosing $c > a_m$ ensures the stability of the closed-loop system.

A.1.3 Conclusion

Ultimately, it can be said that, contrary to what is claimed in [79], the \mathcal{L}_1 stability condition can always be verified, regardless of the class of plants to be controlled. This is done by appropriately designing the filter dynamics. However, the design of the optimal bandwidth of the filter, which guarantees both sufficient stability and robustness margin, is an open challenge of \mathcal{L}_1 adaptive control.

A.2 \mathcal{L}_1 -Spaces and \mathcal{L}_1 -Norms.

Using the definition for the vector norms, we define norms of functions $f : [0, \infty) \rightarrow R^n$ as follows:

\mathcal{L}_1 -norm and \mathcal{L}_1 -space:

The space of piecewise-continuous integrable functions with bounded \mathcal{L}_1 -norm

$$\|f\|_{\mathcal{L}_1} \triangleq \int_0^{\infty} \|f(\tau)\| d\tau < \infty \quad (\text{A.15})$$

is denoted \mathcal{L}_1^n , where any of the vector norms can be used for $\|f(\tau)\|$.

\mathcal{L}_p -Norm and \mathcal{L}_p -Space:

The space of piecewise-continuous integrable functions with bounded \mathcal{L}_p -norm

$$\|f\|_{\mathcal{L}_p} \triangleq \left(\int_0^{\infty} \|f(\tau)\|^p d\tau \right)^{1/p} < \infty \quad (\text{A.16})$$

is denoted \mathcal{L}_p^n . As above, any of the vector norms can be used for $\|f(\tau)\|$. However, for the \mathcal{L}_2 -space it is conventional to use the 2-norm of the vector.

\mathcal{L}_∞ -Norm:

The space of piecewise-continuous bounded functions with \mathcal{L}_∞ -norm

$$\|f\|_{\mathcal{L}_\infty} \triangleq \max_{1 \leq i \leq n} \{ \sup |f_i(\tau)| \} < \infty \quad (\text{A.17})$$

is denoted \mathcal{L}_∞^n . notice that the requirement for the \mathcal{L} -norm to be finite restricts the class of functions that can belong to the \mathcal{L}_p^n space.

Notice that the requirement for the \mathcal{L} -norm to be finite restricts the class of functions that can belong to the \mathcal{L}_p^n space. so as not to be restricted by this, we consider the extended space \mathcal{L}_e^n , defined as the space of functions

$$\mathcal{L}_e^n \triangleq \{ f(t) | f_\tau(t) \in \mathcal{L}^n, \forall \tau \in [0, \infty) \},$$

where $f_\tau(t)$ is the truncation of the function $f(t)$ defined by

$$f(t) = \begin{cases} f(t), & 0 \leq t \leq \tau, \\ 0, & t > \tau. \end{cases}$$

Bibliography

- [1] <http://www.icao.int>. Accessed: 21-04-2014.
- [2] Kasey A Ackerman, Enric Xargay, Ronald Choe, Naira Hovakimyan, M Christopher Cotting, Robert B Jeffrey, Margaret P Blackstun, T Paul Fulkerson, Timothy R Lau, and Shawn S Stephens. Evaluation of an \mathcal{L}_1 adaptive flight control law on calspan's variable-stability learjet. *Journal of Guidance, Control, and Dynamics*, 2017.
- [3] Karim Ahmadi, Davood Asadi, and Farshad Pazooki. Nonlinear \mathcal{L}_1 adaptive control of an airplane with structural damage. *Proceedings of the Institution of Mechanical Engineers, Part G: Journal of Aerospace Engineering*, 233(1):341–353, 2019.
- [4] Brian D. O. Anderson, Thomas Brinsmead, Daniel Liberzon, and a. Stephen Morse. Multiple model adaptive control with safe switching. *International Journal of Adaptive Control and Signal Processing*, 15(5):445–470, August 2001.
- [5] Karl J Åström and Björn Wittenmark. *Adaptive control*. Courier Dover Publications, 2013.
- [6] Reg Austin. *Unmanned aircraft systems: UAVs design, development and deployment*, volume 54. John Wiley & Sons, 2011.
- [7] Sanchito Banerjee, Zhongjie Wang, Bernhard Baur, Florian Holzapfel, Jiaxing Che, and Chengyu Cao. \mathcal{L}_1 adaptive control augmentation for the longitudinal dynamics of a hypersonic glider. *Journal of Guidance, Control, and Dynamics*, 2015.

Bibliography

- [8] Randal W Beard, Jeff Ferrin, and Jeffrey Humpherys. Fixed wing uav path following in wind with input constraints. *IEEE Transactions on Control Systems Technology*, 22(6):2103–2117, 2014.
- [9] Randal W Beard and Timothy W McLain. *Small unmanned aircraft: Theory and practice*. Princeton University Press, 2012.
- [10] Randy Beard, Chengyu Cao, and Naira Hovakimyan. An \mathcal{L}_1 adaptive pitch controller for miniature air vehicles. In *AIAA guidance, navigation, and control conference and exhibit*, page 6777, 2006.
- [11] John H Blakelock. *Automatic control of aircraft and missiles*. John Wiley & Sons, 1991.
- [12] Mogens Blanke, Michel Kinnaert, Jan Lunze, Marcel Staroswiecki, and J Schröder. *Diagnosis and fault-tolerant control*, volume 2. Springer, 2006.
- [13] Marc Bodson. Reconfigurable nonlinear autopilot. *Journal of guidance, control, and dynamics*, 26(5):719–727, 2003.
- [14] Morten Breivik and Thor I Fossen. Principles of guidance-based path following in 2d and 3d. pages 627–634. IEEE, 2005.
- [15] A Brezoescu, Rogelio Lozano, and P Castillo. Lyapunov-based trajectory tracking controller for a fixed-wing unmanned aerial vehicle in the presence of wind. *International Journal of Adaptive Control and Signal Processing*, 29(3):372–384, 2015.
- [16] David Cabecinhas, Carlos Silvestre, Paulo Rosa, and Rita Cunha. Path-following control for coordinated turn aircraft maneuvers. In *AIAA Guidance, Navigation and Control Conference and Exhibit*, volume 35, 2007.
- [17] Chengyu Cao and Naira Hovakimyan. Design and analysis of a novel \mathcal{L}_1 adaptive control architecture with guaranteed transient performance. *IEEE Transactions on Automatic Control*, 53(2):586–591, 2008.
- [18] Chengyu Cao and Naira Hovakimyan. \mathcal{L}_1 adaptive output feedback controller for systems of unknown dimension. *IEEE Transactions on Automatic Control*, 53(3):815–821, 2008.

- [19] Chengyu Cao and Naira Hovakimyan. \mathcal{L}_1 adaptive output-feedback controller for non-strictly-positive-real reference systems: Missile longitudinal autopilot design. *Journal of guidance, control, and dynamics*, 32(3):717–726, 2009.
- [20] Chengyu Cao, Naira Hovakimyan, and Eugene Lavretsky. Application of \mathcal{L}_1 adaptive controller to wing rock. In *AIAA Guidance, Navigation, and Control Conference, Keystone, CO*, 2006.
- [21] Elisa Capello, Giorgio Guglieri, Fulvia Quagliotti, and Daniele Sartori. Design and validation of an \mathcal{L}_1 adaptive controller for mini-uav autopilot. *Journal of Intelligent & Robotic Systems*, 69(1-4):109–118, 2013.
- [22] Elisa Capello, Giorgio Guglieri, and Daniele Sartori. Performance evaluation of an \mathcal{L}_1 adaptive controller for wing-body rock suppression. *Journal of Guidance, Control, and Dynamics*, 35(6):1702–1708, 2012.
- [23] Elisa Capello, Fulvia Quagliotti, and Roberto Tempo. Randomized approaches for control of quadrotor uavs. *Journal of Intelligent & Robotic Systems*, 73(1-4):157–173, 2014.
- [24] Nicola Ceccarelli, John J Enright, Emilio Frazzoli, Steven J Rasmussen, and Corey J Schumacher. Micro uav path planning for reconnaissance in wind. In *American Control Conference, 2007. ACC'07*, pages 5310–5315. IEEE, 2007.
- [25] Qi Chen, Jing Wan, and Jianliang Ai. \mathcal{L}_1 adaptive control of a generic hypersonic vehicle model with a blended pneumatic and thrust vectoring control strategy. *Science China Information Sciences*, 60(3):032203, 2017.
- [26] Namhoon Cho, Youdan Kim, and Sanghyuk Park. Three-dimensional nonlinear path-following guidance law based on differential geometry. In *World Congress*, volume 19, pages 2503–2508, 2014.
- [27] BL Cong, Z Chen, and XD Liu. On adaptive sliding mode control without switching gain overestimation. *International Journal of Robust and Nonlinear Control*, 24(3):515–531, 2014.
- [28] V. Dobrokhodov, E. Xargay, N. Hovakimyan, I. Kaminer, C. Cao, and I. M. Gregory. Multicriteria analysis of an \mathcal{L}_1 adaptive flight control

- system. *Proceedings of the Institution of Mechanical Engineers, Part I: Journal of Systems and Control Engineering*, 227(4):413–427, March 2013.
- [29] Vladimir Dobrokhodov, Isaac Kaminer, Ioannis Kitsios, Enric Xargay, Chengyu Cao, Irene M Gregory, Naira Hovakimyan, and Lena Valavani. Experimental validation of l1 adaptive control: The rohms counterexample in flight. *Journal of Guidance, Control, and Dynamics*, 34(5):1311–1328, 2011.
- [30] Andrei Dorobantu, Austin Murch, B er enice Mettler, and Gary Balas. System identification for small, low-cost, fixed-wing unmanned aircraft. *Journal of Aircraft*, 50(4):1117–1130, 2013.
- [31] Hugh L Dryden and Ira H Abbott. The design of low-turbulence wind tunnels. *Nasa report*, 1949.
- [32] Guillaume JJ Ducard. *Fault-tolerant flight control and guidance systems: Practical methods for small unmanned aerial vehicles*. Springer, 2009.
- [33] Zachary Thompson Dydek. *Adaptive control of unmanned aerial systems*. PhD thesis, Massachusetts institute of Technology, 2010.
- [34] Christopher Edwards, Thomas Lombaerts, and Hafid Smaili. *Fault tolerant flight control*. Springer, 2010.
- [35] Christopher Edwards, Sarah K Spurgeon, and Ashu Akoachere. A sliding mode static output feedback controller based on linear matrix inequalities applied to an aircraft system. *Journal of Dynamic Systems, Measurement, and Control*, 122:656, 2000.
- [36] P Encarnacao and A Pascoal. 3d path following for autonomous underwater vehicle. In *Proc. 39 th IEEE Conference on Decision and Control*. Citeseer, 2000.
- [37] David Erdos, Tal Shima, Evgeny Kharisov, and Naira Hovakimyan. \mathcal{L}_1 adaptive control integrated missile autopilot and guidance. In *AIAA Guidance, Navigation, and Control Conference*, page 4465, 2012.
- [38] J Fei. Robust adaptive vibration tracking control for a micro-electromechanical systems vibratory gyroscope with bound estimation. *IET control theory & applications*, 4(6):1019–1026, 2010.

- [39] Ramon A Suarez Fernandez, Sergio Dominguez, and Pascual Campoy. \mathcal{L}_1 adaptive control for wind gust rejection in quad-rotor uav wind turbine inspection. In *Unmanned Aircraft Systems (ICUAS), 2017 International Conference on*, pages 1840–1849. IEEE, 2017.
- [40] F Frenet. Sur les courbes á doublette courbure. *Toulouse, France*, 1847.
- [41] Irene Gregory, Enric Xargay, Chengyu Cao, and Naira Hovakimyan. Flight test of an \mathcal{L}_1 adaptive controller on the nasa airstar flight test vehicle. page 8015, 2010.
- [42] Irene Gregory, Enric Xargay, Chengyu Cao, and Naira Hovakimyan. Flight test of \mathcal{L}_1 adaptive control law: Offset landings and large flight envelope modeling work. *AIAA Guidance, Navigation, and Control Conference*, page 6608, 2011.
- [43] Irene M Gregory, Chengyu Cao, Enric Xargay, Naira Hovakimyan, and Xiaotian Zou. \mathcal{L}_1 adaptive control design for nasa airstar flight test vehicle. In *AIAA Guidance, Navigation, and Control Conference*, volume 5738, 2009.
- [44] Philip C Gregory. Air research and development command plans and programs. In *Proc. Self Adaptive Flight Control Symp*, pages 8–15. OH: Wright-Patterson Air Force Base, 1959.
- [45] Masanori Harada, Ryuta Ichikawa, Soichiro Watanabe, and Kevin Bollino. \mathcal{L}_1 adaptive control for single coaxial rotor mav. In *AIAA SciTech: Guidance, Navigation, and Control Conference, paper AIAA*, volume 894, 2016.
- [46] Khalil Hassan. *Nonlinear systems*. Prentice-Hall, 2002.
- [47] Fabian Hellmundt, Jens Dodenhoft, and Florian Holzapfel. \mathcal{L}_1 adaptive control with eigenstructure assignment for pole placement considering actuator dynamics and delays. In *AIAA Guidance, Navigation, and Control Conference*, page 1382, 2016.
- [48] Nathan V Hoffer, Calvin Coopmans, Austin M Jensen, and YangQuan Chen. A survey and categorization of small low-cost unmanned aerial vehicle system identification. *Journal of Intelligent & Robotic Systems*, 74(1-2):129–145, 2014.

Bibliography

- [49] Naira Hovakimyan and Chengyu Cao. \mathcal{L}_1 adaptive control theory: Guaranteed robustness with fast adaptation, volume 21. Siam, 2010.
- [50] Naira Hovakimyan, Chengyu Cao, Evgeny Kharisov, Enric Xargay, and Irene M Gregory. \mathcal{L}_1 adaptive control for safety-critical systems. *Control Systems, IEEE*, 31(5):54–104, 2011.
- [51] Liu Hsu and Ramon R Costa. Variable structure model reference adaptive control using only input and output measurements: Part 1. *International Journal of Control*, 49(2):399–416, 1989.
- [52] Petros A Ioannou and Elias B Kosmatopoulos. *Adaptive Control*. Wiley Online Library, 2006.
- [53] Petros A Ioannou and Jing Sun. *Robust adaptive control*. Courier Dover Publications, 2012.
- [54] Hamidreza Jafarnejadsani, Donglei Sun, Hanmin Lee, and Naira Hovakimyan. Optimized \mathcal{L}_1 adaptive controller for trajectory tracking of an indoor quadrotor. *Journal of Guidance, Control, and Dynamics*, 2017.
- [55] Jin Jiang and Xiang Yu. Fault-tolerant control systems: A comparative study between active and passive approaches. *Annual Reviews in control*, 36(1):60–72, 2012.
- [56] Jin Jiang and Youmin Zhang. Accepting performance degradation in fault-tolerant control system design. *Control Systems Technology, IEEE Transactions on*, 14(2):284–292, 2006.
- [57] Wang Jin, Song Bifeng, Wang Liguang, and Tang Wei. \mathcal{L}_1 adaptive dynamic inversion controller for an x-wing tail-sitter mav in hover flight. *Procedia Engineering*, 99:969–974, 2015.
- [58] Yeundeuk Jung, Sungwook Cho, and David Hyunchul Shim. A trajectory-tracking controller design using \mathcal{L}_1 adaptive control for multi-rotor uavs. In *Unmanned Aircraft Systems (ICUAS), 2015 International Conference on*, pages 132–138. IEEE, 2015.
- [59] Isaac Kaminer, Antonio Pascoal, Enric Xargay, Naira Hovakimyan, Chengyu Cao, and Vladimir Dobrokhodov. Path following for small unmanned aerial vehicles using \mathcal{L}_1 adaptive augmentation of commercial

- autopilots. *Journal of guidance, control, and dynamics*, 33(2):550–564, 2010.
- [60] Isaac Kaminer, Oleg Yakimenko, Vladimir Dobrokhodov, Antonio Pascoal, Naira Hovakimyan, Vijay Patel, Chengyu Cao, and Amanda Young. Coordinated path following for time-critical missions of multiple uavs via \mathcal{L}_1 adaptive output feedback controllers. In *AIAA Guidance, Navigation and Control Conference and Exhibit*, page 6409, 2007.
- [61] Evgeny Kharisov. \mathcal{L}_1 adaptive output-feedback control architectures. PhD thesis, University of Illinois at Urbana-Champaign, 2014.
- [62] Evgeny Kharisov and Naira Hovakimyan. \mathcal{L}_1 adaptive output feedback controller for minimum phase systems. In *American Control Conference (ACC), 2011*, pages 1182–1187. IEEE, 2011.
- [63] Ki-Seok Kim, Keum-Jin Lee, and Youdan Kim. Reconfigurable flight control system design using direct adaptive method. *Journal of Guidance, Control, and Dynamics*, 26(4):543–550, 2003.
- [64] Ioan Doré Landau, Rogelio Lozano, and Mohammed M’Saad. *Adaptive control*, volume 51. Springer Berlin, 1998.
- [65] E. Lavretsky. Adaptive output feedback design using asymptotic properties of lqg/ltr controllers. *IEEE Transactions on Automatic Control*, 57:1585–1591, 2012.
- [66] Eugene Lavretsky and Kevin A Wise. Robust adaptive control. In *Robust and Adaptive Control*, pages 317–353. Springer, 2013.
- [67] Hanmin Lee, Steven Snyder, and Naira Hovakimyan. \mathcal{L}_1 adaptive control within a flight envelope protection system. *Journal of Guidance, Control, and Dynamics*, 2017.
- [68] Hanmin Lee, Steven Snyder, and Naira Hovakimyan. \mathcal{L}_1 adaptive output feedback augmentation for missile systems. *IEEE Transactions on Aerospace and Electronic Systems*, 2017.
- [69] Cunjia Liu, Owen McAree, and Wen-Hua Chen. Path-following control for small fixed-wing unmanned aerial vehicles under wind disturbances. *International Journal of Robust and Nonlinear Control*, 23(15):1682–1698, 2013.

Bibliography

- [70] Yu Liu, Gang Tao, and Suresh M. Joshi. Modeling and Model Reference Adaptive Control of Aircraft with Asymmetric Damage. *Journal of Guidance, Control, and Dynamics*, 33(5):1500–1517, September 2010.
- [71] Jie Luo and Chengyu Cao. \mathcal{L}_1 adaptive control with sliding-mode based adaptive law. *Control Theory and Technology*, 13(3):221–229, 2015.
- [72] Timothy G McGee and J Karl Hedrick. Path planning and control for multiple point surveillance by an unmanned aircraft in wind. In *American Control Conference, 2006*, pages 6–pp. IEEE, 2006.
- [73] Alain Micaelli and Claude Samson. Trajectory tracking for unicycle-type and two-steering-wheels mobile robots. Technical report, INRIA, 1993.
- [74] Eli Mishkin and Ludwig Braun. *Adaptive control systems*. McGraw-Hill, 1961.
- [75] Maximilian Muhlegg, Philipp Niermeyer, Guillermo P Falconi, and Florian Holzapfel. \mathcal{L}_1 fault tolerant adaptive control of a hexacopter with control degradation. In *Control Applications (CCA), 2015 IEEE Conference on*, pages 750–755. IEEE, 2015.
- [76] Kumpati S Narendra and Jeyendran Balakrishnan. Adaptive control using multiple models. *Automatic Control, IEEE Transactions on*, 42(2):171–187, 1997.
- [77] Derek R Nelson, D Blake Barber, Timothy W McLain, and Randal W Beard. Vector field path following for miniature air vehicles. *Robotics, IEEE Transactions on*, 23(3):519–529, 2007.
- [78] Pavan Nuthi and Kamesh Subbarao. Experimental verification of linear and adaptive control techniques for a 2-dof helicopter. *Journal of Dynamic Systems, Measurement, and Control*, 2014.
- [79] Romeo Ortega and Elena Panteley. Comments on \mathcal{L}_1 adaptive control: stabilisation mechanism, existing conditions for stability and performance limitations. *International Journal of Control*, 87(3):581–588, 2014.

- [80] John Osborne and Rolf Rysdyk. Waypoint guidance for small uavs in wind. *AIAA Infotech Aerospace*, 193(1-4):1–12, 2005.
- [81] Vijay V Patel, Chengyu Cao, Naira Hovakimyan, Kevin A Wise, and Eugene Lavretsky. \mathcal{L}_1 adaptive controller for tailless unstable aircraft in the presence of unknown actuator failures. *International Journal of Control*, 82(4):705–720, 2009.
- [82] Ron J Patton. Fault-tolerant control: the 1997 situation. *IFAC Proceedings Volumes*, 30(18):1029–1051, 1997.
- [83] Wilfrid Perruquetti and Jean-Pierre Barbot. *Sliding mode control in engineering*. CRC Press, 2002.
- [84] B Peterson and Kumpati S Narendra. Bounded error adaptive control. *Automatic Control, IEEE Transactions on*, 27(6):1161–1168, 1982.
- [85] Franck Plestan, Yuri Shtessel, Vincent Bregeault, and Alexander Poznyak. New methodologies for adaptive sliding mode control. *International journal of control*, 83(9):1907–1919, 2010.
- [86] J-B Pomet and Laurent Praly. Adaptive nonlinear regulation: estimation from the lyapunov equation. *Automatic Control, IEEE Transactions on*, 37(6):729–740, 1992.
- [87] Farzad Pourboghrat and George Vlastos. Model reference adaptive sliding control for linear systems. *Computers & Electrical Engineering*, 28(5):361–374, 2002.
- [88] Ashwini Ratnoo, PB Sujit, and Mangal Kothari. Adaptive optimal path following for high wind flights. In *18th IFAC World Congress, Milano, Italy*, volume 2, 2011.
- [89] Unmanned Aerial Vehicles Roadmap. Roadmap 2005-2030. *Office of the Secretary of Defense*, 4:42–46, 2005.
- [90] Rolf Rysdyk. Unmanned aerial vehicle path following for target observation in wind. *Journal of guidance, control, and dynamics*, 29(5):1092–1100, 2006.
- [91] Daniele Sartori. *Design, Implementation and Testing of Advanced Control Laws for Fixed-wing UAVs*. PhD thesis, Politecnico di Torino, 2014.

Bibliography

- [92] J-A Serret. Sur quelques formules relatives à la théorie des courbes à double courbure. *Journal de Mathématiques pures et appliquées*, pages 193–207, 1851.
- [93] Jean-Jacques E Slotine, Weiping Li, et al. *Applied nonlinear control*, volume 60. Prentice-Hall Englewood Cliffs, NJ, 1991.
- [94] D Soetanto, L Lapierre, and A Pascoal. Adaptive, non-singular path-following control of dynamic wheeled robots. In *Decision and Control, 2003. Proceedings. 42nd IEEE Conference on*, volume 2, pages 1765–1770. IEEE, 2003.
- [95] Haitao Song, Tao Zhang, Guoliang Zhang, and Changjie Lu. Integrated design of interceptor guidance and control based on l1 adaptive control. In *Intelligent Human-Machine Systems and Cybernetics (IHMSC), 2013 5th International Conference on*, volume 1, pages 525–528. IEEE, 2013.
- [96] Toufik Souanef, Ahsene Boubakir, and Walter Fichter. \mathcal{L}_1 adaptive control of systems with disturbances of unknown bounds. In *Advances in Aerospace Guidance, Navigation and Control: Selected Papers of the Third CEAS Specialist Conference on Guidance, Navigation and Control held in Toulouse*, page 151. Springer, 2015.
- [97] Toufik Souanef and Walter Fichter. Adaptive altitude hold of a small uav with switching adaptation laws. In *Automatic Control in Aerospace*, volume 19, pages 212–217, 2013.
- [98] Toufik Souanef and Walter Fichter. Fault tolerant \mathcal{L}_1 adaptive control based on degraded models. In *Advances in Aerospace Guidance, Navigation and Control*, pages 135–149. Springer, 2015.
- [99] Toufik Souanef, Federico Pinchetti, and Walter Fichter. \mathcal{L}_1 adaptive control for systems with matched stochastic disturbance. In *Advances in Aerospace Guidance, Navigation and Control*, pages 297–313. Springer, 2013.
- [100] B. L. Stevens and F. L. Lewis. *Aircraft Control and Simulation*. Wiley, New York, 2003.
- [101] P B Sujit and Srikanth Saripalli. Unmanned aerial vehicle path following. *IEEE Control Systems Magazine*, (February), 2014.

- [102] Donglei Sun, Ronald Choe, Enric Xargay, and Naira Hovakimyan. An \mathcal{L}_1 adaptive backup flight control law for transport aircraft with vertical-tail damage. In *AIAA Guidance, Navigation and Control Conference*, pages 2016–0633, 2016.
- [103] Chang Tan, Gang Tao, Hui Yang, and Fangping Xu. A multiple-model adaptive control scheme for multivariable systems with uncertain actuation signs. pages 1121–1126. IEEE, 2017.
- [104] Gang Tao. *Adaptive control of systems with actuator failures*. Springer, 2004.
- [105] Vadim Ivanovich Utkin. *Sliding modes and their application in variable structure systems*. Mir publishers, 1978.
- [106] Kimon P Valavanis and George J Vachtsevanos. *Handbook of Unmanned Aerial Vehicles*. Springer, 2015.
- [107] Jiang Wang, Vijay Patel, Craig A Woolsey, Naira Hovakimyan, and David Schmale. \mathcal{L}_1 adaptive control of a uav for aerobiological sampling. In *American Control Conference, 2007. ACC'07*, pages 4660–4665. IEEE, 2007.
- [108] Jiang Wang, Vijay V Patel, Chengyu Cao, Naira Hovakimyan, and Eugene Lavretsky. Novel \mathcal{L}_1 adaptive control methodology for aerial refueling with guaranteed transient performance. *Journal of guidance, control, and dynamics*, 31(1):182–193, 2008.
- [109] Enric Xargay, Vladimir Dobrokhodov, Isaac Kaminer, António M Pascoal, Naira Hovakimyan, and Chengyu Cao. Time-critical cooperative control of multiple autonomous vehicles. *IEEE Control Systems Magazine*, 32(5):49, 2012.
- [110] Guang-Hong Yang, Jian Liang Wang, and Yeng Chai Soh. Reliable controller design for linear systems. *Automatica*, 37(5):717–725, 2001.
- [111] Dong Sang Yoo and Myung Jin Chung. A variable structure control with simple adaptation laws for upper bounds on the norm of the uncertainties. *Automatic Control, IEEE Transactions on*, 37(6):860–865, 1992.

Bibliography

- [112] Tansel Yucelen, Wassim M Haddad, and Anthony J Calise. Output feedback adaptive command following and disturbance rejection for nonminimum phase uncertain dynamical systems. *International Journal of Adaptive Control and Signal Processing*, 25(4):352–373, 2011.
- [113] Youmin Zhang and Jin Jiang. Fault tolerant control system design with explicit consideration of performance degradation. *Aerospace and Electronic Systems, IEEE Transactions on*, 39(3):838–848, 2003.
- [114] Youmin Zhang and Jin Jiang. Bibliographical review on reconfigurable fault-tolerant control systems. *Annual Reviews in Control*, 32(2):229–252, December 2008.
- [115] Bingyu Zhou, Harish Satyavada, and Simone Baldi. Adaptive path following for unmanned aerial vehicles in time-varying unknown wind environments. In *American Control Conference (ACC), 2017*, pages 1127–1132. IEEE, 2017.
- [116] Zongyu Zuo and Pengkai Ru. Augmented \mathcal{L}_1 adaptive tracking control of quad-rotor unmanned aircrafts. *Aerospace and Electronic Systems, IEEE Transactions on*, 50(4):3090–3101, 2014.

Resume

TOUFIK SOUANEF

Born in 1972 in Batna, Algeria.

EDUCATION

2004-2006 Military Polytechnic School, Algeria

Magistere (Master) in Control Engineering

1989-1994 National School of Engineers, Algeria

Control Engineer Degree

WORK EXPERIENCE

2018-to date National Polytechnic School of Oran, Algeria

Assistant Professor

2017-2018 University of Science and Technology HB, Algeria

Assistant Professor

2015-2017 Higher School of Aeronautical Techniques, Algeria

Assistant Professor

2011-2015 IFR, University of Stuttgart, Germany

Research Associate

2007-2011 Government Research Institution, Algeria

Research Associate

1996-2004 Flight Training Center, Algeria

Maintenance Engineer

1994-1996 Higher School of Aeronautical Techniques, Algeria

Teaching Assistant